BIOLOGICAL PATHWAYS BASED APPROACHES TO MODEL AND CONTROL GENE REGULATORY NETWORKS

A Dissertation

by

SRIRAM VAKULABARANAM SRIDHARAN

Submitted to the Office of Graduate and Professional Studies of
Texas A&M University
in partial fulfillment of the requirements for the degree of

DOCTOR OF PHILOSOPHY

Chair of Committee,	Aniruddha Datta
Committee Members,	Edward Russell Dougherty
	Shankar Bhattacharya
	Jijayanagaram Venkatraj
Department Head,	Chanan Singh

May 2015

Major Subject: Electrical Engineering

ABSTRACT

The aim of effective cancer treatment is to prolong the patients' life while offering a reasonable quality of life during and after treatment. The treatments must carry their actions/effects in a manner such that a very large percentage of tumor cells die or shift into a state where they stop proliferating. The fundamental issue in systems biology is to model gene interaction via gene regulatory networks (GRN) and hence provide an informatics environment to study the effects of gene mutation as well as derive newer and effective intervention (via drugs) strategies to alter the cancerous state of the network, thereby eradicating the tumor. In this dissertation, we present two approaches to model gene regulatory networks. These approach are different, albeit having a common structure to them.

We develop the GRN under a Boolean formalism with deterministic and stochastic framework. The knowledge used to model these networks are derived from *biological pathways*, which are *partial* and *incomplete*. This work is an attempt towards understanding the dynamics of a proliferating cell and to control this system. Initial part (deterministic) of this work focuses on formulating a deterministic model by assuming the pathway regulations to be complete and accurate. Using these models algorithms were developed to pin-point faults (mutations) in the network and design personalized combination therapy depending on the expression signature of specific output genes.

To introduce stochastic nature onto the model due to incompleteness in the prior biological knowledge, an uncertainty class of models was defined over the biological network. Two such uncertainty class of models are modeled- one over the state transitions and the other over the node transitions in the system. This knowledge is transferred to priors, and the existing Bayesian theory is used to update and converge to a good model. The Bayesian control theory for Markovian processes is applied to the problem of interven-

tion in Markovian gene regulatory networks, while simultaneously updating the model. Via a toy example, it is shown that effective prior knowledge quantification can significantly help in converging on to the actual model with limited information from the system and take advantage of the optimality promised by Bayesian intervention. These control methods however, suffer from computational and memory complexity issues- *Curse of Dimensionality*, to be useful for any network size of biological relevance. To counter these issues associated with Dynamic Programming, suboptimal approximate algorithm known as *Q-learning* and its Bayesian variation are used to save on computational and memory complexities. These sub-optimal approximate algorithms perform very close (but inferior) to optimal policy, but the computational saving, both in terms of time and memory are significant to extend them to networks of larger size.

To Thatha

(Grandfather)

ACKNOWLEDGEMENTS

I would like to express my deepest gratitude to my advisor, Dr. Aniruddha Datta, who made my dissertation possible. I thank him for his steady guidance and inspirational discussions. The great experiences of working with him will definitely benefit the rest of my career. I thank Dr. Edward Dougherty and Dr. Vijay Venkatraj for their time and guiding me in projects and my research and providing such a wonderful research environment. I thank Dr. Shankar Bhattacharya, for serving on my committee and for his support and useful suggestions for the improvement of this work. He was the first person who suggested I go talk with Dr. Aniruddha Datta and work in genomics and system biology. I also want to thank Dr. Rola Barhoumi who has been of immense help in guiding my wet-lab experiments along with Dr. Venktaraj. They have patiently put up with me adapting from engineering to biology and it came at the expense of their time and money. I thank all students and researchers, past and current, at the Genomic Signal Processing Laboratory, especially Dr. Mohammad Shahrokh Esfahani, Dr. Ting Chen, Dr. Fang-Han Hsu, Jason Knight, Dr. Esmaeil Atashpaz Gargari, Dr. Lori Dalton, and Dr. Mohammadmahdi R. Yousefi, for friendship and memories. I would also like to thank Dr. Jay Porter and the Department of Engineering Technology and Industrial Distribution for generously supporting me financially as teaching assistant and later on as a lecturer through out the course my doctoral program at Texas A&M University. I would like to thank all the faculty and staff at Texas A&M University, especially for the administrative support provided by Ms. Tammy Carda of Electrical Engineering and Emma Carrigan of Engineering Technology and Industrial Distribution.

I had the opportunity to meet some really wonderful people who have contributed to my personal and intellectual growth. I especially want to thank Rahul Rangarajan,

Jasmit Kohli, Dr. Giridhar Sekar, Deva Vikram, Adhithya Rengarajan, Avinash Rani, Aditya Muthunarayanan and Venkatesh Ravishanker for some wonderful moments and discussions over the course of my stay in College Station.

Last but not least, I would like to thanks my parents for their patience and understanding. Every time they asked me about my graduation, I would reply next year until finally it has come through. I also want to thank my wife Soumya for her support by taking load of all the household chores as well as managing her work life. She was extremely patient and understanding when finishing up my dissertation.

Sriram Sridharan

College Station

January 14, 2015

NOMENCLATURE

Bach1: BTB and CNC homology 1, basic leucine zipper transcription factor 1

Nrf2: Nuclear factor (erythroid-derived 2)-like 2

PKC: Protein Kinase C

ROS: Reactive Oxygen Species

Keap1: Kelch-like ECH-associated protein 1

ARE: Anti-oxidant Response Element

Ras: Rat Sarcoma

PI3K: Phosphoinositide 3-kinase

PIP2: Phosphatidylinositol 4,5-bisphosphate

PIP3: Phosphatidylinositol (3,4,5)-trisphosphate

PTEN: Phosphatase and tensin homolog

ATM: Ataxia Telangiectasia Mutated

Akt: Protein Kinase B

Mdm2: mouse double minute 2

p53: Tumor protein 53

GSK-3β: Glycogen synthase kinase 3 beta

Bad: BCL2-associated agonist of cell death

Bcl-2: B-cell lymphoma 2

HIF: Hypoxia Inducible Factor

VHL: Von Hippel Lindau tumor suppressor protein

VEGF: Vascular Endothelial Growth Factor

ETC: Electron Transport Chain

HRE: Hypoxia Response Element

PHD: Prolyl Hydroxylase Domain containing proteins

ARNT: Aryl Hydrocarbon Nuclear Trans locator

mRNA: messenger Ribo Nucleic Acid

NADH: Nicotine Amide Dinucleotide (reduced form)

FAD: Flavin Adenine Dinucleotide

GAPDH: Glyceraldehyde Phosphate Dehydrogenase

LDHA: Lactate Dehydrogenase A

PDH: Pyruvate Dehydrogenase

PDK: Pyruvate Dehydrogenase Kinase

ETC: Electron Transport Chain

ATP: Adenosine Tri Phosphate

ADP: Adenosine Di Phosphate

NAD: Nicotine Amide Dinucleotide

TABLE OF CONTENTS

LIST OF FIGURES

LIST OF TABLES

1. INTRODUCTION

1.1 Systems Biology

Systems biology is a biology based interdisciplinary science that studies complex interaction within biological systems using a systems or holistic approach. All the properties, both functional and behavioral, of a biological system are the end result of these interactions. Consequently, precise qualitative and quantitative analysis will lead to newer insights in understanding these systems. In experimental (molecular) biology, the aim is to characterize the molecular constituents of living organisms. By contrast, systems biology tries to treat cells as organized molecular systems. Several approaches in physiology have taken a systems approach. There has been a surge in research in systems biology; this primarily is due to limitations of non-systems approaches along with advances in lots of associated fields such as computer science, genomics, nonlinear dynamical systems, control theory and Bayesian theory. Systems-level understanding is an imprecise notion due to vagueness in defining the system. In this dissertation, we use gene regulatory networks to define the system of interest. However, this is just one aspect of the system. The core of any system is the dynamics it creates and the logic that creates these dynamics. Consequently, in this study, we try to understand and model the logic that creates the dynamics in a biological system. The 3 primary goals of systems biology namely, -Structure Identification, System Dynamics and System Intervention- are explained in detail. Flow chart for systems biology research is shown in Fig. 1.1.

1.1.1 Structure Identification

The first step in any systems level study is to understand the physical structure of the system. The physical structure will help us in identifying both direct and indirect influences between different components of the system. In a biological system (e.g. a cell),

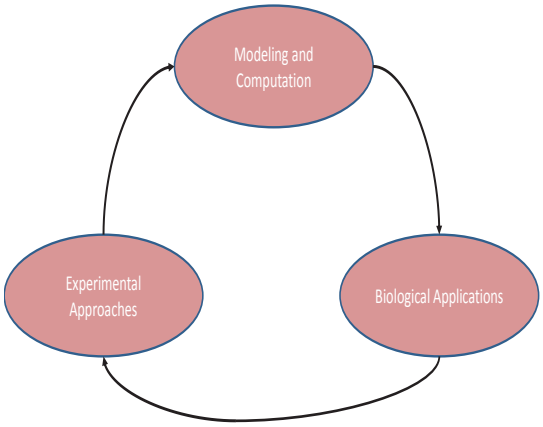

Figure 1.1: Flowchart of systems biology research

the gene regulatory network represents these details. The structure of such a network has been obtained over decades of experimentation involving genes/ proteins of interests and determining the regulatory relationships between them.

1.1.2 System Dynamics

Once the system structure is identified, the system dynamics need to be understood. System dynamics will be mathematical equations representing the state transition of the system given the current and previous states of the system along with all other pertinent information. Intuitively, the state of the system gives us enough information to determine the future course (states) of the system. The structure of the system directly influences the dynamics of the system. One common feature in gene regulatory networks is the presence of negative feedback connections which are important to maintain the stability of the system. Such a configuration is very common in controls literature. This feedback feature can give rise to oscillatory behavior.

1.1.3 System Intervention

The ultimate aim of the two study aspects discussed above is to successfully intervene to alter the behavior of the system. We intend the system to be traversing through states defined to be good rather than bad for a favorable outcome in these situations. In systems biology, this translates to finding therapeutic approaches based on systems level understanding such that there is a favorable prognosis of the ailment. Many of the present day drugs have been developed through effect-oriented screening. It is only recently that molecular targets of drugs have been identified and this information is being used to design better targeted drugs. Success in these newly developed methods will need to exploit the dynamics of the cell to accurately predict the effects of different interventions. This will help us in differentiating favorable outcomes from unfavorable ones.

1.2 Cell Biology: The Living Cell

The word 'cell' is derived from the Latin word 'cellula' meaning a small room. A cell is the most basic unit of life. A cell is the smallest unit capable to replicating itself. Anything smaller than a cell is truly not living. An example of this are viruses which are genetic material, but are not capable of replicating themselves. They usually hijack the replicating machinery of their host to make more copies of themselves. A cell is typically 5-20μm in diameter. Cells are membrane bound units capable of performing different functions. The simplified structure of a cell is shown in Fig. 1.2.

A brief description of the components are given below:

- Cell membrane: The cell membrane is the wall boundary surrounding the cell. It is a selectively permeable membrane made up of lipid bilayer and embedded proteins. All the compartments shown within the cell wall are called as organelles.

- Nucleus: It is the most important organelle and contains most of the genetic infor-

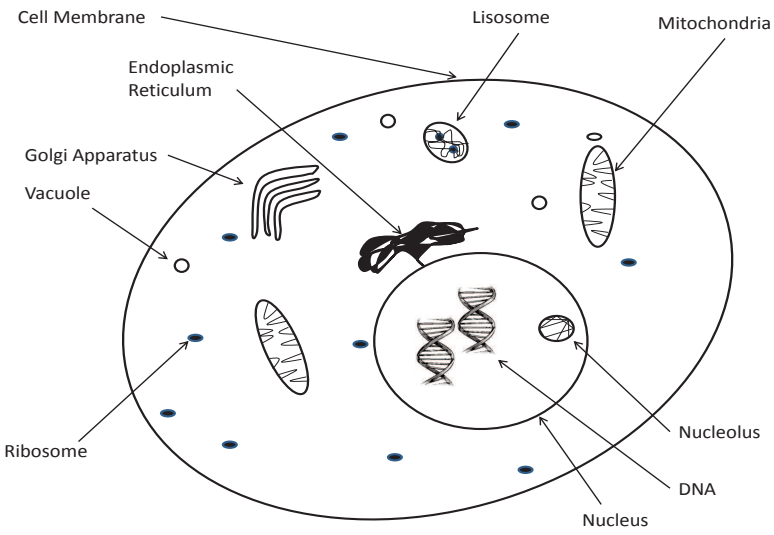

Figure 1.2: A simplified human cell

mation or the DNA. Its function is to maintain integrity of the DNA and control the activities by regulating the expressions of the genes.

- Nucleolus: It is a discrete densely stained structure within the nucleus. Its main role is to assemble ribosomes and also to transcribe ribosomal RNA.

- Endoplasmic Reticulum (ER): This organelle is responsible for synthesizing and transporting all the proteins, lipids and steroids. It also regulates drug metabolism and attachment of receptors onto the cell membrane proteins.

- Ribosome: Ribosomes reads the mRNA and assembles the corresponding the protein sequence.

- Mitochondria: They are the powerhouse of the cell. They are responsible for converting the glucose into ATP, which is used by the cells to meet its energy demand.

- Golgi apparatus: Its primary function is to process and package protein molecules

to be delivered elsewhere within the cell. They are also responsible for intra-cellular communication.

- Lysosome: They destroy all cellular debris by using enzymes. It also helps the cell make new organelles by destroying the old ones.
- Vacuoles: They are used for transporting toxic elements out of cell, maintaining pH and pressure inside the cell.

1.3 DNA, RNA and Protein: Central Dogma of Biology

The ability of cells to sort, retrieve and translate the genetic information is critical for making and maintaining a living organism. The information contained in each cell should also be passed on to its daughter cells at each cell division and also from generation to generation through the reproductive cells. Deoxyribonucleic acid (DNA) are the molecules used to store such genetic information. The famous double strand representations used everywhere is essentially representing the human DNA double-strand. The DNA molecule is double stranded and each strand is composed of combination of 1 out of 4 nucleotides at each position. The 4 nucleotide bases that make up the the DNA are *Adenine* (A), *Guanine* (G), *Cytosine* (C) and *Thymine* (T). The double-strand of the DNA is maintained due to complementary base-pairing property of the nucleotides- A pairs with T through a double bond, while G pairs with C through a triple bond. These settings guarantee that both the strands are equidistant apart all along the length of the DNA molecule. Fig. 1.3 shows the building blocks and single strand of DNA. Two such single strands can be combined to obtain a double-stranded DNA with the pairing rule mentioned above and shown in Fig. 1.4. This double-strand DNA molecule aligns itself in the form of the double helix. Since DNA is double-stranded and satisfy base-pairing rule complete information about one strand will completely determine the second strand of the DNA. The complete information encoded within the DNA depends on the sequence of the each base A, G,

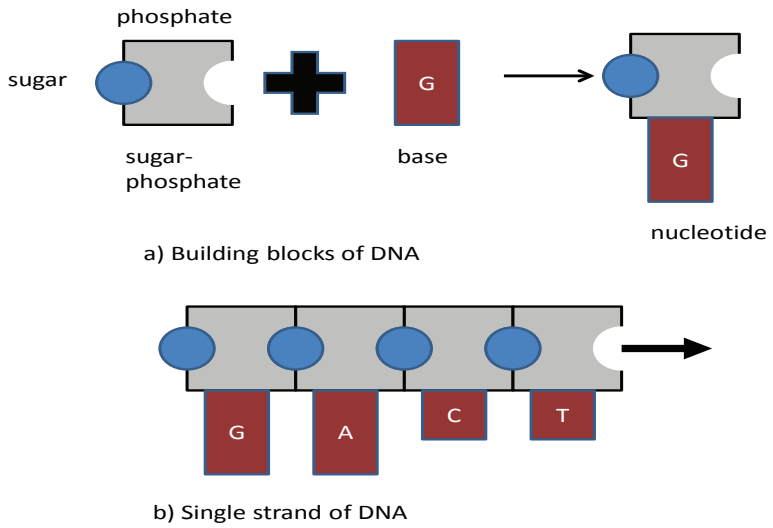

Figure 1.3: Building block of DNA

C and T determines within the DNA. Human genome consists of about 3 billion base-pairs. This can be thought to be a book consisting of 3 billion letters from the alphabet set $\{A, G, C, T\}$. Difference across the different organisms is due to the fact that their DNA sequence is different from each other.

Genes are short stretches of DNA nucleotides consisting of few thousand base-pairs. The human genome consists of about roughly, 25000 genes. Different genes are of different lengths and each gene codes for a specific protein in the body. Genes hold all the information to build and maintain a cell as well as pass this information to its offsprings. Genes have regulatory regions that specify when and how much protein needs to be produced to meet the requirements of the cell. Additionally, there are coding and non-coding regions in DNA. Coding sequence also known as *exon* are the useful region which are known to participate in making the proteins. Non-coding regions also known as *introns* do not have any participation in making the protein. The introns are also known as junk DNA. Coding regions are shown in red and non-coding regions in green in Fig. 1.5.

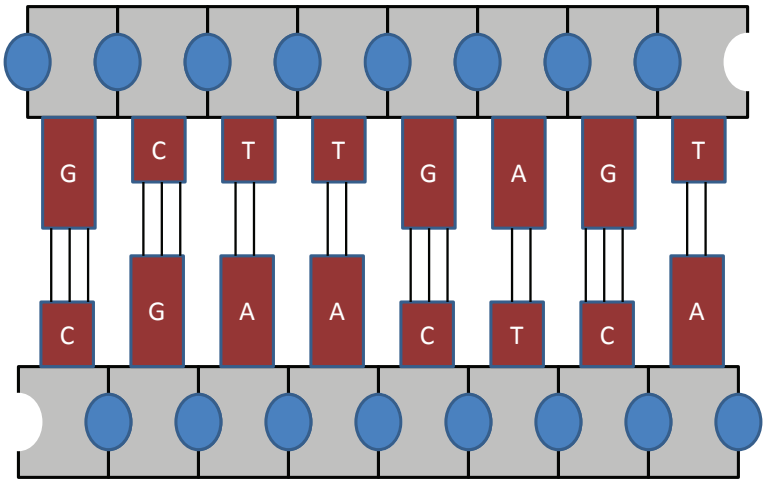

Figure 1.4: Double strand DNA with base-pairings

The word *gene* is derived from the Greek word *genesis* which means *birth*. DNA does not produce the proteins directly, but uses another intermediate step to make them. This intermediate step is where DNA is converted to another type of nucleic acid, RNA (ribonucleic acid). When a particular protein is needed the double-stranded DNA is split and the gene corresponding to the protein is copied into RNA. This process is referred to as *transcription*. The cell then uses the copies of these RNA to create the protein and this process is referred to as *translation*. The use of RNA helps in generating large quantities of protein simultaneously. Each DNA can produce multiple copies of RNA and each RNA can produce multiple molecules of the protein. The RNA nucleotides are also made up of 4 bases- *Adenine* (A), *Guanine* (G), *Cytosine* (C) and *Uracil* (U). Unlike DNA, which is double-stranded and helical in shape, RNA is single-stranded and can take a variety of shapes. Once the DNA is transcribed into RNA the nucleotides are translated to the corresponding protein. Proteins are made up of amino acids. A combination of 3 nucleotides in the RNA describes a single amino acid. This nucleotide triplet is also known as a *codon*. Since RNA is composed of 4 nucleotides a total of 64 codons are possible however, there

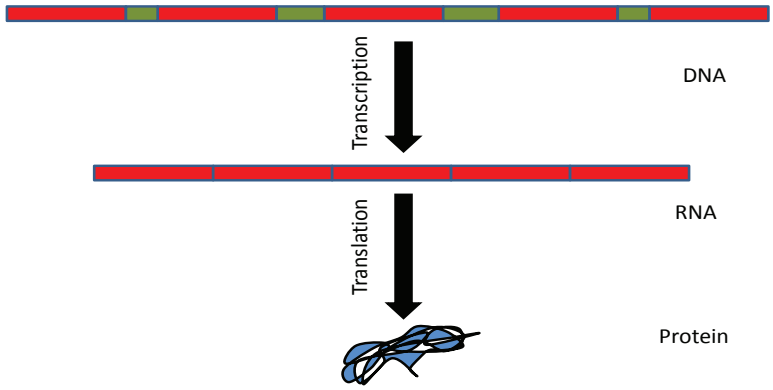

Figure 1.5: Central dogma of molecular biology

are only 20 amino acids that exist in nature and this is due to the redundancy whereby different combinations code for the same amino acid. Table. 1.1 gives all the nucleotide combinations and the amino acids they represent. The *central dogma of molecular biology* is an explanation of information flow in a biological system. It says that information flow is from DNA $\rightarrow$ RNA $\rightarrow$ protein. It is pictorially shown in Fig. 1.5.

1.4 Pathways and Signal Transduction

In multi-cellular organisms, the activities of a cell are carried out by intra- and extra-cellular cues and the signal it receives. Each cell has its own different functionality and its future course is dependent on these signals. For example, whether a cell needs to proliferate or undergo programmed cell death (*apoptosis*) is dependent on a number of different signals it receives. The state of a cell is tightly controlled by these different signals. In a healthy system, there is a balance between the cell death, cell differentiation and cell division. The regulation of these signals is lost in a disease like cancer and the presence of this aberrant signaling makes a disease like cancer very difficult to cure. Cell signaling through electrical pulses is primarily used by neuronal cells to communicate. However, for somatic cells, proteins are used as the primary signaling molecules. Signaling molecules

Table 1.1: Genetic code

Amino acid	**Codon(s)**
Alanine/Ala/A	GCU, GCC, GCA, GCG
Arginine/Arg/R	CGU, CGC, CGA, CGG, AGA, AGG
Asparagine/Asn/N	AAU, AAC
Asparticacid/Asp/D	GAU, GAC
Cysteine/Cys/C	UGU, UGC
Glutamine/Gln/Q	CAA, CAG
Glutamicacid/Glu/E	GAA, GAG
Glycine/Gly/G	GGU, GGC, GGA, GGG
Histidine/His/H	CAU, CAC
Isoleucine/Ile/I	AUU, AUC, AUA
Leucine/Leu/L	UUA, UUG, CUU, CUC, CUA, CUG
Lysine/Lys/K	AAA, AAG
Methionine/Met/M	AUG
Phenylalanine/Phe/F	UUU, UUC
Proline/Pro/P	CCU, CCC, CCA, CCG
Serine/Ser/S	UCU, UCC, UCA, UCG, AGU, AGC
Threonine/Thr/T	ACU, ACC, ACA, ACG
Tryptophan/Trp/W	UGG
Tyrosine/Tyr/Y	UAU, UAC
Valine/Val/V	GUU, GUC, GUA, GUG
Start	AUG
Stop	UAA, UGA, UAG

usually function by changing the three dimensional (3-D) structure of the other molecules to which it binds or communicates. These interactions are usually multivariate in the sense that a single molecule can communicate with a number of other molecules and vice-versa. Because of the inherent difficulty in understanding such information, biologists have used the marginal interactions between these signaling molecules, collectively known as *pathway information*. A pathway is a series of molecules in a cell which are interconnected such that the change in the activity of one of the molecules can cause a change in the activity of other molecules. Meanwhile, signal transduction occurs when a molecule, that is extracellular, binds to a surface receptor in cell and triggers a series of changes in the cell. This is the mechanism by which cells communicate with other cells as well as with itself. A collection of many such pathway segments will constitute a graph/network which indicates the regulatory relationships between the different interacting molecules in the network. Such a network is also referred to as a *gene regulatory network*.

1.5 Homeostasis and Gene Regulation

Homeostasis, from the Greek word meaning *similar* or *steady*, is the property of a system by which the variables are regulated in such a way that the system maintains fairly stable conditions necessary for survival. This word was coined by Walter Cannon in 1926. In the human body this might relate to maintaining the healthy levels of body temperature, water, salt, sugar, protein, fat, calcium and oxygen contents in the blood. The regulatory processes in the body, dynamically maintain the steady-state conditions in the system. Norbert Weiner was able to relate the concepts of homeostasis in living tissues to that of machines. Cybernetics borrows ideas from biology that any existing system has a natural drive towards homeostasis. A simple example in this regard is the control of body temperature close to 98.6^{o}F. When the temperature increases we tend to sweat and when it is too cold we sweat less and reduce blood circulation to prevent loss of heat. In a way

living cells can also be thought up of as cybernetic systems. One fundamental feature in such systems is the presence of negative feedback loops that always tend to counter the externally acting force. The negative feedback arises out of imbalance between the forces that tend to counter each other. Another important factor of these negative feedbacks is that they give rise to oscillatory behavior. The negative feedback takes time to act and such a time lag is also another essential feature of natural systems.

How do biological systems achieve homeostasis?

The most important method through which cells maintain homeostatic conditions is through gene regulation. Of the roughly 25,000 genes present in a human cell, not all of them need to be making protein all the time. A gene that is producing protein is said to be *expressed*, while a gene not producing protein is said to be *not expressed*. The amount of protein produced however, depends on the demand from the system. The regulation of the gene is controlled by multiple feedback pathways. The expression of genes can be considered similar to turning a switch ON or OFF within an electrical circuit [1]. From a systems viewpoint, the living cell is like a multi-input- multi-output (MIMO) feedback system. It is the ON and OFF mechanisms of the genes, along with their feedback signaling that help the systems achieve homeostasis. Understanding such a system is the most important challenge in systems biology.

1.6 Dynamical Systems Modeling

An important aspect of modeling is to understand the dynamics of the gene regulatory network. Due to the associated complexities of these gene regulatory networks, intuition alone will not present a complete understanding of the system. Instead, an explicit mathematical description of the network is required that will explain the system dynamics

completely. A dynamical system is a system whose time evolution of states are defined by mathematical equation. This equation tells us how the system is going to be changing its state from one time point to another. A simple example of a dynamical system is an oscillating simple pendulum. The state along with the equations will define the system completely. The mathematical equations essentially define the model of the system.

The defined model can be a continuous or discrete state system. A continuous system is the one where the value of state variables vary as a real number. Discrete systems are the ones where the state variables can take only certain predefined discrete values. Additionally, the mathematical equations describing the state transitions can be deterministic or stochastic. The biological system is one such dynamical system whose state changes depending on the intra- and extra-cellular signals it receives. As explained previously, a gene can be turned ON or OFF. Though a gene is being expressed when it is turned ON the amount of protein produced depends on the requirements of the cell. Thus, it is a continuous variable and changes its values depending on the demands. However, biological systems' response usually occurs beyond a certain threshold, in the sense that the quantity of the protein determines its activity. Thus protein activity exhibits a switch like behavior [1]. The biological system can thus be modeled as a continuous or a discrete system. So the choice of the type of modeling to use will depend upon other considerations. The continuous time models, using differential equations, provide a more detailed picture of network dynamics, but the number of parameters required apriori is too large, too expensive and usually unavailable. An alternative to this is the use of discrete logic-based models that can provide a good qualitative approximation of the system. The reason for preferring this alternative is that biologists find it easier and more intuitive to describe gene expression in terms of discrete states-ON/OFF. In this dissertation, the biological systems under consideration have all been modeled as discrete-state and discrete-time systems, but both deterministic and stochastic transitions have been considered.

1.7 Research Plan

1.7.1 Modeling Stress Response Pathways

1.7.1.1 Related Works

The gene regulatory relationships considered in these models are deterministic in nature. The p53-Mdm2 gene regulatory network in a deterministic sense was modeled in [2]. Based on the Boolean model thus developed, the authors studied the dynamics of such a system and compared it with available evidence in literature to evaluate the performance.

1.7.1.2 Modeling Oxidative Stress Response Pathways

The significance of oxidative stress response pathways in the human body is discussed. These pathways are modeled as boolean networks and algorithms implemented for understanding the dynamics of the system. The results from simulations are compared with literature evidence to evaluate performance. The model considered is discrete state deterministic model.

1.7.1.3 Modeling Hypoxia Stress Response Pathways

The hypoxia stress response pathways and their relevance to cancer are discussed. These pathways are modeled as boolean networks and algorithms are implemented for understanding the dynamics of the system. The model considered is a discrete state deterministic model.

1.7.2 Fault Detection and Control in Stress Response Pathways: A Deterministic Approach

1.7.2.1 Related Works

As mentioned earlier, the ultimate aim of the modeling and dynamical systems approach is to locate faults in the system and to successfully intervene to correct for their

harmful effects. In [3], growth factor pathways were modeled and drug intervention strategies designed for different pathway mutations. In this dissertation, this work has been improved upon by considering some more factors to make the problem more realistic. The pathways considered in [3] are acyclical in nature, that is, they contain no feedback loops. However, we consider cyclical networks which have feedbacks.

1.7.2.2 Detection of Multiple Faults in a Cyclic Gene Regulatory Network

In [3], the network considered did not have any feedback loops. It is more realistic when the considered network has feedback loops in them. For solving this problem, oxidative stress response pathways along with PI3K/Akt pathways are considered. Input to the system are designed such that they are capable of detecting faults (mutations) in the system based on the signature of output downstream genes.

1.7.2.3 Drug Intervention in a Cyclic Gene Regulatory Network

In [3], due to the absence of feedback loops, the state of the system is static after a few time-steps. In order to consider feedback connections, the hypoxia stress response pathways modeled earlier were augmented with other pathways that play an important role in cancer. In this case due to feedback connections the state of the system is oscillatory. Drug intervention strategies were designed by considering the major pathways influenced by hypoxia.

1.7.3 Control in Signaling Pathways Under Uncertainty: A Stochastic Approach

1.7.3.1 Related Works

The previous methods assumed that the transitions between states happens in a deterministic manner. It is known that biological systems do not behave that way and there is some amount of stochasticity to transitions at every time-step. Perfect knowledge of underlying transition probabilities between states is necessary to design an optimal control

action. We are interested in modeling a Gene Regulatory Network (*GRN*) as a Markov Decision Process (*MDP*). The theory for analysis and control of MDP is very rich. The reader is referred to [4] for a detailed discussion on this topic. In biological systems very little is known about the true dynamics of the system due to the paucity of available data and the costly experiments involved for generating such data. Additionally, variation across biological systems is too confounding to come up with these transition probabilities. To address this uncertainty, one can construct an uncertainty class of models and optimize an objective function across the entire uncertainty class. Previously, biological systems were modeled as Boolean Networks (*BN*) and its probabilistic variant Probabilistic Boolean Network (*PBN*) and intervention techniques designed for such systems [5–10]. In these models it was assumed that the information about the transition probabilities in the system is known or can be generated with some uncertainty about them. To refine these models, prior knowledge in the form of pathways which gives the relational regulation between a pair of genes/proteins was considered [3]. However, the models were deterministic in nature. Furthermore, in these models the mutations were identified and corrective interventions designed based on the signature of chosen downstream genes. This prior knowledge is however, partial and incomplete. Yousefi et. al [11] extended the work by assuming a probability distribution over the state transition probabilities. The probabilities were updated under a Bayesian framework based on data from the system to reduce the uncertainty. The intervention (control) problem was formulated and solved as an optimization problem in the dynamic programming framework.

1.7.3.2 Uncertainty in Stochastic Dynamical System: Bayesian Control

In this current work, prior biological knowledge is incorporated in the form of pathway information. Since there is some uncertainty in the regulation of the pathways, a prior probability distribution is defined over each pathway. The parameters of the distribution,

which determine its shape express the degree of confidence in this prior knowledge. Such information expressed over the pathways is used to generate the Transition Probability Matrix, TPM, which defines the complete dynamics of the model. The observations from the true system are used to update and reduce uncertainties in the designed model. An optimization framework is defined to estimate an optimal intervention action. This action is optimal for the model determined by the prior defined over the system. The objective function for the optimization problem is the expected cost relative to the probability distribution over the uncertainty class and an optimal Bayesian robust intervention policy minimizing this cost function is formulated.

1.7.3.3 Computational Issues: Q-Learning

In [11], the intervention (control) problem was solved under a dynamic programming framework, this however, was computationally intensive and non-tractable for network sizes of a few nodes. Hence , it was not possible to extend these methods to larger practical sized networks. To alleviate this issue, sub-optimal solutions are formulated using the framework of Q-learning. It was seen that not only was there a significant gain in computational issues, but the costs derived in both the methods were comparable to each other.

1.8 Dissertation Outline

The dissertation is organized as follows:

- Section 2: General structure of stress response pathways are introduced. Oxidative stress response pathways are discussed. These pathways are modeled as boolean networks and algorithms implemented for locating the faults (mutations) in the network based on signature of specific genes. The model considered is discrete time deterministic model.

- Section 3: Hypoxia stress response pathways and its relevance in cancer are discussed. These pathways are modeled as boolean networks and algorithms implemented for designing combination drug therapy which will be more effective than treating with a single drug. The model considered is discrete time deterministic model.

- Section 4: Uncertainties in pathways are expressed as a distribution and an uncertainty class representing the system derived. Based on observations from the true system the size of the uncertainty class was reduced using an bayesian update framework. A control scheme was also designed which was adaptive and non-stationary in nature.

- Section 5: Some conclusions and future research directions are outlined.

2. OXIDATIVE STRESS RESPONSE PATHWAYS *

2.1 Introduction

The control of gene expression in eukaryotic organisms is achieved via *multivariate* interactions between different biological molecules such as proteins and DNA [12]. Consequently, in recent years, various genetic regulatory network modeling approaches such as differential equations and their discrete-time counterparts, Bayesian networks, Boolean networks (BNs) and their probabilistic generalizations, the so-called probabilistic Boolean networks (PBNs) [13] have been proposed for capturing the holistic behavior of the relevant genes. Some of these approaches such as differential equations involve finer models and require a lot of data for inference while others such as Boolean networks yield coarse models with lower data requirements for model inference. On the other hand, historically biologists have focused on experimentally establishing marginal cause-effect relationships between different pairs of genes, which when concatenated together leads to what is known as *pathway* information. Biological pathways are used by biologists to represent complex interactions occurring at the molecular level inside living cells [14]. Pathway diagrams describe how the biological molecules interact to achieve their biological function in the presence of appropriate stimuli [15]. At a very simple level, biological pathways represent the graphical interactions between different molecules. However, as already noted, the pathways give only a marginal picture of the regulations (up-regulation or down-regulation) of the different genes/RNAs/proteins by other genes/RNAs/proteins.

The complexity of biological signaling and the prevelance of prior information in the form of pathway knowledge demand that genetic regulatory network models consistent

*This section is reprinted with permission from "Boolean modeling and fault diagnosis in oxidative stress response" by S Sridharan, R Layek, A Datta and J Venkatraj, *BMC Genomics 2012, 13(Suppl 6):S4*. doi:10.1186/1471-2164-13-S6-S4.

with pathway information be developed. Motivated by this, we developed an approach to generate Boolean network models consistent with given pathway information and applied it to studying the p53-mediated DNA damage stress response [2]. In addition, we used a signaling diagram of the *MAP-Kinase* pathways to predict possible location(s) of the single signaling breakdowns, based on the cancer-causing breakdown signature [3]. Moreover, we also made *theoretical* predictions of the efficacy of different combination therapies involving six anti-cancer drugs, which we plan to validate in the near future.

In this work, we first develop a Boolean network model consistent with oxidative stress response pathway information from the biological literature. Thereafter this model is linked with the *PI3k/Akt* pathway and the composite model is used to pinpoint the possible fault locations based on the observed deviations in the apoptotic signature over different time windows. This section is organized as follows. Section 2.2 contains a brief general description of Stress Response Pathways while Section 2.3 presents a discussion specific to the case of oxidative stress. The Boolean network model for oxidative stress response is developed in Section 2.4. The role of mitochondria as the site in a cell where the oxidative stress is generated is discussed in Section 2.5. In Section 2.6, we develop an integrated network linking oxidative stress response to the phenomenon of apoptosis via the $PI3k/Akt$ pathways. Section 2.7 presents an approach for pinpointing fault locations in the integrated network by observing the apoptotic signature in response to certain test stress input sequences. Finally, Section 3.9 contains some concluding remarks.

2.2 Stress Response Pathways

Adaptive stress response pathways are the first responders to chemical toxicity, radiation, and physical insults. The different stress response pathways share a very similar architecture. This architecture has three main components: a transducer, a sensor and a transcription factor (TF) [16]. The transcription factor (TF) is a DNA-binding protein that

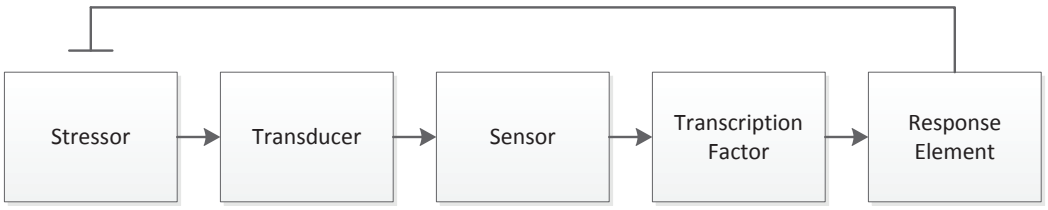

Figure 2.1: General scheme of stress response pathways

interacts with the promoter regions of its target genes via its canonical DNA-binding sites, known as 'response elements' (REs), to activate the expression of the target genes. The sensor is a protein that physically interacts with the transcription factor in the cytosol, sequestering the transcription factor from the nucleus under normal cellular conditions. In addition to its role in cytoplasmic sequestration of the TF, the sensor may direct TF degradation, providing an additional layer of regulatory control. The result of the sensor-TF complexation is to maintain inactivity of the TF under normal cellular conditions, while providing a mechanism that permits activation in response to an appropriate insult to the cell. The transducer is an enzymatic protein, such as a kinase, that conveys a biochemical change from a signaling pathway upstream of the sensor/TF complex in the event of cellular stress. The transducer may directly modify the transcription factor, providing the activating signal or modify the sensor which in turn, destabilizes the sensor/TF complex. Liberated, stabilized, and activated, the transcription factor relocates to the nucleus where it activates its target genes. Generally the sensor and TF are unique for a given stress response pathway unlike transducers which can be shared between different stress response pathways, leading to what is commonly referred to as 'cross-talk' between the pathways. A schematic diagram showing the general architecture of a stress response pathway is shown in Fig. 2.1.

2.3 Oxidative Stress Response Pathways

Oxidative stress is caused by exposure to reactive oxygen intermediaries/species (*ROS*). The stress induced on the cells by electrophiles and oxidants gives rise to a variety of chronic diseases. The outcome of interactions between the cell and oxidants is determined largely by the balance between the enzymes that activate the reactive intermediaries and the enzymes that detoxify these reactive intermediaries [17]. For example, oxidative stress contributes to aging and age-related diseases such as cancer, cardiovascular disease, chronic inflammation, and neurodegenerative disorders. The body has developed a variety of counteractive measures for combating oxidative stress. At elevated concentrations of electrophiles the complex $Keap1$-$Nrf2$ (made up of the transcription factor $Nrf2$ and sensor $Keap1$) is broken and $Nrf2$ is liberated and transported into the nucleus. $Keap1$ has been known to sequester $Nrf2$ in the cytoplasm and also leads to the proteasomal degradation of $Nrf2$. Once the complex is broken, $Nrf2$ is phosphorylated and transported to the nucleus. Inside the nucleus, $Nrf2$ forms heterodimers with small Maf proteins (*SMP*) which then binds to the anti-oxidant response element (*ARE*) and leads to the translation of antioxidant genes, which produces Phase II detoxifying enzymes. The purpose of this is to detoxify the electrophiles to water soluble components. Thus in response to elevated concentrations of electrophiles, various antioxidant proteins are activated [18–22]. The schematic diagram for $Nrf2$ activation is shown in Fig. 2.2. In the rest of this section, the term ARE will be interchangeably used to represent either the antioxidant response element cis enhancer sequence that is upstream of the gene promoters for the antioxidant proteins or the antioxidant genes/proteins themselves. The context will make it clear whether we are referring to the regulatory sequence or to the resulting gene/protein.

We next focus on the procedure by which $Nrf2$ is deactivated. This is carried out by other proteins that stop translation of the antioxidant genes once the electrophiles have

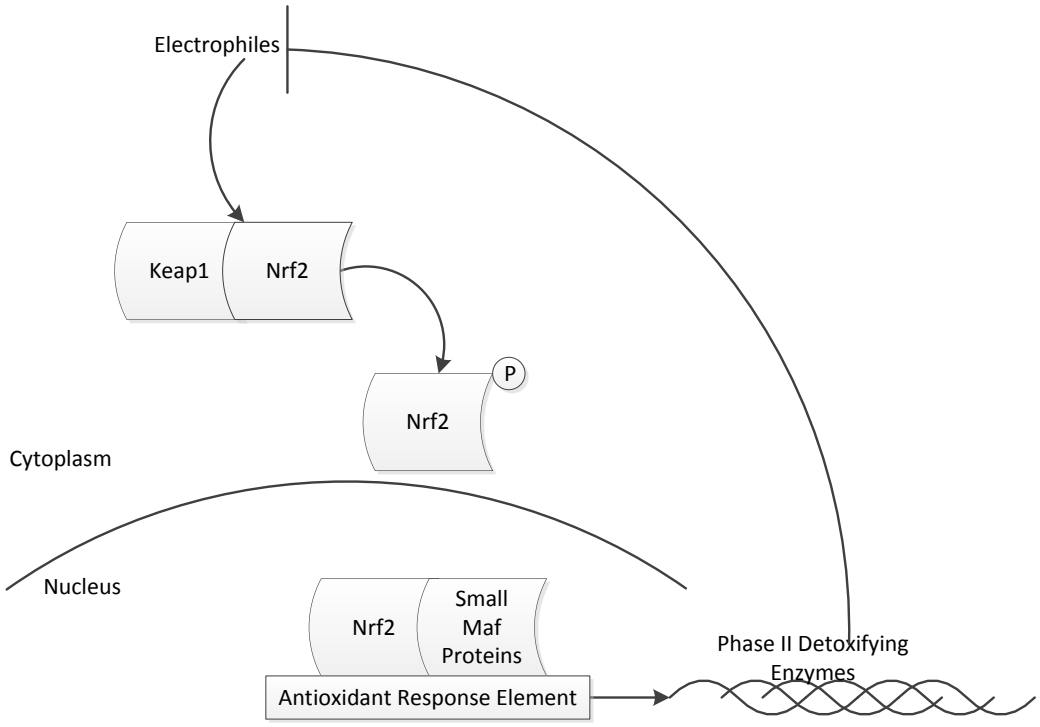

Figure 2.2: Nrf2 activation

been neutralized. For instance, the *Bach*1-*SMP* complex has been known to bind to the same region on the *ARE* as the $Nrf2$-*SMP* complex. Similarly, small Maf proteins are known to form homodimers or heterodimers with other small Maf proteins. These protein complexes are known to bind to the same location on the *ARE* as the $Nrf2$-*SMP* complex. So, once the electrophiles have been eliminated, these protein complexes bind to the *ARE* and displace $Nrf2$ which is then transported back to the cytoplasm. In the cytoplasm, it binds with $Keap1$, which directs its proteosomal degradation [23–26]. The schematic diagram for $Nrf2$ deactivation is shown in Fig. 2.3.

One of the byproducts of normal metabolism is the production of a large number of free radicals. Oxidative stress is caused by the production of free radicals in quantities beyond those that can be handled by the cellular antioxidant system. Indeed, oxidative stress has been implicated in the development of many age-related diseases, including neurodegen-

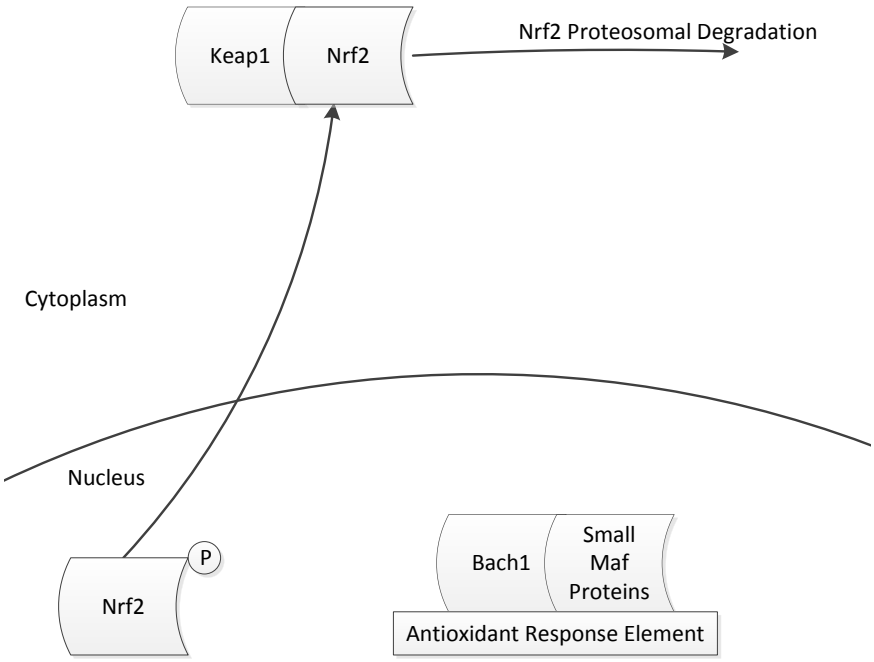

Figure 2.3: Nrf2 deactivation

erative ones, such as Alzheimer's and Parkinson's, and in aging itself. In addition, excess free radicals react with the nucleotides in the DNA resulting in mutations in the long run. Although there are cellular mechanisms to sense and repair the oxidative DNA damage, mutations can accumulate over a period of time and result in a major disease like cancer. In the next section, we develop a Boolean network model for oxidative stress response pathways. This network will be later utilized to analyze different failure modes that can suppress apoptosis and possibly lead to cancer.

2.4 Boolean Network Modeling of Oxidative Stress Response Pathways

Before proceeding to the actual modeling of the specific oxidative stress response pathways, we first formally define the general terms 'pathway' and 'Boolean Network' following the detailed development in [2]. Given two genes/proteins A and B and binary values $a, b \in \{0,1\}$, we define the term *pathway segment* $A \xrightarrow{t:a,b} B$ to mean that if gene/protein A assumes the value a then gene/protein B transitions to b in no more than t subsequent

time steps. A *pathway* is defined to be a sequence of pathway segments of the form $A \xrightarrow{t_1:a,b} B \xrightarrow{t_2:b,c} C$.

A *Boolean Network* (*BN*), $\Upsilon = (V,F)$, on n genes is defined by a set of nodes/genes $V = \{x_1,...,x_n\}$, $x_i \in \{0,1\}$, $i = 1,...,n$, and a list $F = (f_1,...,f_n)$, of Boolean functions, $f_i : \{0,1\}^n \to \{0,1\}$, $i = 1,...,n$ [1]. The expression of each gene is quantized to two levels, and each node x_i represents the state/expression of the gene i, where $x_i = 0$ means that gene i is OFF and $x_i = 1$ means that gene i is ON. The function f_i is called the *predictor function* for gene i. Updating the states of all genes in Υ is done synchronously at every time step according to their predictor functions. At time t, the network state is given by $x(t) = (x_1(t),x_2(t),...,x_n(t))$, which is also called the *gene activity profile* (*GAP*) of the network.

The modeling approach that we will follow here involves using the biological pathway knowledge from the literature and applying Karnaugh map reduction techniques to it to obtain an update equation for each node of the Boolean network [2]. The details specific to the oxidative stress response pathway are discussed next. The pathway segments relevant to the oxidative stress response are given below [18, 19, 21, 24, 27, 28]:

$$ROS \xrightarrow{1:1,0} Keap1 \tag{2.1}$$

$$ROS \xrightarrow{1:1,1} PKC \tag{2.2}$$

$$ROS \xrightarrow{1:a,\bar{a}} Bach1 \tag{2.3}$$

$$Keap1 \xrightarrow{1:b,\bar{b}} Nrf2 \tag{2.4}$$

$$Nrf2, ROS \xrightarrow{1:(1,0),1} Keap1 \tag{2.5}$$

$$PKC \xrightarrow{1:1,1} Nrf2 \tag{2.6}$$

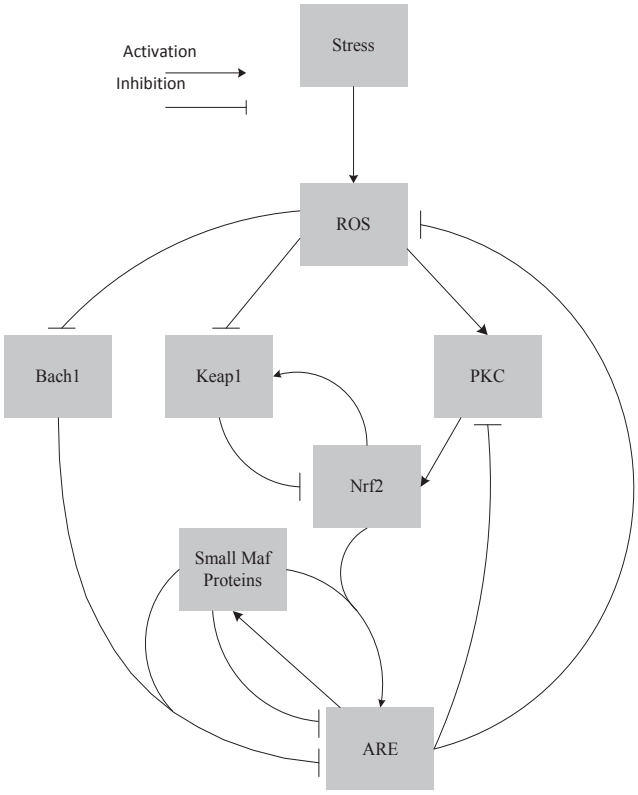

Figure 2.4: Oxidative stress response pathways

$$Bach1, SMP \xrightarrow{1:(1,1),0} ARE \tag{2.7}$$

$$Nrf2, SMP \xrightarrow{1:(1,1),1} ARE \tag{2.8}$$

$$SMP, SMP \xrightarrow{1:(1,1),0} ARE \tag{2.9}$$

$$ARE \xrightarrow{1:1,1} SMP \tag{2.10}$$

$$ARE \xrightarrow{1:1,0} ROS \tag{2.11}$$

$$ARE \xrightarrow{1:1,0} PKC \tag{2.12}$$

In these pathways *ARE* represents the family of antioxidant genes in the sense that if the correct complexes bind to *ARE* it leads to the up-regulation/down-regulation of the

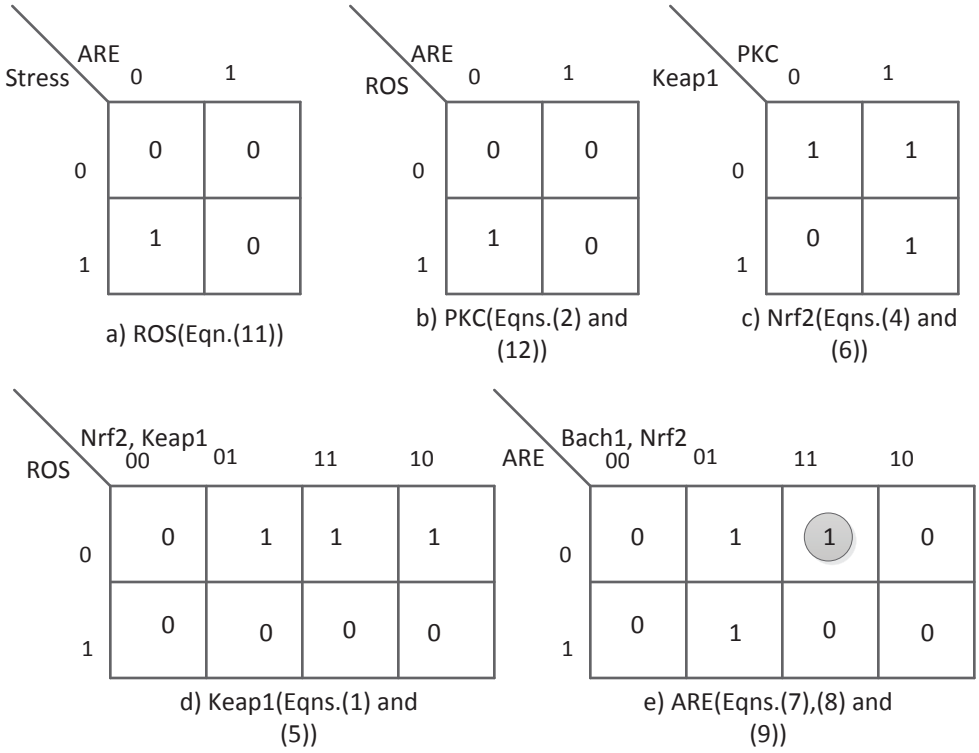

Figure 2.5: Karnaugh maps for deriving the Boolean network of oxidative stress response pathways

appropriate antioxidant gene. These pathway interactions are pictorially represented in Fig. 2.4. In this figure we have used square boxes without making any distinction between whether they represent proteins/genes or a biochemical entity. *ROS* stands for reactive oxidative species which is a biochemical entity. The other entities like *PKC*, $Keap1$, $Nrf2$, $Bach1$ are all proteins and *ARE* (Antioxidant Response Element) is a cis enhancer sequence that is upstream of the gene promoters for the antioxidant proteins or the antioxidant genes/proteins themselves. Also the merged activation ($Nrf2$/*SMP*) or inhibition ($Bach1$/*SMP*) corresponds to dimers formed between these components. The Karnaugh-maps for the genes/proteins are shown in Fig. 2.5.

From the pathways described above and using the Karnaugh-map reduction techniques, the Boolean update equations for each node of the network are deduced. Some logical rea-

soning has been used for determining the equations: 1) the maximum number of predictors for updating a variable is fixed to be 3; 2) Small Maf Protein is assumed to be ubiquitously expressed and the pathway given by Eqn.(2.10) only increases the concentration of SMP, which in conjunction with Eqn.(2.9), binds to ARE and down-regulates the antioxidant gene; 3) a gene being turned on implies that the corresponding protein is being produced although, in reality, this is not necessarily true; and 4) in the case of a conflict in the Karnaugh map, biological knowledge has been used to assign either a 0 or a 1. This last point is demonstrated by a specific example. For instance, in the case of ARE, the entry shown with a grey circle around it says that when both $Bach1$ and $Nrf2$ are upregulated and antioxidant gene is downregulated, then at the next time step antioxidant gene will be upregulated. The biological explanation for such an update is that it corresponds to the situation where, in the presence of $Stress$, $Nrf2$ has been activated and is relocating to the nucleus while the inhibitor $Bach1$ is simultaneously relocating to the cytoplasm prior to the activation of antioxidant gene at the next time step. Such intuitive reasoning has been used to model the system here. One might use a different reasoning which could lead to a different set of update equations. However, since we are concerned only about the final steady-state behavior, such reasoning can be justified as long as the overall system behavior, defined by the update equations, matches the steady-state. As an example, the final update equation for ARE is derived as follows. In the K-maps, the ones are grouped up in pairs of 2,4,8 and so on and each group should have at least one variable staying constant. So for this case there are two groups whose equations correspond to $Nrf2 \cdot (\overline{ARE})$ and $Nrf2 \cdot (\overline{Bach1})$. The final update equation for ARE is the sum of these two equations. Indeed, by working with different sets of update equations, we determined that all biologically plausible ones led to the same/similar attractor behavior. From the set of possible Boolean networks we chose the ones that appealed most to our biological understanding

and the resulting update equations are given below:

$$ROS_{next} = Stress \cdot \overline{ARE} \tag{2.13}$$

$$Keap1_{next} = \overline{ROS} \cdot (Nrf2 + Keap1) \tag{2.14}$$

$$PKC_{next} = ROS \cdot \overline{ARE} \tag{2.15}$$

$$Nrf2_{next} = PKC + \overline{Keap1} \tag{2.16}$$

$$Bach1_{next} = \overline{ROS} \tag{2.17}$$

$$SMP_{next} = 1 \tag{2.18}$$

$$ARE_{next} = Nrf2 \cdot (\overline{ARE} + \overline{Bach1}). \tag{2.19}$$

An equivalent digital circuit with logic gates is shown in Fig. 2.6. Here the lines in bold represent feedback paths. The state transition diagrams resulting from Eqns. (2.13)-(2.19) for the two cases *Stress*=0 and *Stress*=1 are shown in Figs. 2.7 and 2.8 respectively. In these transition diagrams, the genes in the binary state representation are ordered as [*ROS Keap*1 *PKC Nrf*2 *Bach*1 *ARE*] and the binary states are compactly represented by their decimal equivalents. For instance, the binary state (111100) would be represented by the decimal number 60. The states of particular interest are the attractors as they give rise to the steady-state properties of the network. In Fig. 2.7 , the state of interest is the singleton attractor $18(010010)$. On the other hand, in Fig. 2.8 , the states of interest are the seven states forming the attractor cycle. These states are: $18(010010)$, $50(110010)$, $40(101000)$, $44(101100)$, $45(001101)$, $5(000101)$ and $23(010111)$ traversed in that order. They would lead to cyclical/oscillatory behavior in the time domain response.

It is clear from the preceding discussion that some kind of oscillatory behavior of the

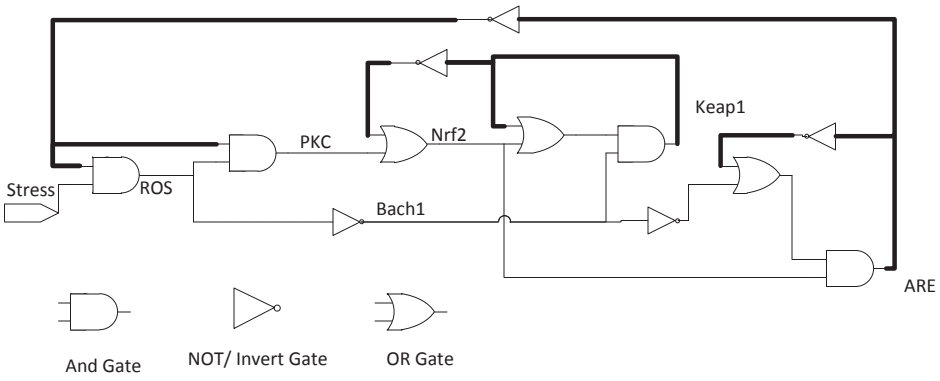

Figure 2.6: Equivalent Boolean network for oxidative stress response

genes will be observed when the external *Stress* input equals 1. On the other hand, when the *Stress* input equals 0, the system will rest in only one state meaning that there will be no oscillation.

2.4.1 Time Domain Simulation Results

The network obtained was simulated using MATLAB by giving an external stress input signal for a duration of 50 $timesteps$, and both the input signal and the responses are shown in Fig. 2.9. The signal *ROS* is a biological manifestation of the external input signal, *Stress* being applied to the network. The biological purpose of this network is to counteract the effect of *ROS* produced in response to the *Stress* input. As we can see from Fig. 2.9 , in the absence of any *Stress* signal, the system reaches the singleton attractor 18(010010). Once *Stress* signals are applied, there are oscillations as theoretically expected from the existence of an attractor cycle. In Reichard *et al*. [23], the cells were treated with Arsenite, a well known activator of $Nrf2$ and an out-of-phase relationship was observed between $Nrf2$ and $Bach1$. Shan *et al*. [26] also showed a similar out of phase relationship. In Katsuoka *et al*. [25] *DEM* (an activator of $Nrf2$) also leads to increased expression of $NQO1$ which is a known anti-oxidant response element. Such an in-phase relationship between $Nrf2$ and the antioxidant gene is also seen in Fig. 2.9. Thus the theoretical predictions made by our Boolean network model for oxidative stress response appear to

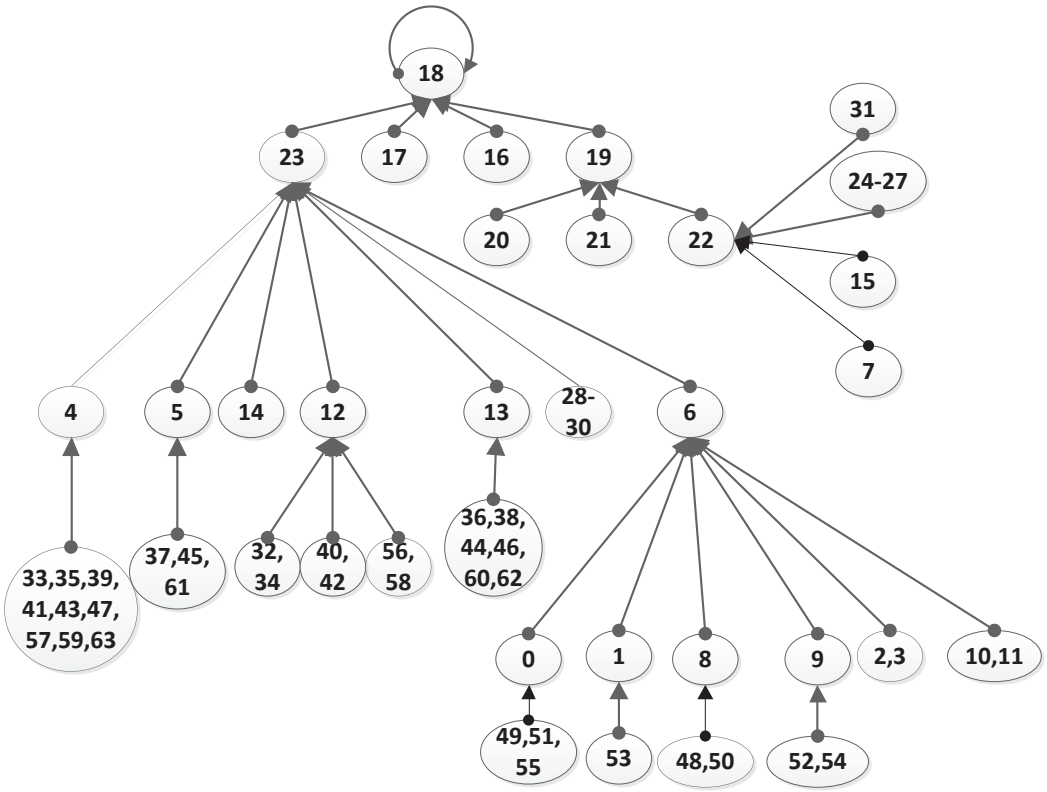

Figure 2.7: The Boolean state transition diagram when the stress input is 0

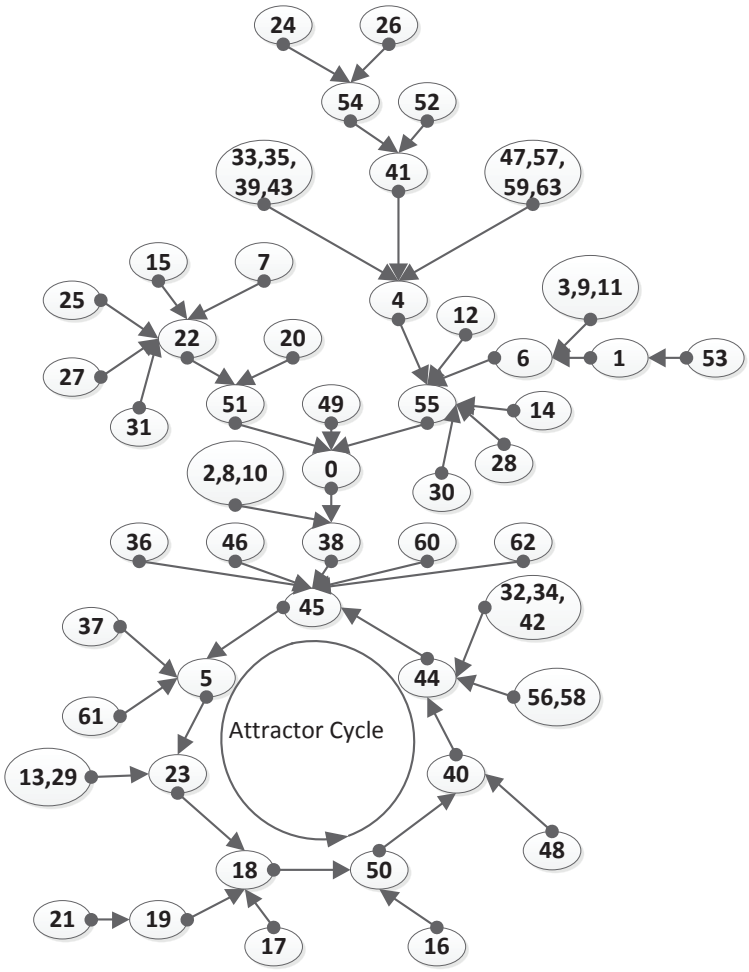

Figure 2.8: The Boolean state transition diagram when the stress input is 1

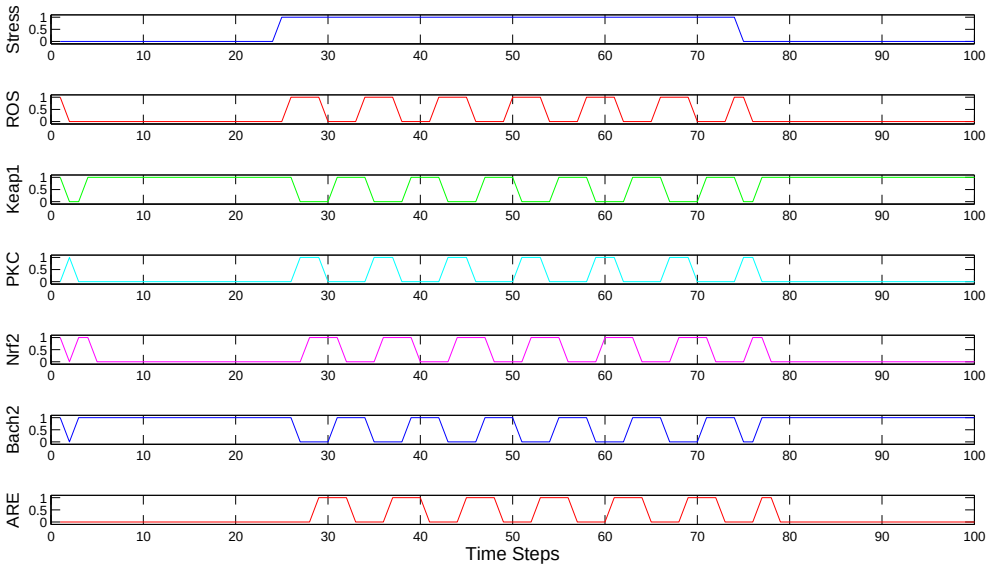

Figure 2.9: Time response behavior of the system in Fig. 2.4

be consistent with experimental observations from the published literature. Note, however, that these experiments consider only two genes/proteins at a time and therefore, there is a need for experimentally studying the simultaneous activities of ROS, $Keap1$, $Nrf2$, PKC, $Bach1$ and ARE in the time domain.

2.5 Mitochondria and Free Radical Generation

Mitochondria play an important role in cellular energy metabolism, free radical generation and apoptosis. It has long been suspected that mitochondrial functions contribute to the development and progression of cancer [29–31]. Over 70 years ago, Otto Warburg proposed that a key event in carcinogenesis is a defect in the respiratory mechanism, leading to increased glycolysis even in the presence of oxygen;this is known as the Warburg effect [32]. The well known function of mitochondria is to generate Adenosine Triphosphate (ATP) molecules providing energy for the survival of the cell through oxidative phosphorylation ($OXPHOS$), which is collectively accomplished by proteins encoded both by nuclear and mitochondrial DNA. Oxidative phosphorylation is a metabolic process, which takes place in mitochondria in which ATP is formed as a result of the transfer of elec-

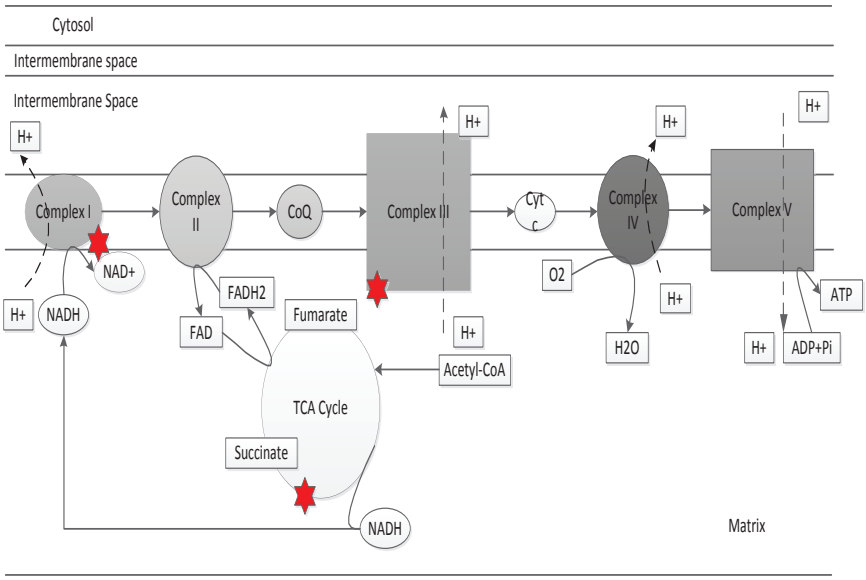

Figure 2.10: Stages of oxidative phosphorylation producing free radicals

trons from $NADH$ or $FADH_2$ to O_2 by a series of electron carriers. $OXPHOS$ is the major source of ATP as well as free radical generation in aerobic organisms. For example, oxidative phosphorylation generates 26 of the 30 molecules of ATP that are formed when a molecule of glucose is completely oxidized to CO_2 and H_2O, although 1 to 2% of the electrons are lost during transfer through the chains leading to free radical generation [33]. Fig. 2.10 [34]shows a schematic representation of the whole process along with free radical generation. The points shown with red stars correspond to the locations where free radicals are generated.

Even though it has been long recognized that increased ROS production in mitochondria leads to genetic instability and progression of cancer, there remain several unanswered questions regarding the complex signaling capacity of this organelle [35]. The DNA is highly susceptible to free radical attacks. Free radicals can break DNA strands or delete bases. These mutations can prove to be carcinogenic. It has been estimated that more than 10,000 hits of oxidative stress occur each day. So it is important to tackle these free radicals at the source of their generation, which is why the mitochondria is also a very

rich source of anti-oxidants. Although cellular mechanisms can tackle this stress, damage accumulates with age. At present altered energy metabolism is considered to be an additional hall mark of cancer progression [36] and these metabolic pathways have been investigated as targets for cancer therapy. In this work, we will specifically focus on the $PI3k/Akt$ pathway which is one such pathway and is described in the following section.

2.6 An Integrated Network for Oxidative Stress Response and Apoptosis

Cancer is an umbrella term for diseases that are associated with loss of cell-cycle control, leading to uncontrolled cell proliferation and/or reduced apoptosis. It is often caused by genetic alterations leading to malfunctioning in the biological pathways [12, 37, 38]. One of the possible cellular responses resulting from oxidative stress is the induction of apoptosis. Thus it is important to develop a network model linking the oxidative stress input to the fate of the cell. In this section, we will do precisely that by considering the oxidative stress response pathways alongside other downstream pathways capable of inducing apoptosis. Specifically, we will focus on the $PI3k/Akt$ pathway. The $PI3k/Akt$ pathway is downstream of the *Ras* gene which is known to play an important role in many cancers. In addition, other genes in the $PI3k/Akt$ pathways are found mutated in many cases of cancer. Oxidative stress often upregulates many of the genes in the $PI3k/Akt$ pathway. The detailed interactions between the oxidative stress response pathway and the $PI3k/Akt$ pathway are shown in Fig. 2.11 [12, 39–41]. Starting with this pathway diagram and utilizing the procedure developed earlier in section 2.4, an equivalent digital circuit in terms of logic gates can be implemented as shown in Fig. 2.12. The above circuit is modeled with two output genes which effectively control the final fate of the cell. *Bad* and *Bcl*2 are known to have pro-apoptotic and anti-apoptotic functions respectively and thus can serve as biomarkers of apoptosis induction. Indeed, it is the delicate balance between the activity of these two genes that dictates the ultimate fate of the cell [42–44]. The pur-

pose of the $Nrf2$-*ARE* pathway in this integrated network is to reduce the average value of *ROS* present in the system, in response to the oxidative stress. This is clear from the plot in Fig. 2.9 : between the time instants from the 25^{th} $timestep$ to the 75^{th} $timestep$ when there is a continuous *Stress* present in the system, the *ROS* present in the system is oscillating between 0 and 1 which implies that its average value is less than '1', which is the value that we would have otherwise had in the absence of the $Nrf2$-*ARE* pathway.

2.7 Classification of Faults in the Integrated Network

In the integrated pathway diagram of Fig. 2.11 , the two genes namely *Bad* and *Bcl*2 are instrumental in deciding the fate of the cell. The preferred status of the two genes, when oxidative stress is not being neutralized, are 1 and 0 respectively since it corresponds to the situation where the pro-apoptotic factor is turned ON and the anti-apoptotic factor is turned OFF. Although a deviation from this state may not signal that the cell is turning cancerous, there is a higher possibility of the cell exhibiting aberrant behavior.

Depending on the final resting status of these two genes, one may be able to characterize the degree of invasiveness of the disease especially if it is being caused by apoptosis suppression. Once it has been determined that a cell is exhibiting aberrant behavior, one would like to pinpoint the location of the fault/error so that the necessary therapeutic intervention(s) can be applied. Since the digital circuit model of Fig. 2.12 uses logic gates, it should be possible to use the fault detection techniques from the Digital Logic literature [45, 46] to pinpoint the fault locations. This will be carried out in this section. An important difference between the results obtained in Layek *et al.* [3] for pinpointing the fault locations in the *MAPKinase* pathways and the results to be presented here is that the digital circuit in Fig. 2.12 involves feedback and its behaviour is, therefore, much more complicated to analyze. However, it should be pointed out that the simpler fault pinpointing methodology presented in Layek *et al*. [3] is much more amenable to biological

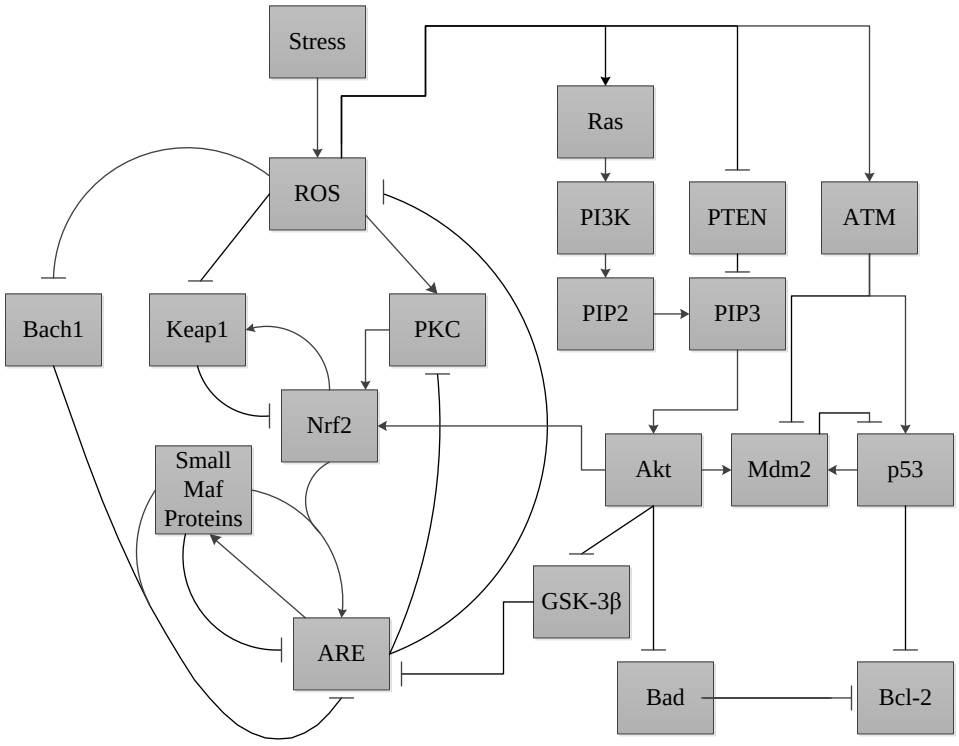

Figure 2.11: Pathway diagram of oxidative stress along with PI3k/Akt

validation via appropriately designed experiments while the same cannot be said about the results to be presented here. Indeed, the results to be presented here show that the pinpointing of the fault locations is theoretically possible even in this case, although the biological feasibility of the methods required is open to question.

We note that the faults in a digital circuit are mainly of two types [45]:

- Stuck-at Faults: As the name implies, this is a fault where a particular line l is stuck at a particular value $\alpha \in \{0,1\}$, denoted by line l,s-a-α (s-a-α means stuck-at-α). This means that the value at that line is always going to be α regardless of the inputs coming in. This can be thought of as something similar to a mutation in a gene, where a particular gene is either permanently turned ON or OFF.

- Bridging Faults : This is the type of fault where new interconnections are introduced among elements of the network. This can be thought of as new pathways being created in the cell. This type of fault is not considered in the current work due to the lack of biological knowledge about new pathways being introduced.

Here, it is appropriate to mention that the biological relevance of each of these two types of faults has been discussed in Layek *et al*. [3].

The digital circuit in Fig. 2.12 has feedback (shown in bold lines) and is, therefore, a sequential circuit. To detect a fault in a sequential circuit we need a test sequence. Let T be a test sequence and let $R(q,T)$ be the response of the fault-free sequential system N starting in the intial state q. Now let the faulty sequential circuit be denoted by N_f where f is the fault. Let us denote by $R_f(q_f,T)$ the response of N_f to T starting in the intial state q_f. A test sequence T detects a fault f iff (if and only if or equivalently this condition is both necessary and sufficient) for every possible pair of intial states q and q_f, the output sequences $R(q,T)$ and $R_f(q_f,T)$ are different for some specified vector $t_i \in T$. The output being observed is the status of $[Bad, Bcl2]$.

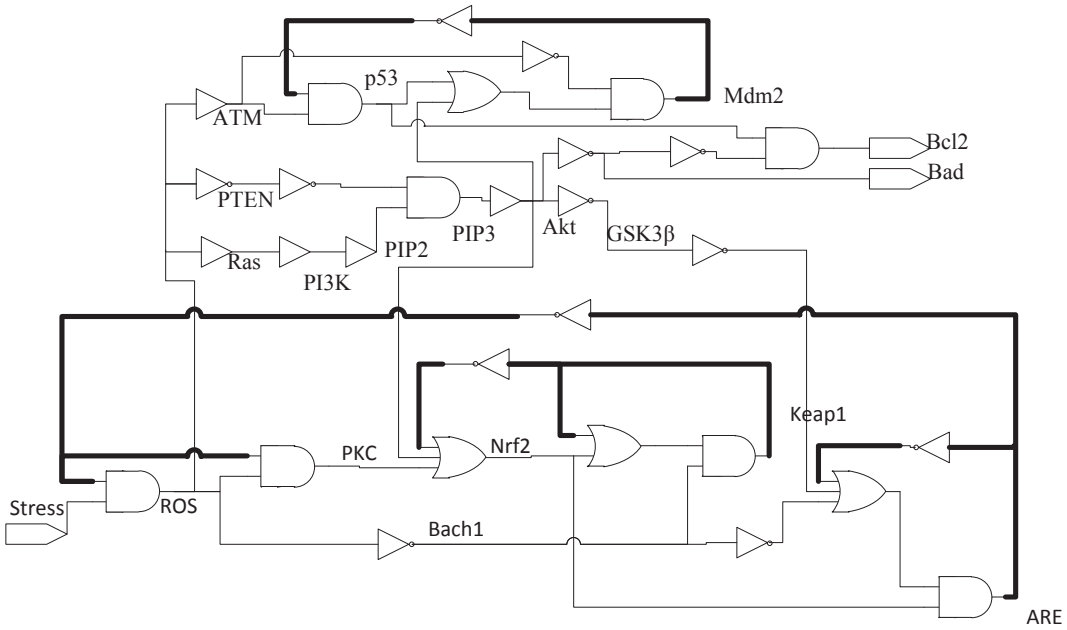

Figure 2.12: Boolean network modeling of Fig. 2.11

Once this output shows a deviation from a desired value, it becomes imperative to pinpoint the possible fault locations which can give rise to the aberrant behaviour. To do so, one can represent the digital circuit of Fig. 2.12 as in Fig. 2.13. The Primary Input(PI) is *Stress* which is the only external signal which the experimenter has control over. The Primary Output's (PO's) are the status of *Bad* and *Bcl*2, which are the only outputs available to the experimenter. The Secondary Output's and Secondary Input's are $[ARE, Keap1, Mdm2]$, which are being fed back into the system. The states of these 3 genes ARE, $Keap1$ and $Mdm2$ determine the internal state of the system. These 3 elements can be considered as memory elements of the system as their previous state is retained by the system and fed back. The input sequence consists of two parts namely a Homing sequence and a Test sequence, denoted by H and T respectively.

The purpose of this procedure is to pinpoint the possible locations for the fault f in N_f, given the output sequence of *Bad* and *Bcl*2 for the normal and faulty circuits. It is assumed that we have no knowledge about the initial status of any of the genes. Knowledge of the

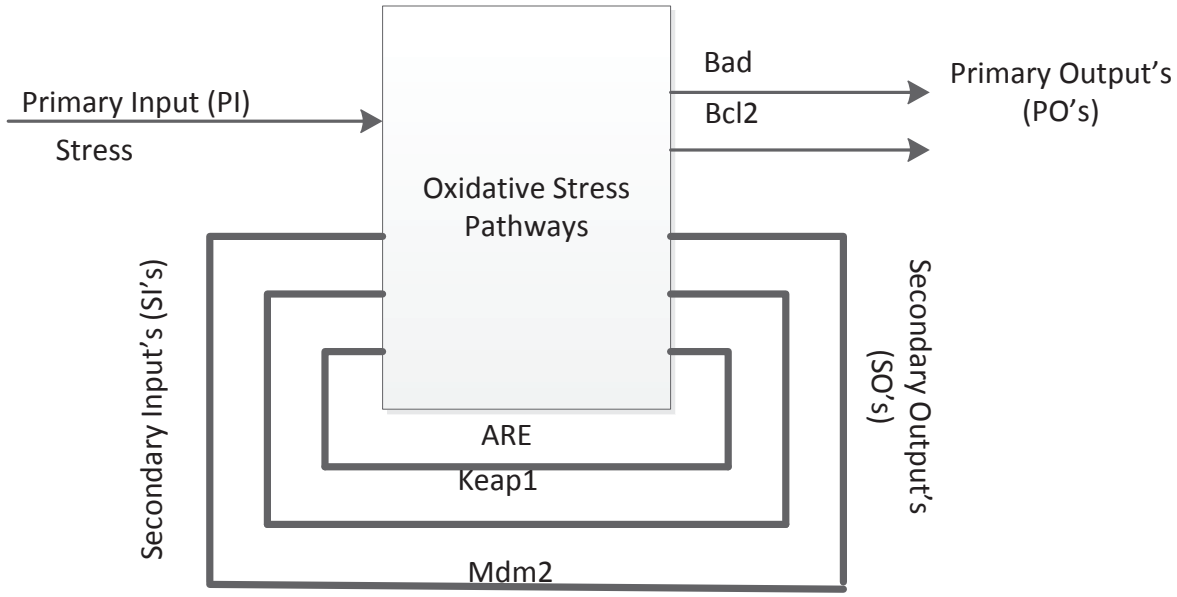

Figure 2.13: Block diagram representation of Fig. 2.12

initial status of the internal states is important as all future computations are based on these values. The Homing sequence is an initial input sequence that brings the network to a known internal state. So, once the Homing Sequence is given to N and N_f, N will come to a known internal state. Note that a similar claim cannot be made about N_f as the fault f is not known apriori. For the circuit in Fig. 2.12 , a possible Homing sequence is [0 0 0 0 0 0 0 0], which brings the internal state of the system to [0 1 0]. This means that if the *Stress* input is zero for eight time steps, then at the end of that period, the internal state of the system becomes [0 1 0], regardless of the initial status of any of the genes in the network. A reason for choosing this Homing sequence is that it implies that no input needs to be given to the system and it evolves to the indicated internal state. In future when we are trying to validate these results experimentally this will be of immense help. If we refer back to Fig. 2.7, we see that regardless of the intial state, within four time steps the trajectory reaches the state ('010010') where ARE=0 and $Keap1$=1. This is consistent with the conclusion that we are getting from the Homing sequence here with the only

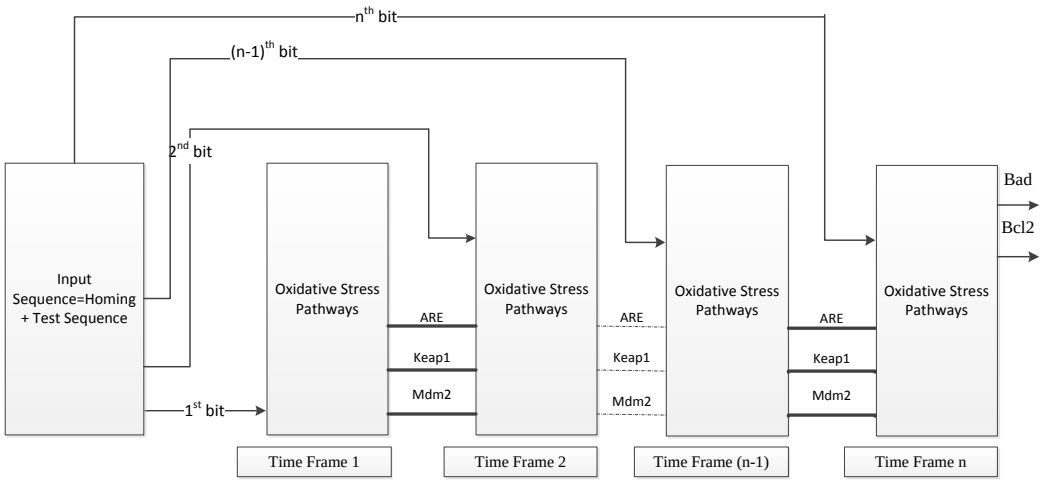

Figure 2.14: Fault detection using time-frame expansion

difference that a slightly longer sequence is required here as the state transition diagram has a higher cardinality than that in Fig. 2.7.

Once the Homing sequence has done its job, the Test sequence(T) is fed into N and N_f, and by comparing the output states of the normal and faulty networks, we can pinpoint the location of the fault in the network, assuming that a single stuck-at-fault has occurred. This can be carried out using the *time-frame expansion method* which is briefly discussed next. The block in Fig. 2.13 is replicated n times with the feedback loops cut-off. The Secondary Output of the k^{th} stage is fed as the Secondary Input for the $(k+1)^{th}$ stage. The Primary Outputs of the first $(n-1)$ stages are neglected. The Primary Outputs of the n^{th} stage of the normal and faulty circuits will be different as the network configurations are different for both. The Primary Input sequence has to be derived so that the error in a line is propagated to the primary output in n time steps, so that a difference is observed at the primary outputs of the normal and faulty circuits [45, 46]. The situation is pictorially represented in Fig. 2.14. Please refer to Appendix A for a simple example that explains the method.

Test Sequence	Faults Detected	
	s-a-0	s-a-1
10100000	Ras, PI3K, PIP2, PIP3, Akt, Keap1	PIP3, Akt, Ras, PI3K, PIP2, PTEN, ARE, PKC, ATM, p53
110101000	PTEN, Nrf2, ATM, Bach1, GSK-3β, p53	Mdm2
101111100	Nrf2, ARE	Bach1, Keap1
11010010101000	Mdm2	
11110001010000		GSK-3β
Undetectable	PKC	

Figure 2.15: Test sequences for detecting single stuck-at-faults.

From the preceding discussion in this section, we know that there are 15 possible genes (this is the total number of genes in Fig. 2.11 , excluding the output genes *Bad* and *Bcl*2) where there could be a mutation. This means that there are 30 cases of faults as a single gene can be mutated as a *s-a*-0 or as a *s-a*-1. We consider all possible cases of single mutation, because in the presence of mutation, the normal and faulty system cannot produce the same output unless, of course, the mutated gene is not a critical one. Based on the methods described earlier in this section, we came up with a list of test sequences for the detection of each gene fault. It is to be noted that the Test Sequences generated here are only for the Homing Sequence considered earlier. For a different Homing Sequence the Test Sequence will also be different. The different test sequences and their ability to detect different single stuck-at faults are tabulated in Fig. 2.15. Here, truncated versions of the same test sequence can be used to detect different faults appearing in the same row. For detecting any particular fault, one would apply the test sequence from the same row truncated at the bit whose color matches that of the particular fault. The mismatch between the outputs of the normal and faulty systems, characterized by the vector $[Bad, Bcl2]$ would then result in the detection of that fault. Thus we have developed a method to pinpoint the possible fault locations in a Boolean network with feedback. The algorithm will work with multiple fault cases too with minor modifications.

2.8 Concluding Remarks

In this section, we have developed a Boolean network model for the oxidative stress response. This model was developed based on pathway information from the current literature pertaining to oxidative stress. Where applicable, the behaviour predicted by the model is in agreement with experimental observations from the published literature. It is our hope that some of the additional predictions here, such as those pertaining to the oscillatory behaviour of certain genes in the presence of oxidative stress, will be experimentally validated in the near future.

We have also linked the oxidative stress response to the phenomenon of apoptosis via the $PI3k/Akt$ pathway. An integrated model based on collectively considering the $PI3k/Akt$ pathways and the oxidative stress response pathways was developed and then used to pinpoint possible fault locations based on the *Bad*-*Bcl*2 apoptotic signatures in response to 'test' oxidative stress inputs. The approach used to achieve this differs significantly from the earlier results in Layek *et al*. [3] since the Boolean network considered here has feedback. The approaches used here and in Layek *et al*. [3] could potentially have a significant effect on cancer therapy in the future as pinpointing the possible fault location(s) in cancer could permit the choice of the appropriate combination of drugs (such as kinase inhibitors) for maximum therapeutic effectiveness. Of course, it should be pointed out that the theoretical procedure presented here for pinpointing fault locations in a biological network with feedback will need to be further simplified before it can be even considered for practical biological validation.

3. HYPOXIA STRESS RESPONSE PATHWAYS *

3.1 Introduction

In this work, we develop a Boolean network model consistent with hypoxia stress response pathway information from the biological literature. After this we consider the major pathways involved in a hypoxic cell and consider targeted therapy in these pathways to upregulate the average apoptotic activity and downregulate both the average cell-survival activity and average energy production through fermentation. Misregulation of each of these activities characterizes the difference between a normal cell and cancer cell. The basic underlying principles of modeling of this work is similar to the ideas used in modeling the oxidative stress response pathways.

3.2 Hypoxia

Hypoxia is a condition in which there is an inadequate supply of oxygen to the tissues of the body. If the oxygen entering inside a cell is not matching the oxygen demand of the same cell, a hypoxic condition is created. Oxygen is rapidly taken up from the blood into the tissues at the level of microcirculation, particularly from the capillaries. Oxygen being highly lipid soluble, it passes through cell membranes. This rate of oxygen diffusion is determined primarily by the PO_2 (partial pressure of oxygen) , the pressure difference between the plasma and cells surrounding the capillaries. The value of PO_2 values is different among different capillaries, however the typical value ranges from 30-40 mmHg. Since cells consume oxygen the PO_2 inside cells is very low. This value drops to less than 1mm Hg (mercury) pressure inside the mitochondria where oxygen is used to generate energy. With increased oxidative metabolism in a tissue, the mitochondria needs to make

*This section is reprinted with permission from " Hypoxia Stress Response Pathways: Modeling and Targeted Therapy" by S Sridharan, R Varghese, A Datta and J Venkatraj, accepted for publication in *BMC Genomics*

more ATP and hence consume more oxygen. Though PO_2 pressure difference drives the diffusion process, an important factor in this is oxygen bound to haemoglobin. As and when oxygen from plasma diffuses to the cells, the PO_2 of plasma drops and this causes oxygen bound to haemoglobin to become free. Therefore, the amount of oxygen bound to hemoglobin is a major factor in determining oxygen delivery to a tissue. Hypoxic stress is caused when the amount of oxygen available in a cell is insufficient to meet the energy demands of that cell. In a living cell, this imbalance between oxygen supply and energy demand arises due to physiological and pathophysiological processes [13]. A cell faces hypoxic stress due to normal physiological variations during fetal development, wound healing, adapting to a high altitude, inflammation etc. [47]. In a developing embryo, hypoxic stress is due to reduced oxygen supply, whereas while doing vigorous exercise, a hypoxic condition is created in the exercising muscles due to an increased demand of energy [48]. The optimum oxygen tension for tubulogenesis, vasculogenesis and angiogenesis in an embryo of a mammal is about 23-38 mm Hg [47]. Different cells in the body have different partial pressures of oxygen that are considered to be normal and a drop in the partial pressure of oxygen below these normal levels, creates a hypoxic condition. The difference of the partial pressures of oxygen between the blood and the mitochondria of the cells is responsible for the transfer of oxygen between blood and all the cells in the body. Hypoxia detection in human beings is carried out by the most vascular tissue in the human body, the carotid body, which is located near the bifurcation of the carotid artery. The partial pressures of inhaled air, arterial blood and venous blood are 150 mm Hg, 100 mm Hg and 40 mm Hg respectively. The carotid body detects the gradient of the partial pressure of oxygen of the arterial blood that flows through the carotid body. The intracellular PO_2 is regularly measured by three hydroxylases. These hydroxylases are named as prolyl hydroxylase domain containing proteins (PHD), namely PHD1, PHD2, and PHD3 [47]. Almost 95% of the oxygen that we breathe in is used up by the reactions of the Electron

Transport Chain (ETC), catalyzed by cytochrome oxidase, to produce energy. A proton gradient is created across the innermost mitochondrial membrane as a result of some redox reactions taking place in the mitochondrial ETC, due to the transfer of electrons from an electron donor to the terminal electron acceptor, oxygen. This proton gradient is used to phosphorylate ADP to form ATP in the presence of ATP synthase. The inhaled air, which has a partial pressure of 150 mm Hg, passes into the alveoli which are the small air sacs located inside the lungs. Oxygen mixes with the water vapor and carbon dioxide (external respiration) and then enters into the arterial blood. Arterial blood carries oxygen to the mitochondria in each and every cell of the body, where it extracts hydrogen from the food to react with oxygen to produce water vapor. Carbon dioxide produced in the mitochondria enters into the venous blood and is expelled from the lungs. The normal partial pressure of oxygen in the arterial blood is 100 mm Hg, and when it falls to 40 mm Hg, it is very dangerous [49]. Oxygen consumption is thus coupled to release of energy in the form of ATP, which is essential for the proper functioning of the cell. Hence, low oxygen tension should be identified and proper adaptation measures should be taken by the cell for survival. To harvest energy from food and to maintain the proper tissue function, an adaptive response must be incorporated to overcome the scarcity of oxygen. The transcription factor HIF (Hypoxia Inducible Factor) has a prominent role in the regulation of gene expression levels by oxygen. HIF achieves this response by regulating the transcription of thousands of hypoxia responsive genes. The interaction of HIF was identified for the first time in erythropoietin (EPO) gene which is involved in angiogenesis [47].

3.3 Hypoxia Stress Response and Pathways: Hypoxia Inducible Factor (HIF) and its Regulation

Hypoxia Inducible Factor (HIF) is a heterodimer comprising of α and β subunits. HIFα consists of 3 subunits, HIF-1α, HIF-2α and HIF-3α.The HIFβ subunit consists of

ARNT which is the aryl hydrocarbon nuclear translocator and ARNT2. HIF-1 transcription factor consists of HIF-1α and HIF-1β (ARNT) [50]. The concentration of oxygen in the cells regulates the HIF-1α subunit, but the HIF-1β subunit is unaffected by the oxygen levels. HIF-1α quickly stabilizes and is accumulated under hypoxic conditions by the inhibition of PHD2, but on re-oxygenation, it is suddenly destroyed and its half-life is less than 5 minutes [51]. This short half-life shows that HIF-1α accumulation is not good for the body. In fact, prolonged hypoxia is observed in most of the tumors. HIF-1α also undergoes hydroxylation of the amino acid proline located in its oxygen dependent degradation (ODD) domain by PHD2. HIF-1α undergoes hydroxylation of the asparagine 803 residue located in the C terminal activation domain (CTAD) by FIH (factor inhibiting HIF) [52]. The hydroxylation of HIF-1α by PHD2 increases its interaction with the tumor suppressor protein, pVHL, the von-Hippel Lindau tumor suppressor protein which marks HIF-1α for degradation with the help of E3 ubiquitin ligase. PHD2 hydroxylates HIF-1α and that creates a binding site for pVHL [53]. Again, the hydroxylation of HIF-1α by FIH reduces the transcriptional activity of HIF-1α by preventing the binding of coactivators p300/CBP to HIF-1α [54]. The hydroxylation of HIF-1α by FIH results in p300/CBP independent transcription of HIF-1α. PHD and FIH require oxygen, iron, α-ketoglutarate (αKG) and ascorbate as substrates to function properly. Oxygen and αKG are the co-substrates required for PHD2 functioning whereas, ascorbate and Fe^{2+} (iron) are the cofactors required for PHD2 functioning. PHD2 hydroxylates HIF-1α and simultaneously PHD2 decarboxylates αKG to succinate. αKG is an anion of α-ketoglutaric acid which is produced by the deamination of glutamate (an intermediate of the citric acid cycle) [55]. During hypoxia, the substrate oxygen required for PHD functioning is not available and hence PHD is inhibited. This results in the activation and stabilization of HIF-1α subunit which enters into the nucleus and binds with HIF-1β subunit to form the HIF heterodimer [53, 54], which is a transcription factor. This HIF transcription factor

binds to the Hypoxia Responsive Elements (HRE) of the target genes and this interaction drives the transcription in a hypoxia responsive manner, up regulating the genes involved in angiogenesis (EPO), vasculogenesis (VEGF), glycolysis (GLUT1, PDK1, LDHA), etc.

The Electron Transport Chain (ETC) directs the electron transport between the electron donors NADH (nicotinamide adenine dinucleotide) and FADH2 (flavin adenine dinucleotide) and the terminal electron acceptor oxygen. ETC takes place inside the mitochondria where O_2 is reduced to H_2O, NADH is oxidized to NAD^+ and succinate in the presence of the SDH (succinate dehydrogenase) enzyme is converted to fumarate. The proton gradient generated across the mitochindrial membrane, pumps protons inside the mitochondrial space which converts ADP (adenosine di phosphate) to ATP (adenosine tri phosphateuses) using the enzyme ATP Synthase. This whole process is what is referred to as oxidative phosphorylation. Some of the electrons will not be transferred from the electron donor through the complexes I-IV to the terminal electron acceptor, and there may be premature electron leakage through complexes I and III forming reactive oxygen species (ROS) such as superoxide that creates oxidative stress [56]. During hypoxia, the ETC is inhibited since there is not enough oxygen available, which generates even more ROS thereby creating an oxidative stress [57]. This oxidative stress does not allow iron to cycle between the different oxidation states which results in PHD inhibition since iron is one of the cofactors required for PHD to function properly. PHD inhibition results in the accumulation and stabilization of HIF-1α which results in the induction of anti-apoptotic as well as apoptotic genes depending on the extent of hypoxia [58]. Activation of the transcription factor HIF-1α results in a shift from aerobic metabolism to anaerobic metabolism. Pyruvate kinase is a glycolytic enzyme that converts PEP (phosphoenolpyruvate) to pyruvate. PK-M2 (pyruvate kinase muscle isozyme 2) is one of the isozymes of pyruvate kinase [59]. PHD3 hydrolyzes PK-M2 on proline-403/408, and the hydrolyzed PK-M2 interacts directly with HIF-1α subunit which enhances the binding of HIF-1 to

the HRE of the target genes. But, PKM2 itself is a hypoxia target gene since a hypoxia responsive element (HRE) was observed in the intron 1 of PK-M2 [60]. PK-M2 promotes the Warburg effect [61,62]. PK-M2 is identified in almost all the cancer cells and is essential for rapidly dividing cells since quicker energy harvesting is possible by shifting from aerobic to anaerobic metabolism [63]. PDK1 (pyruvate dehydrogenase kinase 1) is also a HIF-1 target gene. PDK1, which is a hypoxia target gene, inhibits the action of the enzyme PDH (pyruvate dehydrogenase) which converts pyruvate to AcCoA (acetyl-co enzyme A). Hence, pyruvate is unable to enter into the citric acid cycle and is trapped in the cytosol and the rate of glycolysis is increased. This explains the Warburg effect and the relationship between prolonged glycolysis and HIF-1 activation. So, in effect PK-M2 catalyzes the conversion of PEP to pyruvate and PHD3 hydrolyzes PK-M2 and the hydrolyzed PK-M2 enters the nucleus and interacts with HIF-1α subunit and enhances the binding of HIF-1 to the hypoxia responsive elements of the target genes. But, PK-M2 and PHD3 are hypoxia target genes. Moreover, PDK does not allow pyruvate to enter into the citric acid cycle and traps pyruvate in the cytosol. Pyruvate inhibits PHD which stabilizes HIF-1α, but PDK1 itself is a HIF-1 target gene. Most of the glycolytic enzymes like GLUT1, LDHA, ALDA etc. are the hypoxia target genes and this explains the feed forward mechanism for HIF-1α activation and increased rate of glycolysis. PHD2 hydrolyzes HIF-1α and the hydrolyzed HIF-1α is degraded by the VHL tumor suppressor protein. But, PHD2 itself is a hypoxia target gene [64]. This feed-back inhibition acts a regulative control for hypoxic response when normoxia is re-established. Thus, HIF-1:PHD2 linked transcription sets up the appropriate HIF-1 signaling to face the hypoxic stress effectively.

3.4 Stress Response Pathways

In biology, almost all the knowledge and information is usually available as signaling pathways. This information is unable to represent the multivariate interactions between the

genes, even though it can give a pictorial representation of the univariate interactions. It is also possible that two or more pathways can share the same genes or the same node. Thus, a biological pathway gives a clear cut idea of the marginal relationship between different genes in that pathway, but fails to provide information about how these genes interact globally when they are present in different pathways. The main aim of this work is to generate a Boolean network whose state transitions realize the hypoxic stress response pathways. The resulting Boolean network obtained shows dynamic behavior which is consistent with the experimental results and observations from published literature [13, 65]. By incorporating the expert knowledge obtained from the biological pathways, the cardinality of the search space of the network can be reduced. The main drawback of the pathway knowledge is that it provides only partial information and that too restricted to a specific context. By mathematically modeling the multivariate interaction between the genes in a pathway, these networks can be used to differentiate between normal cell behavior and diseased cell behavior. By working with the genetic regulatory networks instead of the biological pathways, the holistic behavior of the genes can be captured and the appropriate therapeutic interventions can be developed. The aim of biological pathway modeling is to marginally capture the causal interactions taking place inside a cell when a stimulus or stress is applied. Stress response pathways constitute an important set of pathways studied in the biological literature. The main aim of adaptive stress response pathways is to understand the transcription of cytoprotective genes in the presence of stress [16]. If a stress is applied to a cell exogenously such as xenobiotic, radiation, heat etc. the cell responds via several highly conserved adaptive stress response pathways that will try to attenuate the consequences of this stress and re-establish the homeostasis. The rapid response of the stress response pathways can be attributed to their special architecture. Basic components of this architecture include a transcription factor, a sensor and a transducer. A schematic diagram of the architecture of the stress response pathways is shown below [65] in Fig. 3.1.

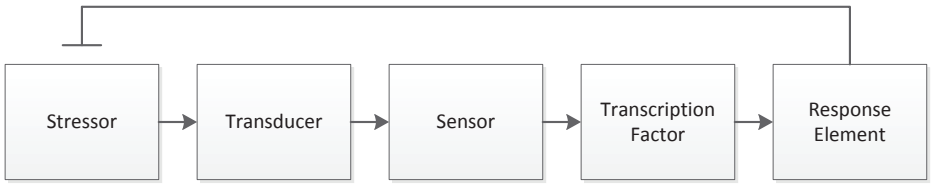

Figure 3.1: General scheme of stress response pathways

A transcription factor is a protein which binds to the DNA through the response elements within its promoter region and thus activates or upregulates the expression of the target genes. During the absence of stress, the transcription factor is prevented from entering into the nucleus with the help of a protein known as a sensor. It interacts with the transcription factor in such a way that the transcription factor is sequestered in the cytoplasm. When a cell is faced by a stress, an enzymatic protein, transducer, transfers a cue from a pathway which lies upstream of the sensor/transcription factor complex. The transducer either modifies the transcription factor or modifies the sensor which destabilizes the sensor/transcription factor complex. The activated transcription factor then enters the nucleus and is able to upregulate the target genes.

3.5 Boolean Network Modeling

Given two genes/proteins A and B and binary values $a,b \in \{0,1\}$, we define the term *pathway segment* $A \xrightarrow{t:a,b} B$ to mean that if gene/protein A assumes the value $'a'$ then gene/protein B transitions to $'b'$ in no more than t subsequent time steps. A *pathway* is defined to be a sequence of pathway segments of the form $A \xrightarrow{t_1:a,b} B \xrightarrow{t_2:b,c} C$. A *Boolean Network* (*BN*), $\Upsilon = (V,F)$, on n genes is defined by a set of nodes/genes $V = \{x_1,...,x_n\}$, $x_i \in \{0,1\}$, $i = 1,...,n$, and a list $F = (f_1,...,f_n)$, of Boolean functions, $f_i : \{0,1\}^n \to \{0,1\}$, $i = 1,...,n$. The expression of each gene is quantized to two levels, and each node x_i represents the state/expression of the gene i, where $x_i = 0$ means that gene i is OFF and $x_i = 1$ means that gene i is ON. The function f_i is called the *predictor function* for gene i. Updat-

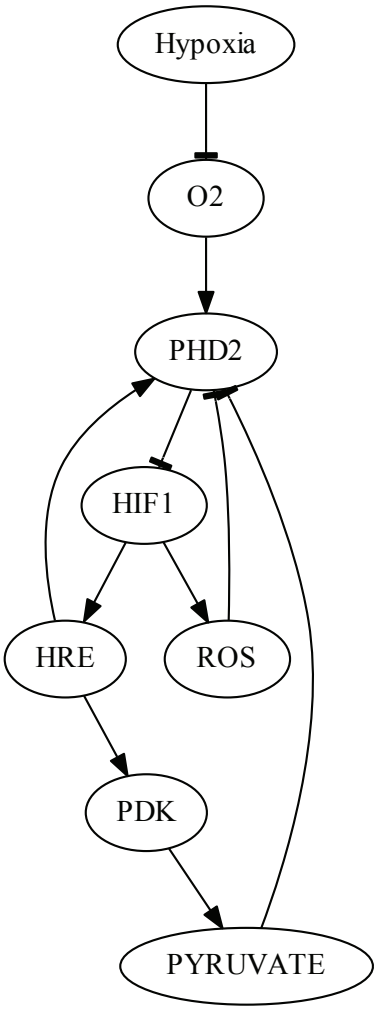

Figure 3.2: Hypoxia stress response pathways

ing the states of all genes in Υ is done synchronously at every time step according to their predictor functions. At time t, the network state is given by $x(t) = (x_1(t), x_2(t), ..., x_n(t))$, which is also called the *gene activity profile* (*GAP*) of the network. The prior biological knowledge of the hypoxia stress response pathways is used to arrive at the Boolean network describing hypoxia stress response activity. The Karnaugh map (K-map) reduction technique is used to obtain an update equation for each and every node [13, 65]. The hypoxia stress response pathways is shown below in Fig. 3.2.

The pathway segments from the pathways in Fig. 3.2 are given by:

$$Hypoxia \xrightarrow{1:1,0} O_2 \tag{3.1}$$

$$O_2 \xrightarrow{1:1,1} PHD2 \tag{3.2}$$

$$PHD2 \xrightarrow{1:a,\bar{a}} HIF1 \tag{3.3}$$

$$HIF1 \xrightarrow{1:1,1} HRE \tag{3.4}$$

$$HRE \xrightarrow{1:1,1} PDK \tag{3.5}$$

$$HRE \xrightarrow{1:1,1} PHD2 \tag{3.6}$$

$$PDK \xrightarrow{1:1,1} PYRUVATE \tag{3.7}$$

$$PYRUVATE \xrightarrow{1:1,0} PHD2 \tag{3.8}$$

$$HIF1 \xrightarrow{1:1,1} ROS \tag{3.9}$$

$$ROS \xrightarrow{1:1,0} PHD2 \tag{3.10}$$

From the above described pathway segments, and applying the technique of K-map reduction explained [13], the update equation for each and every gene is obtained. The state space is defined as [PHD2,HIF,HRE,ROS,PDK,PYRUVATE]. This resulted in a set of possible Boolean networks, out of which the one that matched the most to the prior literature knowledge was chosen. The update equations are given below. From the set of possible Boolean networks we chose the ones that appealed most to our biological understanding and the resulting update equations are given below:

$$O_{2next} = \overline{Hypoxia}, \tag{3.11}$$

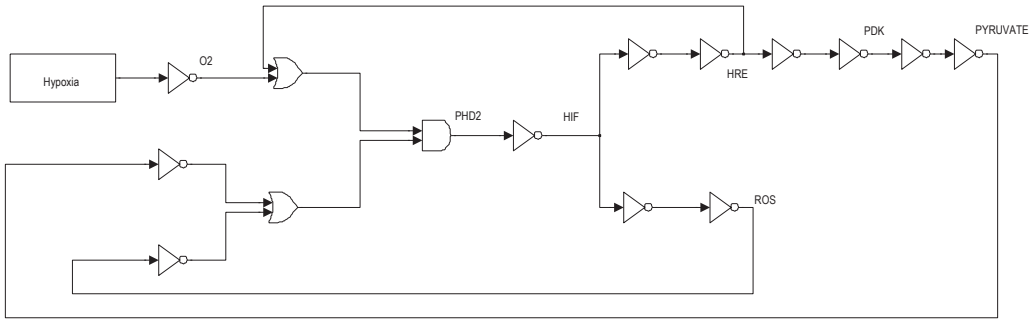

Figure 3.3: Digital equivalent of hypoxia stress response pathways

$$PHD2_{next} = (\overline{PYRUVATE} + \overline{ROS}) \cdot (O_2 + HRE), \tag{3.12}$$

$$HIF_{next} = \overline{PHD2}, \tag{3.13}$$

$$HRE_{next} = HIF, \tag{3.14}$$

$$ROS_{next} = HIF, \tag{3.15}$$

$$PDK_{next} = HRE, \tag{3.16}$$

$$PYRUVATE_{next} = PDK. \tag{3.17}$$

This Boolean network will have two different contexts based on the value of the hypoxic stress, i.e., when Hypoxia=0 and when Hypoxia=1. The resulting equations are expressed as a digital circuit and shown in Fig. 3.3 The state transition diagrams resulting from the above equations for the two cases, Hypoxia=0 and Hypoxia=1, are shown in Figs. 3.4 and 3.5 respectively.

In these transition diagrams, the genes in the binary state representation are ordered as [PHD2, HIF, HRE, ROS, PDK, PYRUVATE] and the binary states are compactly represented by their decimal equivalents. For instance, the binary state (111100) would be represented by the decimal number 60. The states of particular interest are the attractors as they give rise to the steady-state properties of the network. In Fig. 4, the state

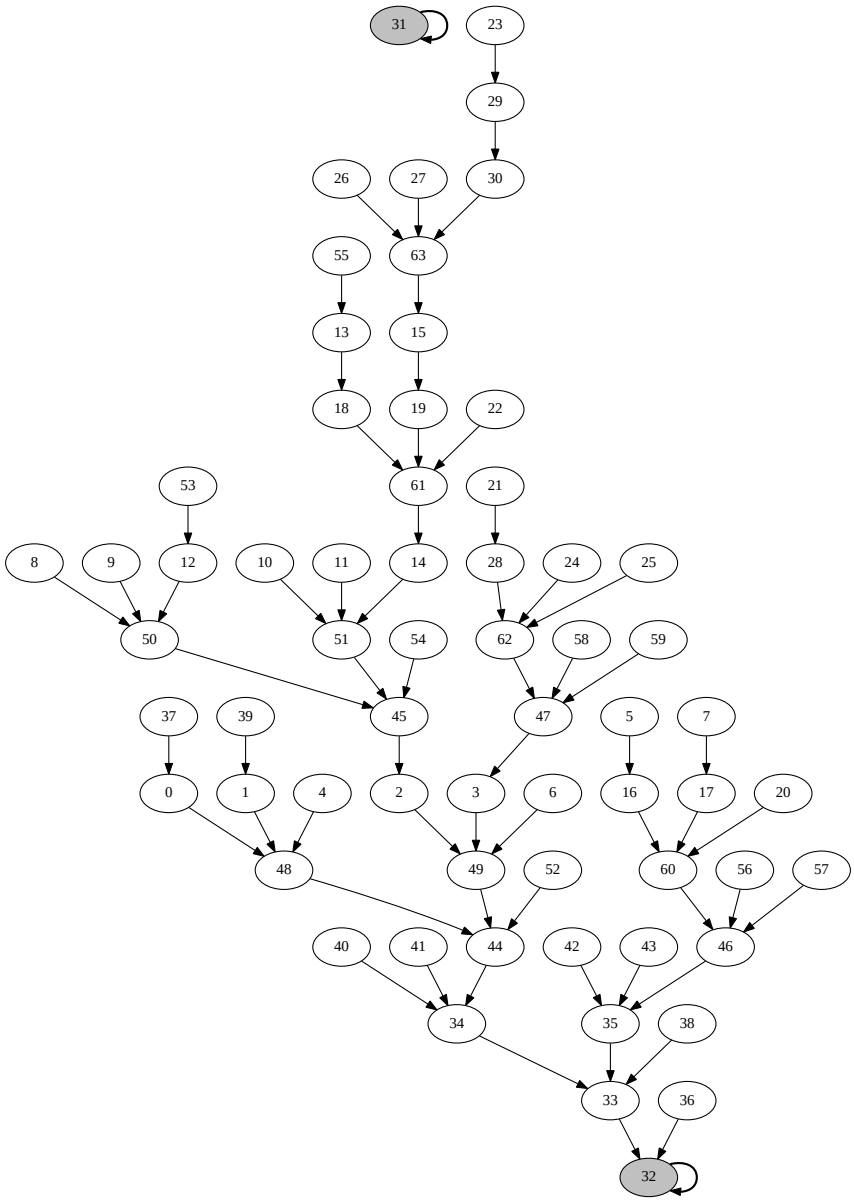

Figure 3.4: State transition diagram with hypoxia=0

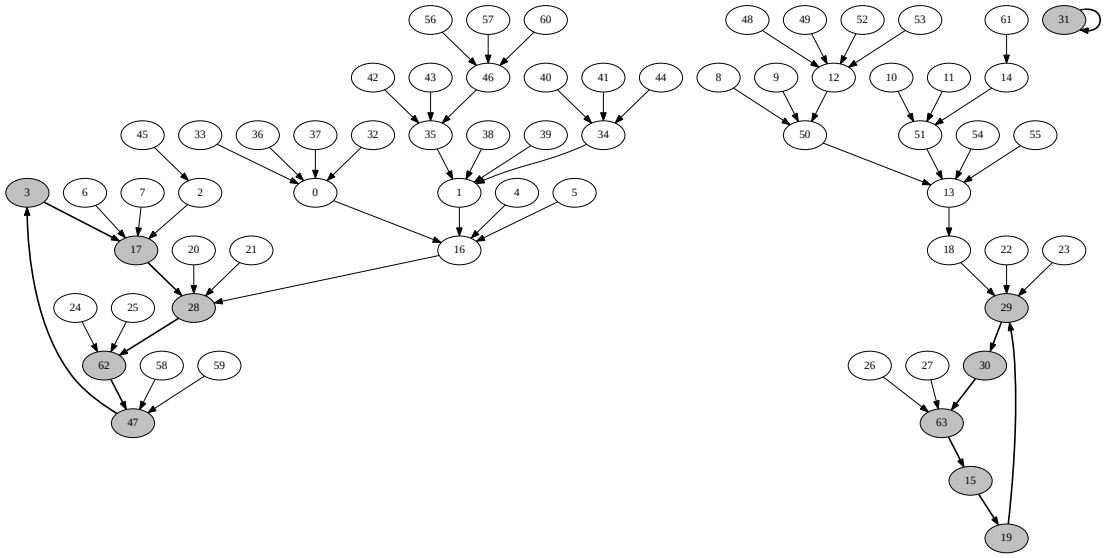

Figure 3.5: State transition diagram with hypoxia=1

of interest is the singleton attractor 32(100000). On the other hand, in Fig. 5, the state space is partitioned. Hence the final attractor cycle will depend on the starting state, one of them cycling through $47 -> 3 -> 17 -> 28 -> 62 -> 47$ and other through $63 -> 15 -> 19 -> 29 -> 30 -> 63$. This would lead to cyclical/oscillatory behavior in the time domain response when Hypoxia = 1. There is a singleton attractor, 31(011111) in both cases of Hypoxia = 0 and Hypoxia = 1 which is not biologically feasible. Spurious attractors of this type do arise in Boolean network modeling. When such networks are derived from pathway information, the ill-posed nature of the inverse problem makes the appearance of spurious attractors even more likely. The equations derived were simulated using MATLAB by giving an external stress input signal for a duration of 100 timesteps, and both the input signal and the responses are shown in Figs. 3.6 and 3.7. From the plot in Fig. 3.7, one can reasonably expect to see oscillations in the presence of hypoxic stress similar to the p53-MDM2 oscillations induced by DNA damage. It would be interesting to experimentally verify if this is indeed the case. In Fig. 3.7, the two time response corresponds to the two steady-state attractor cycles.

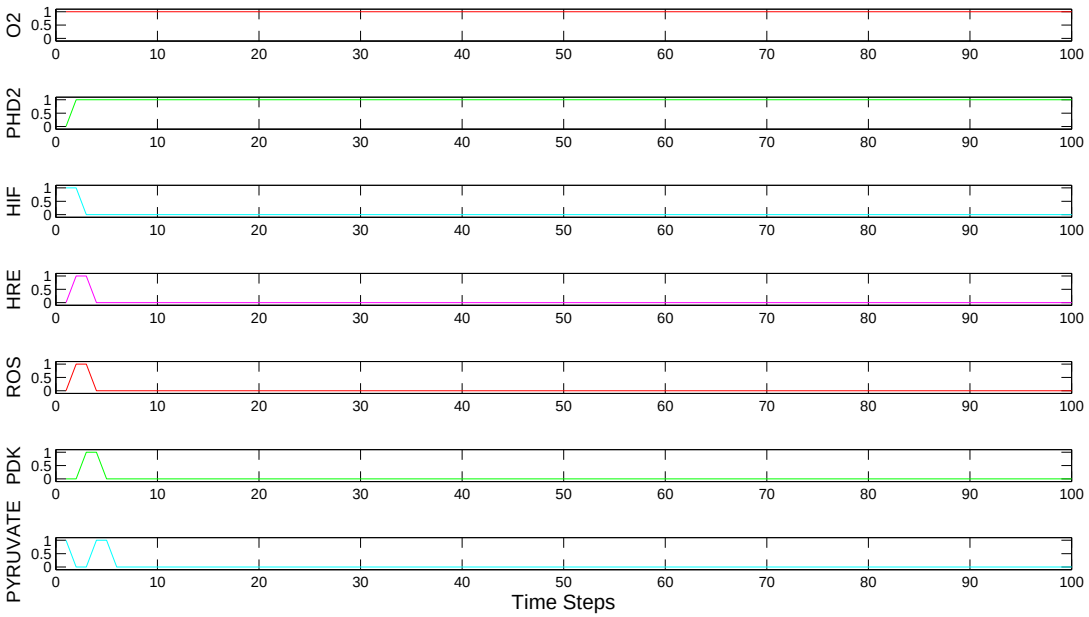

Figure 3.6: Time response behavior when hypoxia=0

3.6 Targeting Hypoxia in Cancer Therapy

Hypoxia is a feature of most solid tumors. It is known to promote malignant progression, metastatic capacity, resistance to chemotherapy and leads to poor patient prognosis. In normal tissues, the oxygen supply will depend on the metabolic requirements [66]. However in tumors the oxygen requirement is way higher than the supply and this leads to some areas in the tissue where there is inadequate oxygen. Increased levels of hypoxia are consistently correlated with genetic instability, tumor progression and poor patient prognosis [67]. Hypoxia is a very prominent characteristic displayed by solid tumors, since rapidly dividing aggressive solid tumor development and progression demands a lot of energy. This energy demand makes oxygen become a limiting factor. As the tumor grows to about 2-3 mm in diameter, the normal oxygen supply is unable to meet the increased energy demand of cancer tissues. Tumor cells that are beyond the diffusion distance for oxygen ($>70\mu$m) are exposed to low levels of oxygen. The cells adapt to this scarcity of oxygen, by creating new blood vessels from the already existing blood vessels (tumor an-

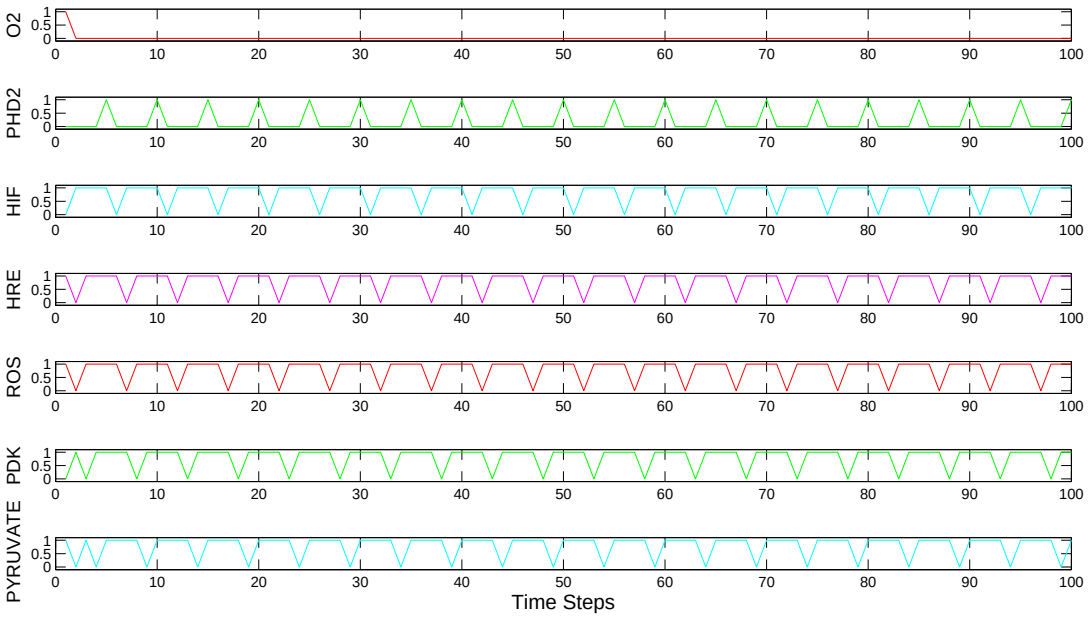

(a)

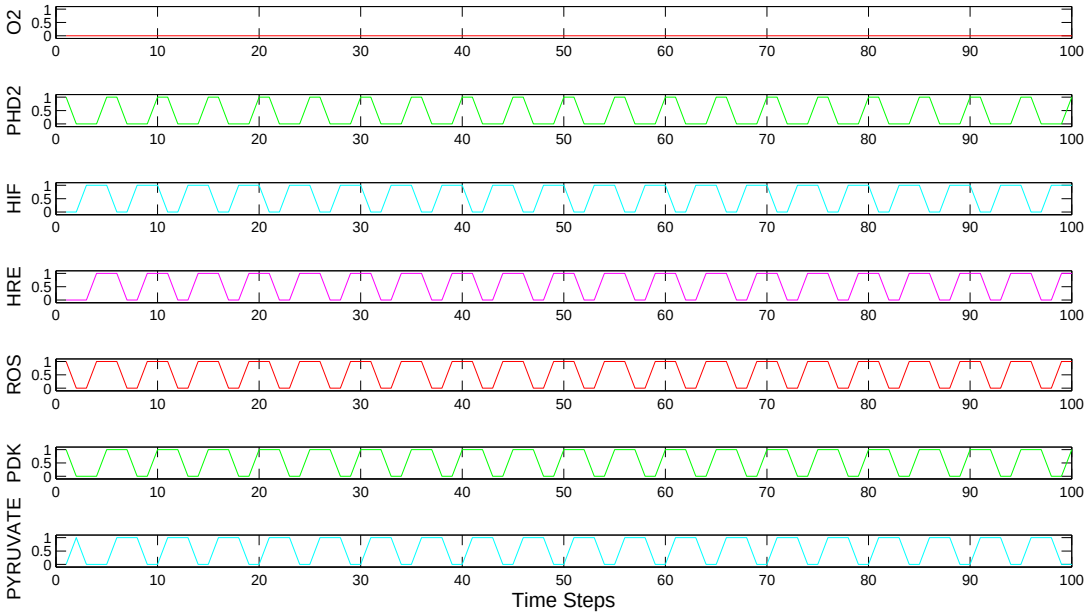

(b)

Figure 3.7: Time response behavior when hypoxia=1

giogenesis) and also by increasing the glycolytic flux for easy and faster anaerobic energy production. Moreover, an adaptive response is mounted through recruiting enzymes, transcription factors and via triggering specific protein signaling cascades. HIF-1α achieves the cellular response to hypoxia through activating the transcription of thousands of hypoxia responsive genes. Furthermore, HIF-1α functions as a master regulator of cellular and systemic homeostatic response to hypoxia through activating transcription of several genes including those involved in energy metabolism, angiogenesis, apoptosis and other genes whose protein products increase the oxygen delivery or facilitate metabolic adaptation to hypoxia. HIF-1α thus plays an essential role in embryonic vascularization, tumor angiogenesis and patho-physiology of ischemic diseases. Finally, the alternatively spliced transcript variants encoding different isoforms have been identified for this gene, although the exact functions of the isoforms are currently unknown. HIF-1α activates the transcription of genes that are involved in crucial aspects of cancer biology including angiogenesis, cell survival, glucose metabolism and invasion [68]. One of the hallmarks of cancer is a metabolic switch from the TCA cycle to Glycolysis as a main source of energy production [36]. This is known as the Warburg effect and was observed by Otto Warburg in the 1920s. HIF-1α is also known to up-regulate enzymes involved in glycolysis. There is lot of work in the literature that discusses the importance of hypoxia in cancer biology. It has been long recognized that therapeutically targeting hypoxia might alleviate some of the negative characteristics associated with cancer cells.

The identification of targets that mediate response in the hypoxic cell in response to hypoxia is important because inhibition of these targets could lead to cell death. The main oxygen-responsive signaling pathways that mediate cellular response to hypoxia involve the HIF family of transcription factors, unfolded protein response (UPR) and mammalian target of rapamycin (mTOR) [69]. In conditions of severe hypoxia, HIF-1α is activated and leads to the regulation of HIF family of transcription factors which includes VEGF

(angiogenesis), GLUT1 (glucose transporter), almost all enzymes involved in glycolysis. Severe hypoxia also leads to mistakes in protein folding which contributes to ER stress or UPR. During UPR, the cell tries to conserve energy by stopping translation of proteins and directs all misfolded to proteins to undergo degradation in the endoplasmic reticulum (ER). One of the pathways through which UPR is mediated is through the PERK pathway. Hypoxia also causes a drop in ATP levels which mediates a response through the mTOR pathway. Metabolic reprogramming in tumor cells called the Warburg effect is in part mediated by HIF-1α and mTOR. But this switch is also regulated by p53 and PI3K/Akt pathways as well. The downstream effects of these mediate apoptotic or cell-survival regulators.

3.7 Boolean Model and Targeted Therapy Under Persistent Hypoxia

We used results published in the literature to get all the necessary pathways [69–72].Here we try to model a hypoxic cell considering three major phenomena- apoptosis, cell survival and the Warburg effect. The pathways related to these phenomena are included in the above figure. After modeling based on the Boolean network explained previously, we apply the different drug combinations to see which one provides the maximum benefit. Benefit is measured in terms of three quantities a) up-regulation of average activity of Bad (Bcl-2 associate death promoter)gene, b) down-regulation of average activity of Bcl-2 (B-cell CLL/lymphoma 2) gene and c) down-regulation of ATP produced through fermentation (Warburg effect). Effective drug combination is defined as the combination with maximum benefit, in terms of the factors described above and minimum number of drugs in order to reduce the side effects of treatment.

3.7.1 Description of Drugs

There are 8 drugs used in this simulation. We include a brief description of each.

a) Metformin: An anti-diabetic drug suspected to have anti-tumor properties. In the path-

way it is shown to activate AMPK.

b) Dorsomorphin: A cell-permeable pyrrazolopyrimidine compound that inhibits AMPK kinase activity.

c) Dimethyloxalylglycine: Dimethyloxalylglycine is a cell permeable prolyl-4-hydroxylase inhibitor, which upregulates HIF-1α by suppressing the activity of prolyl-hydroxylase.

d) Echinomycin: Echinomycin is a peptide antibiotic. It intercalates into DNA at two specific sites, thereby blocking the binding sites of HIF-1α.

e) Avastin: Bevacizumab (trade name Avastin, Genentech/Roche) is an angiogenesis inhibitor, a drug that slows the growth of new blood vessels. It is licensed to treat various cancers, including colorectal, lung, breast (outside the USA), glioblastoma (USA only), kidney and ovarian.

f) Pottasium dichloroacetate: Salts of DCA have been studied as potential drugs because they inhibit the enzyme pyruvate dehydrogenase kinase.

g) Bromopyruvic acid: It is an inhibitor of hexokinase which is an enzyme involved in the first step of glycolysis.

h) Sodium oxamate: Structural analog of pyruvate, inhibits L(+)-lactate dehydrogenase and derails the entire gluconeogenic pathway.

The major pathways along with the drugs that act on these are shown in Fig. 3.8. The drugs are shown in green rectangular boxes in the above pathway diagram. We have used the following abbreviations PDC (Pottasium dichloroacetate), BA (Bromopyruvic Acid), SO(Sodium Oxamate), DMOG (Dimethyloxalylglycine). We did not abbreviate the name of the drugs Metformin, Dorsomorphin, Echinomycin, Avastin. We modeled the pathways in Fig. 3.8 as a Boolean model to simulate the effects of the various drugs.

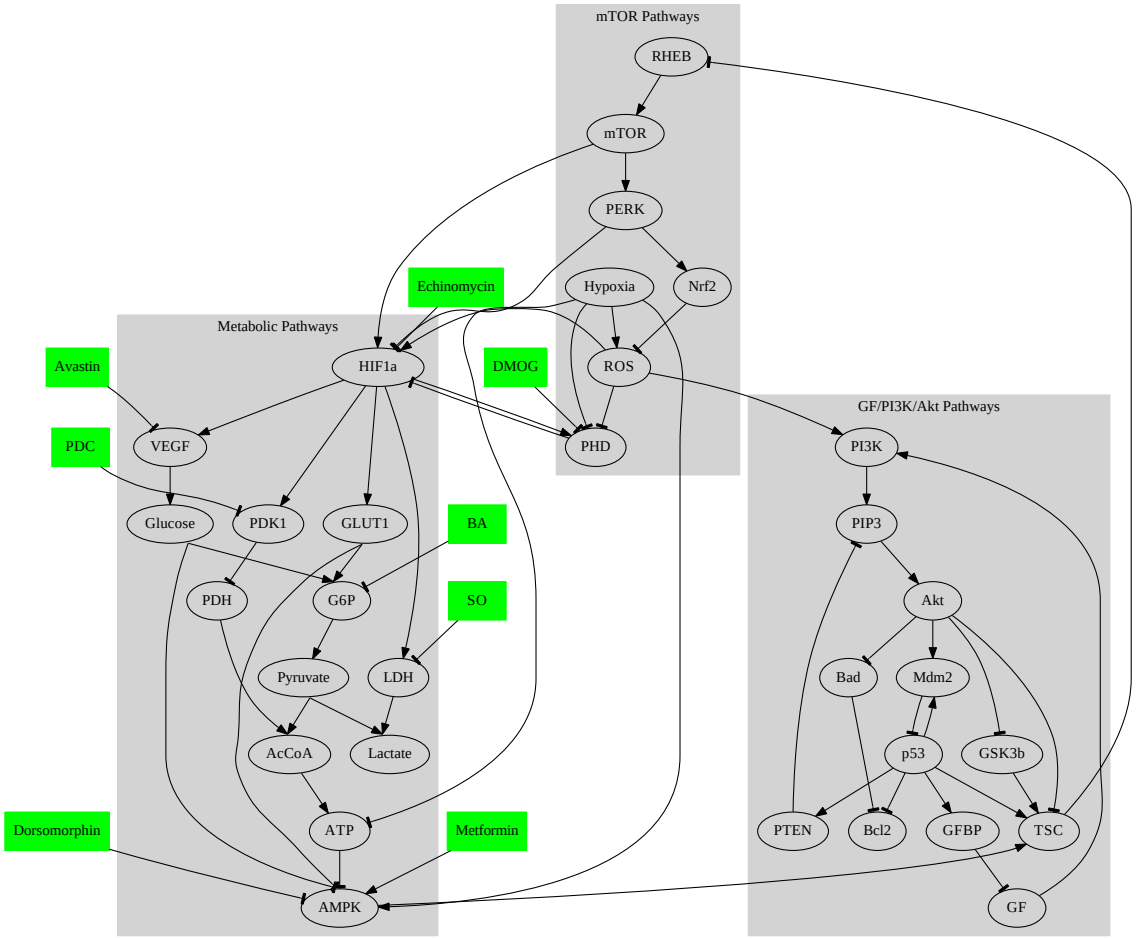

Figure 3.8: Pathway diagram incorporating pathways from apoptosis, cell-survival and the Warburg effect

Table 3.1: Effective drug combinations

Dorsomorphin	DMOG	Echinomycin	Avastin	PDC	BA	SO
0	0	0	0	1	0	1
1	0	0	0	0	0	1
1	0	0	0	0	1	0
0	1	0	0	1	0	1
1	0	0	0	0	1	1
1	0	0	0	1	0	1
1	0	0	0	1	1	0
1	0	0	1	0	0	1
1	0	0	1	0	1	0
1	0	1	0	0	0	1
1	0	1	0	0	1	0
1	1	0	0	0	0	1
1	1	0	0	0	1	0

3.7.2 Example Simulation

We consider a case of persistent hypoxia and no mutations and see how to intervene in such a system. We will choose a starting state that is unfavorable to the system and see what kind of intervention is best. Let the starting state correspond to Hypoxia=1, ROS=1, GF=1, GFBP=0, Lactate=1, VEGF=1, Bad=0, Bcl2=1. We will assume random states for the other variables in the system. We simulated for all 192 drug combinations. We have 8 drugs and this corresponds to 2^8=256 combinations. We however ignore the combinations where Metformin(AMPK activator) and Dorsomorphin(AMPK inhibitor) are both present so that eliminates 64 drug combinations, this leaves us with 192 (=256-64) combinations. As mentioned earlier the effective drug combination is defined as one provides the maximum benefit. Benefit is measured in terms of three quantities a) up-regulation of average activity of Bad, b) down-regulation of average activity of Bcl-2 and c) down-regulation of ATP produced through fermentation (Warburg effect). Effective drug combination is defined as the combination with maximum benefit, in terms of the factors described above

and minimum number of drugs(3 maximum) in order to reduce the side effects of treatment. We only show the drug combinations which yieded maximum benefit, there are other drug combinations which yielded a overall positive effct but was lesser than the benefit provided by the combinations in Table 3.1. Table 3.1 shows all favorables drug response where all the three criteria were found to be satisfied, and the effective gain in each category was the highest, with minimum number of drug combinations.

3.8 Discussion

In Table 3.1, we identify combinations of 2 or 3 drugs are more effective in tackling the problem at hand rather than administering a single targeted drug. Dorsomorphin, an AMPK inhibitor has been shown to reverse the mesenchymal phenotype of breast cancer intiating cells [73]. As explained in [74], EMT or Epithelial to Mesenchymal Transition is an important feature of carcinogenesis and Dorsomorphin has been shown to reverse the Mesenchymal phenotype. DMOG is an indirect activator of HIF-1α. It works by inhibiting PHD's and stabilizing HIF-1α. It is also known to upregulate VEGF, GLUT1, however it does not increase mRNA levels of HIF-1α [75, 76]. Fannale et. al were able to experimentally validate that hypoxia negatively regulates breast cancer cell growth during short term in vitro exposure [77], this can be achieved by adding DMOG to stabilize HIF-1α. They also noticed that it led to changes in DNA damage repair pathways which can induce apoptosis or necrosis. Since DMOG upregulates GLUT1 which increases uptake of glucose [76], this can be counteracted by adding BA (Bromopyruvic Acid), SO(Sodium Oxamate) [78, 79]. Dorsomorphin is a known inhibitor of Bone Morphologic Protein (BNP) whose role in cancer is contested as pro- or anti-tumor, but they are known to induce angiogenesis [80, 81]. Our results suggest that using these drugs in combination will prevent angiogenesis and since Dorsomorphin also affects AMPK it will also down-regulate PI3K/Akt pathways. We notice that Echinomycin (an HIF-1α inhibitor) did not

appear in any of the favorable combinations which had only 2 drugs. Echinomycin always appreared in combinations with two more drugs as shown in Table 3.1. This has been experimentally seen and suggested that inhibiting just HIF-1α alone may not be sufficient to halt angiogenesis and tumor growth. Hence, HIF-1α inhibitor needs to be used in combination with other drugs that are unfavorable to the tumor microenvironment [82]. Anti-angiogenesis therapy has shed new light for cancer treatment but its effectiveness is still not completely validated [83]. It has been experimentally validated that glycolysis inhibitors aid the anti-VEGF treatment of Avastin in coloretal cancer [83]. One reason for this evidence points to the fact that one outcome of hypoxic environment is resistance to Avastin. In [83] they use BA (Hexokinase II inhibitior) in combination with Avastin to get favorable outcome in terms of tumor volume and survival. Our boolean model predicts that this drug combination along with Dorsomorphin (BA+Avastin+Dorsomorphin) or just Dorsomorphin with BA leasds to favorable outcomes. The reason for newer drug combinations is because when simulations are performed they are repeated under different cellular conditions. Hence, the combination needs to be specifically tailored for each patient. Additionally, we also see that Avastin in combination with Sodium oxamate and Dorsomorphin will also be an effective combination. Sodium Oxamate is known to be an inhibitor of glycolysis [84, 85]. It was also seen that Avastin by itself will not lead to favorable outcomes as compared to using it with other drugs in combination [86]. Dicholoroacetate is a used for cancer therapy as suppressor of Warburg effect [87]. It is one of the characteristics of cancer cells whereby they use Glycolysis (even in presence of oxygen) to meet the majority of their energy needs. Dichloroacetate works by inhibiting the enzyme pyruvate dehydrogenase kinase (*PDK*), increases the flux of pyruvate into the mitochondria, promoting glucose oxidation over glycolysis. This reverses the suppressed mitochondrial influenced apoptosis in cancer and results in suppression of tumour growth in vitro and in vivo [87]. Here our model predicts drugs in combination with other drugs to

treat cancer, which might be required since cancer cells have ability to bypass blockades through other pathways. Epidemiological studies of Metformin, an anti-diabetic drug have been suggested to have anti-cancer properties. Table 3.1 does have a single drug combination that has Metformin in the drug cocktail. Simulations with Metformin in combination with other drugs yielded conflicting results. By conflicting results we mean that the response was better by treating with Metformin in some cases and opposite in some other cases. All the drug combinations shown in Table 3.1 without Metformin in the combination, gave a positive effect on treatment for the different starting conditions. We made a literature survey to the check this ambiguity. We found that current preclinical and clinical knowledge suggests that patients exhibiting hyperinsulinemia and tumors expressing insulin receptor, LKB1 and TSC2 would only benefit from metformin but not others with normal insulin levels and tumors lacking expression of insulin receptor (INSR), LKB1 and TSC2 [88]. The gene LKB1 was not part of the BN model presented, it is brought into discussion due to the role it plays in activating AMPK. Metformin also acts to activate AMPK and inhibit mTOR. So LKB1 upregulated in a Boolean model implies that AMPK is also upregulated. However, the direct, insulin-independent effects of metformin originate from LKB1-mediated activation of AMPK and a reduction in mTOR signaling and protein synthesis in cancer cells. So the gene LKB1 was used to emphasize one of the mechanisms through which Metformin acts to suppress mTOR. It has also been experimentally validated that Metformin's actions varies based on the level of glucose. A recently published work suggests that clinical trials of Metformin have yielded conflicting results [89] further complicating the issue. Some studies point to AMPK as a tumor suppressor, whereas others seem to suggest that it can be a promoter of tumor growth. We are encouraged, at this point that the predictions made by our model is supported by data from real world.

3.9 Concluding Remarks

Cancer cells are known to thrive in altered micro-environmental niches, including in a hypoxic nitch. We have investigated via simulations the dynamics and response of cells to hypoxia while also incorporating other major pathways that may be altered at hypoxic stages. The biological pathways involved in cell growth and metabolic regulation were mapped to a Boolean network. The equivalent digital circuit was used to identify drug combinations that may be most effective in reducing the negative effects of Hypoxia while giving maximum advantage. We incorporated the drug intervention points into our model allowing us to test different combination therapies in terms of their efficacy in mitigating the effects of faults in the network. Although the predictions from the current model we developed to ameliorate hypoxia based tumor aggressiveness is encouraging, as it agrees with several of the drugs used in current cancer therapy, we however need to proceed with caution in the sense that some of the drug combinations suggested here may still fail to work. This may be due to cross-talk with other pathways, feedback loops and other molecules directly influencing the pathways in question and other mutations that might be present. Nevertheless, this is a good starting point where there is agreement between theoretical simulation, albeit literature based and real world. This we believe can help us fast-track to test optimal intervention techniques.

4. INTERVENTION UNDER UNCERTAINTY IN GENE REGULATORY NETWORKS

4.1 Introduction

The primary goal in translational genomics is to construct a model of gene regulatory networks such that the model class a) incorporates rule-based dependencies between genes that allow to study the global network dynamics, b) is able to cope up with uncertainty in model selection and c) allows to design, implement and test effective therapeutic strategies for intervening in gene regulatory networks (GRNs). Considering a model-based approach, with an engineering perspective, an "effective strategy" can be formulated as the optimal solution to an optimization problem over the costs associated with each strategy, where the cost is computed within an assumed model. Most previous studies have modeled these systems under the assumption of perfect knowledge of the state transition rules. This however, is not the case especially when dealing with biological systems owing to the inherent complexity in understanding the response of the system to various stimuli under various cellular conditions. The dearth of knowledge about the true dynamics of the system is due to limited availability of data and costly experiments involved to generate such data. The available information is usually on a local scale in the form of *biological pathways*. Additionally, variation across biological system is too confounding to come up with the exact dynamics for such systems. Nonetheless, the existing knowledge, i.e. signaling pathways, can be utilized to impose some constraints on the dynamics of the system. This can lead to an uncertainty class of dynamical systems, rather than one single (and perhaps inaccurate) model and optimize an objective function across the entire uncertainty class. The solution to the optimization function will determine the optimal control strategy for the system.

Previously biological systems were modeled under the Markovian dynamical systems framework as Boolean Networks (BNs) and its probabilistic variant Probabilistic Boolean Networks (PBNs). PBNs have an advantage over BNs to account for stochastic state transitions. As a dynamical system there will change of state of the system which are called transitions. Associated with each state change is a probability value defined the transition probabilities. The transition rules in a BN/PBN can be characterized using a Markov chain with known transition probability matrix (TPM). For a Markov chain, the TPM describes the complete dynamics of the system. For these models, optimal intervention strategies have been designed assuming that the information about the transition probabilities in the system is known or can be generated with some uncertainty in them [5–10]. To refine these models, prior knowledge in the form of pathways which gives the relational regulation between a pair of genes/proteins is incorporated into the model [3, 65]. However, these models were deterministic in nature. Furthermore, in these models the mutations were identified and corrective interventions designed based on the signature of chosen downstream genes.

We are interested in modeling a GRN as a Markov Decision Process (MDP). The theory for analysis and control of MDP is very rich. The reader is referred to [4] for detailed discussion on this topic. In this current work, prior biological knowledge is incorporated in the form of biological pathway information, but with some uncertainty. The uncertainty in the regulation of pathways is defined as a prior probability distribution is defined over the system. The parameters of the distribution, which determines its shape expresses the confidence on this prior knowledge. This information expressed over the pathways is used to generate a family of TPMs, which defines the complete dynamics of the model. The observations from the true system is used to update and reduce the size of the uncertainty class of the designed model. The system is also assumed to have a true underlying transition matrix $\tilde{\phi}$ (unknown but state observable). Since intervention is the ultimate goal of

modeling GRN's, an optimization framework is defined to estimate an optimal action at each state. This action is optimal for the model determined by the prior defined over the system. The objective function for the optimization problem is the expected cost relative to the probability distribution over the uncertainty class and formulate an optimal Bayesian robust intervention policy minimizing this cost function. Since the model will be updated at every time epoch the designed intervention will be *non-stationary* and *adaptive*.

The theory of optimal Bayesian intervention in Markovian systems goes back to 1950s. Bellman [90] considered the two-armed bandit problem with discounted cost and used the term *adaptive control* for process with unknown transition probabilities. He proposed the solution for this problem could be obtained by equivalently formulating it as a dynamic program. Then, Martin [91] extended these concepts to apply control theory to systems where the system transition probabilities are unknown, but can be estimated using observations about the system states. The fundamental theory of optimal Bayesian intervention in Markovian system has been recently applied to a Markovian gene regulatory networks [11], in which a gene regulatory network is modeled by a Markov chain. Nonetheless, owing to incompleteness and partial knowledge, it is virtually impossible to have one single TPM that represents the system completely. This uncertainty in the system is expressed as a family of probability distributions. The parameters of the probability distribution function is known as *hyperparameters*. The initial parameters of the distribution, also known as *prior hyperparameters* are updated based on observation from the system to obtain the *posterior hyperparameters*. Conjugate distributions are probability distributions in which *prior* and *posterior* belong to the same family of distributions. Then, instead of dealing with the prior and posterior distributions we need to keep track of only the hyperparameters of the prior and posterior distributions. We consider two such distributions to express our uncertainty about the biological system under consideration- Dirichlet and Beta distributions. The optimization framework is based on Bellman's *Principle of Op-*

timality. It was however, observed that the method suffers from extreme computational and memory requirements, even for network of reasonable size. Hence, we also designed sub-optimal methods so that the intervention problem can be solved much faster with reasonable performance. The section is divided into 3 major topics- Model Convergence, Bayesian Optimal Intervention and Bayesian Sub-optimal Intervention.

4.2 Problem Description: Modeling

A Boolean network (BN) is composed of n nodes, $V = (v^1, v^2, ...v^n)$ and a list of Boolean functions, $F = (f^1, f^2, ...f^n)$ describing the functional relationships between the various nodes. Each of these nodes represent a gene/protein. A Boolean formalism is used to represent the state of each gene. The expression of each gene is quantized to two levels, and each node v^i represents the state/expression of the gene i, where $v^i = 0$ means that gene i is OFF and $v^i = 1$ means that gene i is ON. At time k, the network state is given by $v(k) = (v_1(k), v_2(k), ..., v_n(k))$, which is also called the *gene activity profile* (GAP) of the network. The idea of GAP is same as the state of the system, since it consists of the states of all the genes in the Boolean network. The Boolean function $f^i : (0,1)^{pr_i} \rightarrow (0,1)$ determines the value of node i at time $k+1$ given the value of its predictor/parent nodes (pr_i) at time k. We assume a synchronous update scheme for the nodes which means that all the nodes of the BN update simultaneously. The complete dynamics of the BN is defined by the transition probabilities between all the states. This is usually represented in the form of a TPM. Thus, given a system in a particular state i, the next state j of the system is dependent on the transition probabilities vector associated with state i. Since these transitions are stochastic in nature and has Markov property we can represent the BN by an equivalent Markov chain. The TPM of a BN denoted by P, gives all information about the transition probabilities between the states of the system. Since the state of the genes are represented by 0 or 1 we use the decimal equivalent to represent the GAP of the system.

For a system with n genes, the GAP varies from 0 to $2^n - 1$. Let $Z_k \in S, k = 0, 1, ..2^n - 1$ be the stochastic process that defines the transitions for this system. Starting from a state $i \in S$ the system moves to a new successor state $j \in S$ with to a state transition probability $P_{ij} = P(Z_{k+1} = j | Z_k = i)$. This value corresponds to the $(i, j)^{th}$ element of the TPM. The sum of the elements of each row of the TPM which corresponds to a state i adds up to 1, since it is a valid probability distribution. The important task thus, is to generate a family of TPMs along with the entries that reasonably explains the dynamical system under consideration. Once a model is available which describes the system based on our current knowledge we will intervene the system externally to affect the states visited by it.

4.2.1 Uncertainty Quantification

If we assume that we have complete knowledge of the system then all the entries of the TPM are fixed entries. Since such knowledge in a biological system is partial and incomplete, it is not possible to determine the exact transition probabilities i.e, there is an uncertainty about the transition probabilities and hence the next state of the system. Instead of having a fixed entry for each element of P, we define a probability distribution expressing uncertainty in the system transition probabilities. This will give rise to a family of TPMs rather than just one. Two models used to quantify this uncertainty are discussed.
a) The first model quantifies the uncertainty over the state (GAP) transition probabilities.
b) The second model expresses the uncertainty over each node (gene) transition probabilities.
In the first model the uncertainty is directly expressed over the state transition probabilities of the TPM. We can associate with each state i, an uncertainty probability distribution of transition probability to the successor state j which will correspond to a row of the TPM. In the second model instead of expressing the uncertainty over the GAP, it is defined over each gene (node) of the network. For each gene/node $(v^k, k \in (1, ...n))$, a conditional prob-

ability table C^k,$k \in (1,...n)$ is defined. These tables gives the probability of the next state of the gene of interest (v^i) given the state of the genes predicting gene i (pr_i). Previously, in this dissertation the node transition probabilities are considered to be deterministic- 0 or 1, but now a probability distribution is defined over each of these transition probabilities. Samples from these distributions can be appropriately combined to obtain a family of TPMs which will represent our uncertainty class. A specific case of the model TPM referred to as *expected TPM* is discussed in Section. 4.3.4. It is calculated from the expected value of all the uncertainty distributions over the transition probabilities. This TPM will be stochastic in nature. As more information about the system is obtained, the hyperparameters of the distribution is updated so that mean of the distribution is as close to the actual transition values in the true system. In the ideal case of variance of the distribution being zero, the probability distribution will be a point distribution at the mean value defined by its parameters. This model will represent the true system. The primary difference in the approaches of the two methods is one defines the uncertainty over the GAP of the network and the other one defines the uncertainty over each node (gene) of the system.

4.3 Nominal Model Formulation

We will discuss about how the uncertainty class is defined and how these models converge to the true model. These models will also be the basis for the intervention problems discussed from Section 4.4 onwards.

4.3.1 Dirichlet Distribution Prior Model: Uncertainty Over State Transitions

Dirichlet distribution denoted by Dir(α), is a family of continuous multivariate probability distribution parametrized by a vector α of positive reals. It is a multivariate generalization of the Beta distribution. The parameters of the distributions are referred to as the hyperparameters. The transition matrix (P) gives the probabilities of transitioning from a given state i to the next state j under action a expressed as $P_{ij}(a)$. We express the uncer-

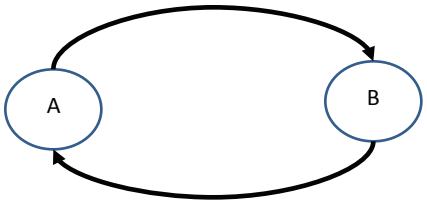

Figure 4.1: 2-gene toy example

$$\begin{array}{c} \\ \overline{AB} \\ \overline{A}B \\ A\overline{B} \\ AB \end{array} \begin{array}{c} \begin{array}{cccc} \overline{AB} & \overline{A}B & A\overline{B} & AB \end{array} \\ \begin{pmatrix} \alpha_{11} & \alpha_{12} & \alpha_{13} & \alpha_{14} \\ \alpha_{21} & \alpha_{22} & \alpha_{23} & \alpha_{24} \\ \alpha_{31} & \alpha_{32} & \alpha_{33} & \alpha_{34} \\ \alpha_{41} & \alpha_{42} & \alpha_{43} & \alpha_{44} \end{pmatrix} \end{array}$$

Figure 4.2: Uncertainties in the state transition probabilities as parameters of Dirichlet distribution

tainty in the state transition probabilities as a conjugate family of probability distributions over the uncertainty class where each row (state) of the TPM follows a Dirichlet distribution with parameter vector α. Assuming that the rows of the TPM are independent, the posterior probability distribution will again be a Dirichlet distribution with updated parameter vector α. Thus, the uncertainty in the system is expressed directly over the state or *gene activity profile* of the system. The reason for choosing a Dirichlet distribution is since that the *GAP* of the system is distributed multinomially, a Dirichlet distribution is a conjugate prior for the Multinomial distribution.

Since the probability distribution is defined over the *GAP* for a system with n genes the size of the parameter matrix will be $2^n \times 2^n$. Every time the system state changes for state i to state j the corresponding value of α_{ij} is updated. For the 2-gene system if Fig. 4.1 the size of the α matrix will be 4×4 as shown in Fig. 4.2. Each row of the matrix in Fig. 4.2 gives the parameters of the Dirichlet distribution used to obtain the various transition probabilities from the state corresponding to that row.

4.3.2 Beta Distribution Prior Model

Beta distribution denoted by Beta(α, β) is a family of continuous probability distributions defined between [0, 1] parametrized by two positive shape parameters α and β. Instead of assuming a prior distribution over transitions between states we express the prior distributions over the *parents* and *child* in the network i.e, over each node of the network. We assume that once the status of the *parents* are completely known the state of the *child* is uniquely determined and is not influenced directly/indirectly by the other nodes. This comes from the assumption that our BN has the property of *Bayesian Nets*. Every node in a bayesian net has an associated conditional probability transition (CPT) table which quantizes the direct influence of parents on the child node. At any given instant the gene *i* is either ON or OFF due to the boolean formalism we have adopted. Consider the pathway and the associated CPT table for gene C as shown in Fig. 4.3. A and B are the parent genes, while C is the child gene. The state of C in the current step depends on the states of A and B in the previous time step. The uncertainty in these transition probabilities is expressed in terms of Beta distribution parameters α's and β's as shown in Fig. 4.4. In Fig. 4.3, the letters A, B and C correspond to the genes and in Fig. 4.4 the letters a, b, c and d correspond to the mean value of the probabilities. The meaning of the entry in row 1 of the table is $\overline{P}(C_k = 0 \mid A_{k-1} = 0, B_{k-1} = 0) = a$ which implies that $\overline{P}(C_k = 1 \mid A_{k-1} = 0, B_{k-1} = 0) = (1-a)$, since it is a Bernoulli distribution. The symbol $\overline{P}$ refers to the mean or expected value of the transition probability. Similarly, the other entries in the table will correspond to the other states for the predictors (A and B) and state of the child gene (C). Such CPT tables will always have 2 columns (state 0 or 1 of child gene) and the number of rows is 2^{pr_i}, where pr_i is the number of predictors/parents. The reason for using a Beta distribution to express the uncertainty in the CPT table is because Beta distribution is a conjugate prior for Bernoulli distribution. In this case since the

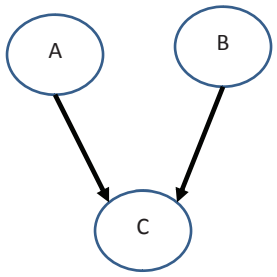

Figure 4.3: General layout pathway regulation conditional probabilities

$$\begin{array}{c} \\ \overline{A}\overline{B} \\ A\overline{B} \\ \overline{A}B \\ AB \end{array} \begin{array}{c} \overline{C} \\ \begin{pmatrix} \alpha_1, \beta_1 \\ \alpha_2, \beta_2 \\ \alpha_3, \beta_3 \\ \alpha_4, \beta_4 \end{pmatrix} \end{array} \qquad \begin{array}{c} \\ \overline{A}\overline{B} \\ A\overline{B} \\ \overline{A}B \\ AB \end{array} \begin{array}{cc} \overline{C} & C \\ \begin{pmatrix} a & (1-a) \\ b & (1-b) \\ c & (1-c) \\ d & (1-d) \end{pmatrix} \end{array}$$

Figure 4.4: Uncertainties in gene regulation as parameters of beta distribution and its mean value

uncertainty is expressed over pathways where the *child* can have values 0 or 1, we need to keep track of only parameters of state 0 of the child since the parameters of state 0 is related to state 1 by $\alpha_1 = \beta_0$ and $\beta_1 = \alpha_0$ due to mirror-symmetry property. Thus, for every row in a CPT table a unique pair of α and β will specify the dynamics completely. Similarly, there will be CPT table associated with each node of the boolean network.

4.3.3 Hyperparameters Update

The purpose of creating an uncertainty class is to represent our limited knowledge about the system. But as our understanding of the system improves we would like to update the hyperparameters of the distribution and reduce the size of our uncertainty class. One of the biggest challenge in bayesian work is the design of prior that represents the system. This itself is an area of research and the readers are referred to [92] and references therein for more exposure to the topic. We will be discussing the whole premise of the problem with uniform priors which represents the condition where the value of all the

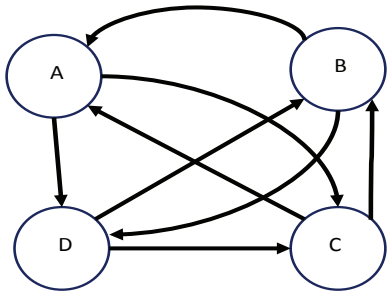

Figure 4.5: 4 gene network for simulation results

hyperparameters equals 1. This corresponds to a condition where we have no knowledge or understanding of the system. However, the same procedure can also be applied to other prior values as well. We consider the 4-gene network shown in Fig. 4.5 for our simulations. The dynamics of this network is defined by the true but unknown TPM ($\tilde{\phi}$) given in Table. B.1. We can say looking at Fig. 4.5 that $Pa(A)$=B,C, $Pa(B)$=C,D, $Pa(C)$=A,D and $Pa(D)$=A,B, where Pa stands for *Parents*. We are only interested in the interactions and not the nature of the interactions since it is a synthetic example. The starting uncertainty hyperparameter matrix defined as α_{diri} and $\alpha\beta_{beta}$ are shown in Table. 4.1 and 4.3. The update process for the uncertainty parameter matrix for both distribution depends on the current state i and next state j. As an example we will consider the situation when the system transitions from i='0000' and j='1011'.

a) For Dirichlet distribution it is straight forward and the value of α corresponding to the transition from '0000' to '1011' is incremented by 1, since this transition is observed and counted as a success. The updated matrix is shown in Table. 4.2. After this we repeat the whole process for the next time-step.

b) For the Beta distribution the update process is a little more complicated. We need to calculate all *Parents* and *Child* combination and then update the values. The values of *parents* are

Table 4.1: Initial Dirichlet hyperparameters

$$\begin{pmatrix}
1 & 1 & 1 & 1 & 1 & 1 & 1 & 1 & 1 & 1 & 1 & 1 & 1 & 1 & 1 & 1 \\
1 & 1 & 1 & 1 & 1 & 1 & 1 & 1 & 1 & 1 & 1 & 1 & 1 & 1 & 1 & 1 \\
1 & 1 & 1 & 1 & 1 & 1 & 1 & 1 & 1 & 1 & 1 & 1 & 1 & 1 & 1 & 1 \\
1 & 1 & 1 & 1 & 1 & 1 & 1 & 1 & 1 & 1 & 1 & 1 & 1 & 1 & 1 & 1 \\
1 & 1 & 1 & 1 & 1 & 1 & 1 & 1 & 1 & 1 & 1 & 1 & 1 & 1 & 1 & 1 \\
1 & 1 & 1 & 1 & 1 & 1 & 1 & 1 & 1 & 1 & 1 & 1 & 1 & 1 & 1 & 1 \\
1 & 1 & 1 & 1 & 1 & 1 & 1 & 1 & 1 & 1 & 1 & 1 & 1 & 1 & 1 & 1 \\
1 & 1 & 1 & 1 & 1 & 1 & 1 & 1 & 1 & 1 & 1 & 1 & 1 & 1 & 1 & 1 \\
1 & 1 & 1 & 1 & 1 & 1 & 1 & 1 & 1 & 1 & 1 & 1 & 1 & 1 & 1 & 1 \\
1 & 1 & 1 & 1 & 1 & 1 & 1 & 1 & 1 & 1 & 1 & 1 & 1 & 1 & 1 & 1 \\
1 & 1 & 1 & 1 & 1 & 1 & 1 & 1 & 1 & 1 & 1 & 1 & 1 & 1 & 1 & 1 \\
1 & 1 & 1 & 1 & 1 & 1 & 1 & 1 & 1 & 1 & 1 & 1 & 1 & 1 & 1 & 1 \\
1 & 1 & 1 & 1 & 1 & 1 & 1 & 1 & 1 & 1 & 1 & 1 & 1 & 1 & 1 & 1 \\
1 & 1 & 1 & 1 & 1 & 1 & 1 & 1 & 1 & 1 & 1 & 1 & 1 & 1 & 1 & 1 \\
1 & 1 & 1 & 1 & 1 & 1 & 1 & 1 & 1 & 1 & 1 & 1 & 1 & 1 & 1 & 1 \\
1 & 1 & 1 & 1 & 1 & 1 & 1 & 1 & 1 & 1 & 1 & 1 & 1 & 1 & 1 & 1
\end{pmatrix}$$

Table 4.2: Updated Dirichlet hyperparameters

$$\begin{pmatrix}
1 & 1 & 1 & 1 & 1 & 1 & 1 & 1 & 1 & 1 & 1 & 2 & 1 & 1 & 1 & 1 \\
1 & 1 & 1 & 1 & 1 & 1 & 1 & 1 & 1 & 1 & 1 & 1 & 1 & 1 & 1 & 1 \\
1 & 1 & 1 & 1 & 1 & 1 & 1 & 1 & 1 & 1 & 1 & 1 & 1 & 1 & 1 & 1 \\
1 & 1 & 1 & 1 & 1 & 1 & 1 & 1 & 1 & 1 & 1 & 1 & 1 & 1 & 1 & 1 \\
1 & 1 & 1 & 1 & 1 & 1 & 1 & 1 & 1 & 1 & 1 & 1 & 1 & 1 & 1 & 1 \\
1 & 1 & 1 & 1 & 1 & 1 & 1 & 1 & 1 & 1 & 1 & 1 & 1 & 1 & 1 & 1 \\
1 & 1 & 1 & 1 & 1 & 1 & 1 & 1 & 1 & 1 & 1 & 1 & 1 & 1 & 1 & 1 \\
1 & 1 & 1 & 1 & 1 & 1 & 1 & 1 & 1 & 1 & 1 & 1 & 1 & 1 & 1 & 1 \\
1 & 1 & 1 & 1 & 1 & 1 & 1 & 1 & 1 & 1 & 1 & 1 & 1 & 1 & 1 & 1 \\
1 & 1 & 1 & 1 & 1 & 1 & 1 & 1 & 1 & 1 & 1 & 1 & 1 & 1 & 1 & 1 \\
1 & 1 & 1 & 1 & 1 & 1 & 1 & 1 & 1 & 1 & 1 & 1 & 1 & 1 & 1 & 1 \\
1 & 1 & 1 & 1 & 1 & 1 & 1 & 1 & 1 & 1 & 1 & 1 & 1 & 1 & 1 & 1 \\
1 & 1 & 1 & 1 & 1 & 1 & 1 & 1 & 1 & 1 & 1 & 1 & 1 & 1 & 1 & 1 \\
1 & 1 & 1 & 1 & 1 & 1 & 1 & 1 & 1 & 1 & 1 & 1 & 1 & 1 & 1 & 1 \\
1 & 1 & 1 & 1 & 1 & 1 & 1 & 1 & 1 & 1 & 1 & 1 & 1 & 1 & 1 & 1 \\
1 & 1 & 1 & 1 & 1 & 1 & 1 & 1 & 1 & 1 & 1 & 1 & 1 & 1 & 1 & 1
\end{pmatrix}$$

Table 4.3: Initial beta hyperparameters

A_t / $(B,C)_{t-1}$	0
00	α_{1A}=1,β_{1A}=1
01	α_{2A}=1,β_{2A}=1
11	α_{3A}=1,β_{3A}=1
10	α_{4A}=1,β_{4A}=1

B_t / $(C,D)_{t-1}$	0
00	α_{1B}=1,β_{1B}=1
01	α_{2B}=1,β_{2B}=1
11	α_{3B}=1,β_{3B}=1
10	α_{4B}=1,β_{4B}=1

C_t / $(D,A)_{t-1}$	0
00	α_{1C}=1,β_{1C}=1
01	α_{2C}=1,β_{2C}=1
11	α_{3C}=1,β_{3C}=1
10	α_{4C}=1,β_{4C}=1

D_t / $(A,B)_{t-1}$	0
00	α_{1D}=1,β_{1D}=1
01	α_{2D}=1,β_{2D}=1
11	α_{3D}=1,β_{3D}=1
10	α_{4D}=1,β_{4D}=1

Pa(A=1)=0,

Pa(B=0)=0,

Pa(C=1)=0,

Pa(D=1)=0 and

the *child* values are A=1, B=0, C=1 and D=1. The CPT tables are maintained for the condition when $child = 0$. So observinf a $child = 0$ is a success, while $child = 1$ is a failure. In each of the CPT tables, if state of $child = 0$, then α values corresponding to the above combination of parents are updated. If state of $child = 1$, then β values corresponding to the above combination of parents are updated. The updated $\alpha\beta_{beta}$ is shown in Table. 4.4.

4.3.4 Expected Transition Matrix

The *expected transition matrix (ETM)* gives the expected values of the transition probabilities from state *'i'* to state *'j'*, $\bar{P}_{ij}(a) = E[P_{ij}(a)]$, which is used in Eq. (4.11),(4.12), to be discussed later. The expectation is calculated over the entire uncertainty class. These expected values are calculated using the mean of the uncertainty distributions defined by

Table 4.4: Updated beta hyperparameters

A_t / $(B,C)_{t-1}$	0
00	α_{1A}=1,β_{1A}=2
01	α_{2A}=1,β_{2A}=1
11	α_{3A}=1,β_{3A}=1
10	α_{4A}=1,β_{4A}=1

B_t / $(C,D)_{t-1}$	0
00	α_{1B}=2,β_{1B}=1
01	α_{2B}=1,β_{2B}=1
11	α_{3B}=1,β_{3B}=1
10	α_{4B}=1,β_{4B}=1

C_t / $(D,A)_{t-1}$	0
00	α_{1C}=1,β_{1C}=2
01	α_{2C}=1,β_{2C}=1
11	α_{3C}=1,β_{3C}=1
10	α_{4C}=1,β_{4C}=1

D_t / $(A,B)_{t-1}$	0
00	α_{1D}=1,β_{1D}=2
01	α_{2D}=1,β_{2D}=1
11	α_{3D}=1,β_{3D}=1
10	α_{4D}=1,β_{4D}=1

the parameter vector α for Dirichlet and parameters (α,β) for Beta distribution. For the problems under consideration we assume that the networks have the property of bayesian networks, i.e. given the state of the parents/predictors of a gene (g), the state of the gene g is uniquely defined by its parents/predictors and it is independent of the state of the other nodes/genes in the network. Thus, if we extend the same principle from node (gene) to state we come up with the following relationship for probability of transition from state S_k to state S_{k+1}

$$P(S_{k+1}|S_k) = \prod_{g=1}^{n} P(v_{k+1}^g|Pa(v_k^g)) \tag{4.1}$$

In the above equation the left hand side gives the probability of transition from state S_k to state S_{k+1} and the right hand side specifies this probability as product of probabilities of individual gene probabilities given its predictors at the previous time step. So if we calculate the expected values in Eq.(4.1), we calculate the expected values of transitions from current state to next state. Thus, Eq.(4.1) can be rewritten as

$$E(P(S_{k+1}|S_k)) = E\Big\{\prod_{g=1}^{n} P(v_{k+1}^{g}|Pa(v_k^g))\Big\} \tag{4.2}$$

The factors inside the product sign are the probability distribution of the gene's state at time k+1 as a function of state of its predictors/ parents at a time k. Since this is a design parameter fixed by the user we assume that these distributions are uncorrelated, hence Eq.(4.2) can be written down as

$$\begin{aligned} E(P(S_{k+1}|S_k)) = E\Big\{P(v_{k+1}^{1}|Pa(v_k^1))\Big\}\times \\ E\Big\{P(v_{k+1}^{2}|Pa(v_k^2))\Big\}\cdots^{n}\cdots \times E\Big\{P(v_{k+1}^{n}|Pa(v_k^n))\Big\} \end{aligned} \tag{4.3}$$

Now each of the expectation in the right hand side correspond to the expected values of transitions of individual genes given the state of its predictors. Thus, the expected transition probabilities from state *'i'* to state *'j'* has been broken down to individual products of expected transition probabilities of individual genes gives the state of its predictors i.e, individual CPT tables. For a Dirichlet distribution with parameters (α_1, α_2, $\cdots$, α_{2^n}) the expected value is given by $\left(\frac{\alpha_1}{\sum_{i=1}^{2^n}\alpha_i}, \frac{\alpha_2}{\sum_{i=1}^{2^n}\alpha_i}, \cdots, \frac{\alpha_k}{\sum_{i=1}^{2^n}\alpha_i}\right)$. For a Beta distribution defined by parameters (α,β) the expected value is given by $\frac{\alpha}{\alpha+\beta}$. The ETM will be denoted by the symbol ϕ and $\phi_{ij}(a)$ defines the probability of transitioning from state i to state j under the control action a. Once we obtain the ETM we can conclude that $\bar{P}_{ij}(a) = E[P_{ij}(a)] = \phi_{ij}(a)$.

4.3.4.1 Dirichlet Distribution Prior: Expected Transition Matrix

As with any distribution Dirichlet distribution has a mean or expected value that is used for computations as discussed in Section 4.5. We define the *expected transition matrix*, ETM ϕ for this case as in Eq. (4.4).

$$\phi = \begin{pmatrix} \alpha_{11}/A & \alpha_{12}/A & \alpha_{13}/A & \alpha_{14}/A \\ \alpha_{21}/B & \alpha_{22}/B & \alpha_{23}/B & \alpha_{24}/B \\ \alpha_{31}/C & \alpha_{32}/C & \alpha_{33}/C & \alpha_{34}/C \\ \alpha_{41}/D & \alpha_{42}/D & \alpha_{43}/D & \alpha_{44}/D \end{pmatrix} \tag{4.4}$$

where $A = \alpha_{11} + \alpha_{12} + \alpha_{13} + \alpha_{14}$

$B = \alpha_{21} + \alpha_{22} + \alpha_{23} + \alpha_{24}$

$C = \alpha_{31} + \alpha_{32} + \alpha_{33} + \alpha_{34}$

$D = \alpha_{41} + \alpha_{42} + \alpha_{43} + \alpha_{44}$. In this case the rows of the TPM are independent Dirichlet distributions and altering one value of α will only alter the entries in that row.

4.3.4.2 Beta Distribution Prior: Expected Transition Matrix

The mean conditional probability transition matrix for the 2-gene system in Fig. 4.1 are shown in Fig. 4.6. In Fig. 4.6, a_1, a_2, b_1 and b_2 denotes the expected values of the transitions which are calculated from the mean of the distribution function that we have defined. Once such an information about all the genes in a specific network is available they can be used to determine a unique ETM, ϕ. We take a 2-gene regulatory network example shown in Fig. 4.1 to show how we evaluate the ETM, ϕ. Let the subscript 1 and 2 denote the respective probabilities for genes A and B. We use both the mean CPT's in Fig. 4.6 to evaluate the mean transiton probabilities between the states. Thus, what we achieve is we combine the probability distributions over the nodes into probability distribution over the states. The ETM ϕ will be given by Eq. (4.5).

$$\phi = \begin{pmatrix} a_1a_2 & a_1(1-a_2) & (1-a_1)a_2 & (1-a_1)(1-a_2) \\ a_1b_2 & a_1(1-b_2) & (1-a_1)b_2 & (1-a_1)(1-b_2) \\ b_1a_2 & b_1(1-a_2) & (1-b_1)a_2 & (1-b_1)(1-a_2) \\ b_1b_2 & b_1(1-b_2) & (1-b_1)b_2 & (1-b_1)(1-b_2) \end{pmatrix} \tag{4.5}$$

$$\begin{array}{c} \\ \overline{B} \\ B \end{array}\begin{array}{c} \begin{array}{cc} \overline{A} & A \end{array} \\ \begin{pmatrix} a_1 & 1-a_1 \\ b_1 & 1-b_1 \end{pmatrix} \end{array} \qquad \begin{array}{c} \\ \overline{A} \\ A \end{array}\begin{array}{c} \begin{array}{cc} \overline{B} & B \end{array} \\ \begin{pmatrix} a_2 & 1-a_2 \\ b_2 & 1-b_2 \end{pmatrix} \end{array}$$

where a_1=$\alpha_1/(\alpha_1+\beta_1)$, b_1=$\alpha_2/(\alpha_2+\beta_2)$, a_2=$\alpha_3/(\alpha_3+\beta_3)$ and b_2=$\alpha_4/(\alpha_4+\beta_4)$.

Figure 4.6: Mean conditional probabilities transition values for the system

We see here in comparison to Dirichlet distribution model the different rows of the final ETM ϕ are dependent on each other which is a realistic feature. As more and more information is available we update the values of α's and β's and thus the error between ϕ and $\tilde{\phi}$ reduces with time.

4.3.5 Model Convergence

Let the true CPT tables for the 4 genes in Fig. 4.5. We use these true CPT tables to construct the true TPM for simulations shown in Table B.1. We call this the true TPM since for the actual system the probabilities are not defined as probability distribution but instead by a single value expressing the transitions. In a real system we do not need to construct any TPM since it has an underlying dynamics. We start with a uniform prior for both the Dirichlet($\alpha = 1$) and Beta distribution ($\alpha = 1$, $\beta = 1$). This ensures the expected values of all initial entries in the CPT tables to be 0.5. The ETM will be of size 16×16, with each entry equal to 1/16. If we have more information, informative prior should be used for the hyperparameters so that the model converges with the true system faster.

We let the system evolve under its true dynamics given by the true TPM from one state to another and update the hyperparameters of the distribution. We show the norm of the distance between true TPM and ETM after 10, 100, 1000, 10000 100000 and 1000000 steps of simulation in Fig. 4.8. As we can infer the Beta distribution prior model converges

$(B,C)_{t-1}$ \ A_t	0	1
00	0.85	0.15
01	0.25	0.75
11	0.35	0.65
10	0.05	0.95

$(C,D)_{t-1}$ \ B_t	0	1
00	0.8	0.2
01	0.35	0.65
11	0.25	0.75
10	0.1	0.9

$(D,A)_{t-1}$ \ C_t	0	1
00	0.95	0.05
01	0.2	0.8
11	0.2	0.8
10	0.05	0.95

$(A,B)_{t-1}$ \ D_t	0	1
00	0.9	0.1
01	0.25	0.75
11	0.25	0.75
10	0.1	0.9

Figure 4.7: True CPT values

at a faster rate than Dirichlet model. The value of the mean CPT tables and the expected TPM after 100 and 10000 time-steps after the simulations are shown in Appendix B. We see that as we have more and more observations the model CPT's are very close to the true CPT's. It is verified that with 10 million time-steps the values of the model CPT's were very close to the true CPT's.

4.4 Nominal Problem Formulation: Intervention

Intervention in Markovian systems refers to sequential decision making problems in which actions taken at discrete time steps alter the underlying dynamics of the system. The dynamics are altered in such a way that the controlled system spends more time in good states than the uncontrolled system. To model the effect of interventions we assume that the networks can be intervened using an external control vector of length m, $c = (c_1, c_2, ...c_m)$. The control scheme of length m suggests that in the n gene network, only m genes can be externally intervened. Since we are using a Boolean formalism to express gene expression, it is intuitive to use a similar formalism for the control inputs as well, i.e.,

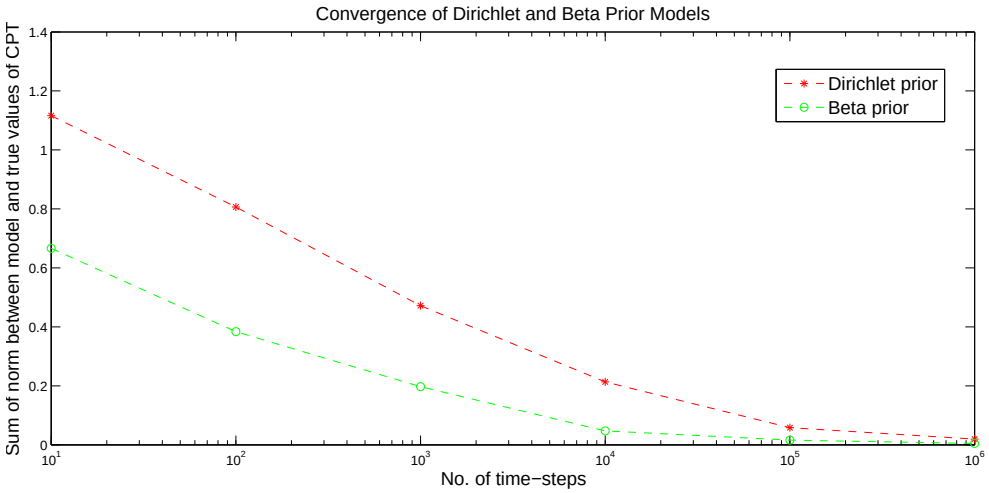

Figure 4.8: Norm between true TPM and ETM

each $c_i \in (0,1)$. $c_i = 0$ implies that the control i is absent and $c_i = 1$ means that we need to intervene by applying the control signal i. The control input is also represented by its decimal equivalent $\mathscr{C} \in (0,1,...2^m - 1)$. The control applied to the system influences the transition probabilities and hence the TPM. To define the relationship between the TPM without intervention and TPM with intervention we need to understand that what happens in the event of external intervention in state i. When the system is externally intervened the state i changes to $\tilde{i}$ and hence the new elements of the controlled TPM $P(a)$ is defined as

$$P_{ij}(a) = P(Z_{k+1} = j | Z_k = i, \mathscr{C} = a) = \begin{cases} P_{ij}, \text{if } a = 0, \\ P_{\tilde{i}j}, \text{if } a \neq 0. \end{cases} \tag{4.6}$$

In the above equation a denotes the decimal equivalent of the control inputs, $a \in (0,1,..2^m - 1)$. The decision maker has the ability to observe the time evolution of the states over the horizon which may be finite of infinite. At each time-step k, upon observing the state, the decision maker chooses an optimal action a (as solution of an optimization problem) that will subsequently alter the dynamics of the system. Associated with each current state i,

the next state j and control action a a cost $g_{ij}(a)$ is accrued. This cost reflects our degree of desirability of various states. The control action a is decided based on the total cost we will accrue over the horizon by choosing different actions. An *intervention policy*, denoted by μ, is a prescription for taking actions from set $\mathscr{C}$ at time k. This mapping does not have to deterministic in nature but can be a function of history. However, we assume that we have a deterministic policy that is optimal. We desire an intervention policy $\mu \in M$ such that the objective function

$$J_P^{\mu}(i) = \lim_{N\to\infty} E_i^{\mu}\Big\{ \sum_{k=0}^{N-1} \lambda^k g z_k z_{k+1}(a) \Big\} \tag{4.7}$$

is minimized. We denote this optimal cost as $J^*(i)$. λ is a discount factor and $\lambda \in (0,1)$ and determines the rate of convergence of the value. $gz_kz_{k+1}(a)$ is an user defined cost function dependent on current state z_k, next state z_{k+1} and applied control action a. The above formulation is called *Discounted Cost Infinite Horizon Problem*. This optimization problem is solved by formulating a set of simultaneous functional equations and a mapping $TJ : S \to \mathbb{R}$, obtained by applying the dynamic programming mapping to any function $J : S \to \mathbb{R}$ for all $i \in S$ defined by

$$TJ(i) = \min_{a\in A}\Big\{ \sum_{j\in S} P_{ij}(a) g_{ij}(a) + \lambda \sum_{j\in S} P_{ij}(a) J(j) \Big\} \tag{4.8}$$

The optimal cost function J^* is a fixed point of the mapping T. The optimal policy can be determined by the convergence, optimality and uniqueness theorems outlined in [93].

4.5 Optimal Bayesian Intervention

In real-world applications perfect knowledge of the TPM will be unavailable or too expensive to acquire. So we characterize the system probabilistically and optimize with regard to this uncertainty class as explained in the previous sections. The results in this

section are derived in [91]. Let

$$\Omega = \Bigg\{ P : P \text{ is } |S| \times |S|, P_{ij} \geq 0, \sum_{j \in S} P_{ij} = 1 \text{ for all } i, j \in S \quad ,$$

denote the class of all valid uncontrolled TPMs (*uncertainty class*). The uncertainty about the matrix P is characterized by a prior probability density $\pi(P)$. At every stage k of the problem an observation is made immediately after applying the intervention and this information to update the prior probability distribution to a posterior distribution. We call the combination of state and probability distribution $(i, \pi(P))$ as a *hyperstate*. Hyperstate completely defines the system since it has information on the current state of the system and also the hyperparameters of the distribution specifying all the transition probabilities. The posterior probability density, when the system transitions from state i to state j under control a is given by

$$\pi'(P : i, a, j) = \begin{cases} cP_{ij}\pi(P), \text{if } a = 0, \\ c'P_{ij}\pi(P), \text{if } a \neq 0, \end{cases} \tag{4.9}$$

where c and c' are normalizing constants dependent on i, j and a. In this case however, all the uncertainties in transition probabilities are defined over the biological pathways. Now for the intervention problem, the equations for the problem formulated as an equivalent dynamic programming needs to be redefined to incorporate this prior density as

$$J_P^{\mu}(i, \pi) = \lim_{N \to \infty} E_{i,\pi}^{\mu} \Big\{ \sum_{k=0}^{N-1} \lambda^k g z_k z_{k+1}(a) \Big\}, \tag{4.10}$$

here the expectation is taken not only w.r.t to the random stochastic process but also the prior probability π. The goal is now to minimize this objective function. We denote the optimal cost as $J^*(i, \pi)$. We can solve the above objective function by forming an

equivalent dynamic programming as formulated above. The equations are defined as

$$TJ(i,\pi(P)) = \min_{a\in A}\Big\{\sum_{j\in S}\bar{P}_{ij}(a)g_{ij}(a)+ \\ \lambda\sum_{j\in S}\bar{P}_{ij}(a)J(j,\pi'(P:i,a,j))\Big\}, \tag{4.11}$$

for all $i \in S$, where $\bar{P}_{ij}(a) = E[P_{ij}(a)]$ w.r.t prior density π. It has been proved that there exists a unique bounded set of optimal costs J^* satisfying

$$J^*(i,\pi(P)) = \min_{a\in A}\Big\{\sum_{j\in S}\bar{P}_{ij}(a)g_{ij}(a)+ \\ \lambda\sum_{j\in S}\bar{P}_{ij}(a)J^*(j,\pi'(P:i,a,j))\Big\}, \tag{4.12}$$

which is the fixed point of the operator T. Since both prior and posterior distributions are chosen to be conjugate distributions, instead of keeping track of closed form expressions of the probability distributions we just need to keep track of the parameters defining the distributions. The distribution with which the variable is defined is called the *likelihood*. The likelihood over the state transitions the likelihood is Multinomial distribution, while the distribution over the regulation of a single gene (CPT table) is Bernoullis distribution. We consider two such models of prior probability distribution- Dirichlet distribution (along with Multinomial likelihood) characterized by parameter α and Beta distribution (along with Bernoullis likelihood) characterized by two parameters α and β to represent the uncertainty class of the system. The Dirichlet distribution is expressed over the entries of the TPM P, but the Beta distribution is defined over each node/gene of the network. The pseudo-code for the control problem using probability distribution prior is shown in

algorithm 4.5.1. The prior information could be the parameters of the Dirichlet or Beta distribution.

Algorithm 4.5.1: INTERVENTION USING UNCERTAINTY CLASS MODEL(h)

$Starting\ state(i),\ Prior\ information(h)$

$Cost\ function(g_{ij}(a,j)),\ True\ unknown\ TPM(\tilde{\phi})$

top :

$a^{\star} \leftarrow f(i, g_{ij}(a,j), h)$

$Next\ state(j) \leftarrow \tilde{\phi}(a^{\star}, i)$

$h_{updated} \leftarrow f'(i,j,h)$

$h \leftarrow h_{updated}$

$i \leftarrow j$

goto *top*

In the above f and f' are used to indicate that the variable on the left is a function of the arguments.

4.6 Q-learning

The proposed methods in the previous sections uses successive approximation to solve for the optimal costs which determines the control action. These methods will fail if we try to extend it beyond a small number of genes. The Beta model is even more computationally intensive than Dirichlet model due to the way the ETM (ϕ) is being evaluated. We are more interested in the Beta model since we can incorporate the uncertainty over the pathways which is the prior knowledge available in biological systems. However, the more computationally difficult task in this whole solution is solution using Dynamic Programming which suffers from *Curse of Dimensionality*. For each time step, the total number of computations to determine the optimal control action is $(|A| \times |S|)^K$, $|A|$ is number of

control actions, $|S|$ is number of states, K is number of steps in successive approximation. These computations increase exponentially with increase in number of states and becomes intractable. To avoid these intractability issues we make use of approximate solutions to solve for the costs. This is part of machine learning called Reinforcement Learning of which we use a specific technique called *Q-learning*. Reinforcement learning principles allow an agent to make good informed action at every time-step by just exploring the environment and observing the rewards for each state-action pair. By repeating the process for a very long time and ideally for infinitely long the agent can gradually converge on the estimates of values for each state that will allow the agent to act optimally. Here we model the nominal problem as a infinite-horizon discounted cost seeking to minimize this cost. Let $J^*(i)$ denote the optimal expected discount reward as explained in Eq.(4.7) that is achievable from state i. Let $Q^*(i,a)$ denote the value of executing action a at state i and then executing the optimal action from there on. $J^*(i)$ and $Q^*(i,a)$ are related to each other and is denoted by:

$$Q^*(i,a) = \min_{a \in A} \Big\{ \sum_{j \in S} P_{ij}(a) g_{ij}(a) + \lambda \sum_{j \in S} P_{ij}(a) J^*(j) \Big\}, \tag{4.13}$$

$$J^*(i) = \min_{a \in A} Q^*(i,a) \tag{4.14}$$

The optimal Q-factor vector Q^* is the unique fixed point of the mapping F defined for all (i,a) by

$$FQ(i,a) = \min_{a,a' \in A} \Big\{ \sum_{j \in S} P_{ij}(a) g_{ij}(a) + \lambda \sum_{j \in S} P_{ij}(a) Q(j,a') \Big\}, \tag{4.15}$$

Eq.(4.15) is the same as Eq.(4.8). These two equations have the same computational complexity. If we have accurate information about the system dynamics we can use a system simulator to converge to the $Q^*(i,a)$ for all $i \in S$ and $a \in A$. Then this matrix is used

to design the optimal action based on Eq.(4.14). For the time evolution of the dynamical system the Q-values are updated until some convergence criteria is met. The update equation for *Q-values* for every state-action pair (i,a) when using a system simulator is given by Eq. (4.6).

$$Q^{k+1}(i,a) = (1-\alpha)Q^k(i,a) + \alpha[g_{ij}(a) + \lambda \min_{a' \in A} Q^k(j,a')] \tag{4.16}$$

$for\ \alpha \to 0$ as $k \to \infty$.

once the Q-values converge the optimal Q-value for the state-action pair can be estimated as

$$Q^*(i,a) = Q^\eta(i,a) \tag{4.17}$$

4.7 Approximate Bayesian Intervention Using Q-learning

In this section we show and explain the modified Bayesian Dynamic Programming equations to incorporate concepts from Section.4.5, 4.6. We again define a prior probability distribution (both Dirichlet and Beta) over the system. Once the system makes transition from state i to state j according to applied action a and the TPM ($\tilde{\phi}$), the prior probability function updated to obtain the posterior probability function as per Eq.(4.9). Now the optimal solution J^* is given by Eq.(4.12). We can relate $J^*(i,\pi(P))$ to $Q^*(i,a,\pi(P))$ as

$$J^*(i,\pi(P)) = \min_{a \in A} Q^*(i,a,\pi(P)) \tag{4.18}$$

$$Q^*(i,a,\pi(P)) = Q^\eta(i,a,\pi(P)) \tag{4.19}$$

Algorithm 4.7.1: APPROX. BAYESIAN Q-LEARNING($\pi(P)$)

MAIN : $Starting\ state(i), Prior\ information(\pi(P))$

$Cost\ function(g_{ij}(a)), True\ unknown\ TPM(\tilde{\phi})$

η *is no. of iterations*

$k \leftarrow 0$

Determine expected transition matrix using $\pi(P)$

subroutine : *while* $k < \eta$

Choose a random control action, a^k

Apply random action a^k *to state i in ETM*

and determine next state j

$Update : Q^{k+1}(i,a) = (1-\alpha)Q^k(i,a) +$

$$\alpha[g_{ij}(a) + \lambda \min_{a' \in A} Q^k(j,a')]$$

$k = k+1$

$i \leftarrow j$

goto subroutine

$Q^*(i,a,\pi(P)) = Q^\eta(i,a,\pi(P)), \forall i \in S$ *and* $a \in A$

$J^*(i,\pi(P)) = \min_{a \in A} Q^*(i,a,\pi(P))$

$a^* = argmax_{a \in A} J^*(i,\pi(P))$

Apply a^* *to actual system and*

observe real transition to state j

Update prior to obtain posterior $\pi'(P)$

$\pi(P) \leftarrow \pi'(P)$

$i \leftarrow j$

goto MAIN

In all of the above equations $\bar{P}_{ij}(a) = E[P_{ij}(a)] = \phi_{ij}(a)$ so we use the *expected transition matrix* model to find the transitions on applying random control and updating *Q-matrix* according to Eq.(4.6). The approximate *Q-learning* algorithm shown in algorithm 4.7.1 combines aspects of model-free and model-based learning. The algorithm 4.7.1 was implemented for both Dirichlet and Beta prior and the discounted cost evaluated.

4.8 Cost and Convergence Simulation Under Control for a 4-gene Example

We consider a 4-gene network defined by the following true but unknown TPM, $\tilde{\phi}$. The network is shown in Fig. 4.5. The predictors/parents (*Pa*) are known to be *Pa*(*A*)=(*B*,*C*), *Pa*(*B*)=(*C*,*D*), *Pa*(*C*)=(*A*,*D*) and *Pa*(*D*)=(*A*,*B*). In a true biological system knowledge of the system will determine the predictors. The system is modeled using the methods described in Sections. 4.3.4.1 and 4.3.4.2 and it is shown here that modeling with a Beta prior gives a lower expected cost in comparison to a Dirichlet prior. To make comparisons easier, both the system such that the starting model is the ETM ϕ is same for both the models. This is done by choosing a uniform distribution for both the Beta and Dirichlet distributions. This tells us when we have very little or no prior knowledge about the system since we assume all the transition probabilities are set to be equal. The starting uncertainty parameter matrix defined as α_{diri} and $\alpha\beta_{beta}$ are shown in Table. 4.1 and 4.3. The update process for the uncertainty parameter matrix for both distribution depends on the current state i and next state j and also control a as discussed previously. On applying control a changes state of system to $\tilde{i}$ and the next state is j. Thus, if we know current state i (after applying control a) and next state j the updated matrices are obtained as explained. We show that the cost is optimal in a Bayesian sense. This means over the whole uncertainty class our action will be optimal, though it might be sub-optimal for a specific TPM. For this we draw 100 samples each from the Dirichlet and Beta distributions. This will be representative of the uncertainty class and will be used to design 100 different TPM's.

4.8.1 Simulation

We simulated the network in Fig. 4.5 from all starting condition *0,1,2...15* and evaluated the average accumulated cost and the convergence between the true TPM ($\tilde{\phi}$) and model TPM (ϕ). The algorithm was implemented as follows.

- The parameters used for optimal DP simulation are: $\lambda = 0.2, K = 3$.

  The parameter used for sub-optimal Bayesian Q-learning are: initial Q-matrix=0, $\gamma = 0.8, \alpha = \eta/(\eta+1), \eta = 10000$.

  The cost function $g_{ij}(a)$ is defined by $g_{ij}(a) = \begin{cases} 0, \text{ if } a = 0, \ j \text{ is good} \\ 2, \text{ if } a = 0, \ j \text{ is bad} \\ 0.1, \text{ if } a = 1, \ j \text{ is good} \\ 2.1, \text{ if } a = 1, \ j \text{ is bad} \end{cases}$

  The control action available was assumed to only down-regulate gene C if it is up-regulated.

- We started with a uniform prior for both the dirichlet and beta distribution. The idea was to show quicker convergence and lower cost scheme in the case of modeling and having prior distribution over pathways (Beta) rather than having prior distribution over the states (Dirichlet).

- Using the prior we evaluated the model ETM.

- Using this model ETM, we evaluated the optimal control action using the method of successive approximation and Bayesian Q-learning.

- We applied this control action to the the true TPM which represents the true system and observe a transition.

Table 4.5: Comparison of costs across different methods

$Method$	J_{DP}^{beta}	J_{DP}^{diri}	J_{Q}^{beta}	J_{Q}^{diri}
$Cost$	1.517	1.521	1.523	1.527

- This transition gives a discounted cost which is already predefined and this is added to the previously accumulated discounted cost.
- Based on the above transitions the prior is updated to obtain the posterior which gives us the model TPM. The *norm* of the distance between true system and model.
- The whole process is repeated for same starting condition multiple times (100) over 100 networks generated from the uncertainty class. Every time the simulation is run the path is going to be different due to stochastic nature of the transitions. We then average out the accumulated cost and *norm* between true system and model over all initial starting states assuming them to be equally likely.
- The final cost and convergence plots are shown in Table 4.5 and Fig. 4.9.

4.9 Conclusions

In this section we developed a stochastic model of a GRN. The uncertainty over the model were introduced as probability distributions over two critical aspects of the system, namely the state and the nodes of the GRN. We showed that updating the model with data from the system helps us to reduce the size of the uncertainty class and converge to the true system. We also defined an optimization framework to estimate optimal control actions over the uncertainty class. The estimated control action is going to be optimal over the uncertainty class and not over every individual network. The optimal methods however, suffered from extreme computational and memory complexities and we had to implement sub-optimal methods to not only solve the problem in reasonable time but also to scale

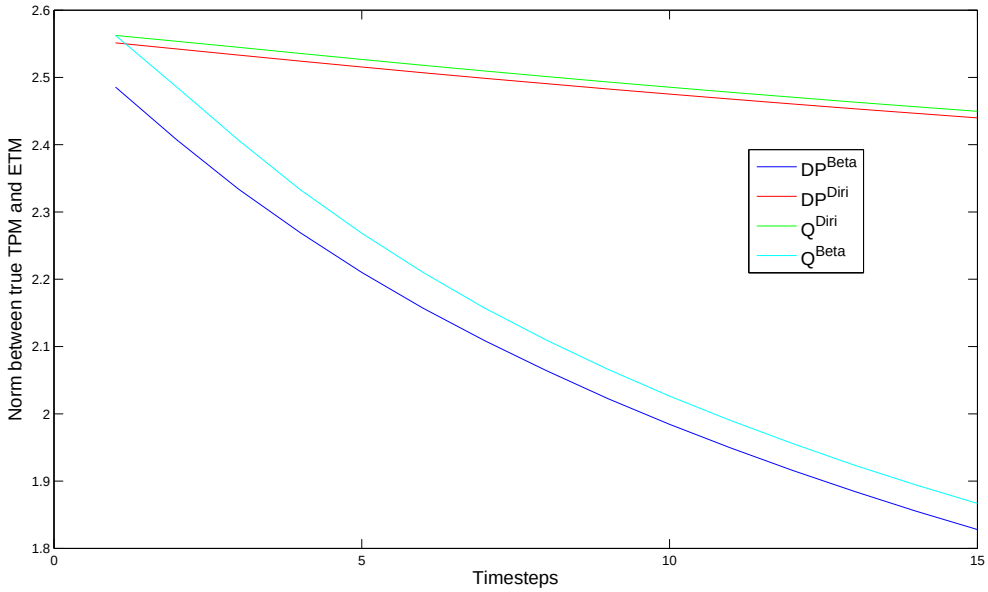

Figure 4.9: Convergence of model to true system across different methods

the size of the network to incorporate more number of nodes. The sub-optimal methods worked reasonably well. We feel that this kind of work has a strong potential in context of cancer genomics- both for network inference and network intervention.

5. CONCLUSIONS

Traditionally, drug discoveries have been performed by identifying functionality of individual components, rather than looking at their overall systemic properties. Considering only a few aspects of a complex system has led to very limited success in treating complex diseases like cancer. Now over years of work it is evident that many of the complex diseases are not caused by just one single factor- a gene, a protein, or biochemical reaction, but a combination of many factors. With this is mind it becomes imperative to study the global dynamical properties of integrated and interacting networks of biological components. Systems biology is gradually becoming the norm to understand biology from a holistic point of view. With the current advancement in biology including high-throughput data (next-gen sequencing), more health related issues are being pursued from a genetic angle. This effort has led us in recent years to catalog the human genome, and in a position to amend the traditional methods of treating complex health problems.

Most of the work in biology so far has focused on understanding univariate interactions. However, to understand genetic diseases including cancer it is important to focus on the multivariate interactions in these systems. Biological systems are observed to show circuit/ network like properties however, we have not exploited these properties for better understanding until recently. Gene regulatory networks represent these biological systems which are highly structured but incredibly complex to understand. With this in mind, it is imperative to improve our understanding of gene-regulatory networks. There are many aspects to systems biology, one of them being modeling and studying the dynamical properties of the gene regulatory networks, which has been the focus of this dissertation. This systems based approach will aid and enhance our success in drug design and discovery by finding good treatment strategy. This has been another focus in this dissertation.

In this dissertation, logic synthesis is used to model and study the gene regulatory networks. The constructed models are used to determine the faults in the networks based on the signature of few output genes. A similar approach was used to test drug efficacy by measuring the profiles of downstream genes. These results can be used to determine the faults and then based on the faults determine the optimal drug combination. To make the models more realistic, stochastic nature of transitions are introduced and control algorithms for these developed based on a Bayesian framework.

It is shown that the task of modeling of gene regulatory network is a non-trivial task. The non-triviality of the task is due to the very limited understanding of the dynamics of these systems. We have tried to circumvent this limitation by using prior knowledge in the form of biological pathways as well as introduce uncertainty over the prior knowledge. We have validated some of our simulation results using experimental results from other researchers work. We have met with some success in this regard. This motivates us to pursue this line of research in the future to validate the actual dynamical system as predicted by our model. This would however, require time-series data acquisition of the gene regulatory network which we plan to pursue in immediate future.

Some of the research questions of immediate interests will be:

- Modeling for multiple fault scenario since there are multiple mutations/faults in a network.
- Validating the dynamical model in vitro and in vivo.
- Validating the fault detection strategies.
- Validating the drug intervention strategies.

REFERENCES

[1] Stuart Kauffman. *The Origins of Order: Self Organization and Selection in Evolution*. New York, NY: Oxford University Press, 1993.

[2] R. Layek, A. Datta, and E. R. Dougherty. From biological pathways to regulatory networks. *Molecular Biosystems*, 7:843–851, 2011.

[3] R. Layek, A. Datta, M. Bittner, and E. R. Dougherty. Cancer therapy design based on pathway logic. *Bioinformatics*, 27:548–555, 2011.

[4] M L Putterman. *Decision Processes: Discrete Stochastic Dynamic Programming*. Wiley Interscience, New York, 2009.

[5] Ilya Shmulevich, Edward R Dougherty, Seungchan Kim, and Wei Zhang. Probabilistic Boolean networks: a rule-based uncertainty model for gene regulatory networks. *Bioinformatics*, 18(2):261–274, 2002.

[6] I Shmulevich, E.R. Dougherty, and Wei Zhang. From Boolean to probabilistic Boolean networks as models of genetic regulatory networks. *Proceedings of the IEEE*, 90(11):1778–1792, 2002.

[7] Aniruddha Datta, Ashish Choudhary, Michael L. Bittner, and Edward R. Dougherty. External control in Markovian genetic regulatory networks: the imperfect information case. *Bioinformatics*, 20(6):924–930, 2004.

[8] Ashish Choudhary, Aniruddha Datta, Michael L. Bittner, and Edward R. Dougherty. Intervention in a family of Boolean networks. *Bioinformatics*, 22(2):226–232, 2006.

[9] R. Pal, A Datta, and E.R. Dougherty. Optimal infinite horizon control for probabilistic Boolean networks. In *American Control Conference, 2006*, pages 668–673, 2006.

[10] Ranadip Pal, Aniruddha Datta, Michael L. Bittner, and Edward R. Dougherty. Intervention in context-sensitive probabilistic Boolean networks. *Bioinformatics*, 21(7):1211–1218, 2005.

[11] Mohammadmahdi R Yousefi and Edward R Dougherty. A comparison study of optimal and suboptimal intervention policies for gene regulatory networks in the presence of uncertainty. *EURASIP Journal on Bioinformatics and Systems Biology*, 2014(1):1–13, 2014.

[12] R. A. Weinberg. *The Biology of Cancer*. Garland Science, Princeton, 2006.

[13] A. Datta and E. Dougherty. *Introduction to Genomic Signal Processing with Control*. CRC Press, Boca Raton, 2007.

[14] G. A. Viswanathan, J. Seto, S. Patil, G. Nudelman, and S. C. Sealfon. Getting started in biological pathway construction and analysis. *PLoS Computational Biology*, 4:e16, 2008.

[15] P. Saraiya, C. North, and K. Duca. Visualizing biological pathways: requirements analysis, systems evaluation and research agenda. *Information Visualization*, pages 1–15, 2005.

[16] S. O. Simmons, C. Y. Fan, and Ram Ramabhadran. Cellular stress response pathway system as a sentinel ensemble in toxicological screening. *Toxicological Sciences*, 111:202–225, 2009.

[17] G. Storz and J. A. Imlay. Oxidative stress. *Current Opinion in Microbiology*, 2:188–194, 1999.

[18] T. W. Kensler, N. Wakabayashi, and S. Biswa. Cell survival responses to environmental stresses via the Keap1-Nrf2-ARE pathway. *Annual Review of Pharmacology and Toxicology*, 47:89–110, 2007.

[19] J. M. Lee and J. A. Johnson. An important role of Nrf2-ARE pathway in the cellular defense mechanism. *Journal of Biochemistry and Molecular Biology*, 37:139–143, 2004.

[20] F. Hong, K. R. Sekhar, M. L. Freeman, and D. C. Liebler. Specific patterns of electrophile adduction trigger Keap1 ubiquitination and Nrf2 activation. *Journal of Biological Chemistry*, 280:31768–31775, 2005.

[21] K. Itoh, N. Wakabayashi, Y. Katoh, T. Ishii, T. O'Connor, and M. Yamamoto. Keap1 regulates both cytoplasmic-nuclear shuttling and degradation of Nrf2 in response to electrophiles. *Genes to Cells*, 8:379–391, 2003.

[22] S. K. Niture and A. K. Jaiswal. Prothymosin mediates nuclear import of the INrf2/Cul3 Rbx1 complex to degrade nuclear Nrf2. *Journal of Biological Chemistry*, 284:13856–13868, 2009.

[23] J. F. Reichard, G. T. Motz, and Alvaro Puga. Heme oxygenase-1 induction by Nrf2 requires inactivation of the transcriptional repressor Bach1. *Nucleic Acids Research*, 35:7074–7086, 2007.

[24] S. Dhakshinamoorthy, A. K. Jain, D. A. Bloom, and A. K. Jaiswal. Bach1 competes with Nrf2 leading to negative regulation of the antioxidant response element (ARE)-

mediated NAD(P)H:quinone oxidoreductase 1 gene expression and induction in response to antioxidants. *Journal of Biological Chemistry*, 280:16891–16900, 2005.

[25] F. Katsuoka, H. Motohashi, J. D. Engel, and M. Yamamoto. Nrf2 transcriptionally activates the mafG gene through an antioxidant response element. *Journal of Biological Chemistry*, 280:4483–4490, 2005.

[26] Y. Shan, R. W. Lambrecht, S. E. Donohue, and H. L. Bonkovsky. Role of Bach1 and Nrf2 in up-regulation of the heme oxygenase-1 gene by cobalt protoporphyrin. *FASEB Journal*, 20:2651–2653, 2006.

[27] O. H. Lee, A. K. Jain, V. Papusha, and A. K. Jaiswal. An auto-regulatory loop between stress sensors INrf2 and Nrf2 controls their cellular abundance. *Journal of Biological Chemistry*, 282:36412–36420, 2007.

[28] H. C. Huang, T. Nguyen, and C. B. Pickett. Phosphorylation of Nrf2 at Ser-40 by protein kinase C regulates antioxidant response element-mediated transcription. *Journal of Biological Chemistry*, 277:42769–42774, 2002.

[29] J. Goh, L. Enns, S. Fatemie, H. Hopkins, J. Morton, C. Pettan-Brewer, and W. Ladiges. Mitochondrial targeted catalase suppresses invasive breast cancer in mice. *BMC Cancer*, 11:191, 2011.

[30] F. Sotgia, U. E. Martinez-Outschoorn, and M. P. Lisanti. Mitochondrial oxidative stress drives tumor progression and metastasis: should we use antioxidants as a key component of cancer treatment and prevention? *BMC Medicine*, 9:62, 2011.

[31] R. K. Bai, S. M. Leal, D. Covarrubias, A. Liu, and L. J. C. Wong. Mitochondrial genetic background modifies breast cancer risk. *Cancer Research*, 67:4687–4694, 2007.

[32] Leonardo M. R. Ferreira. Cancer metabolism: The Warburg effect today. *Experimental and Molecular Pathology*, 89:372–380, 2010.

[33] M. Inoue, E F Sato, M Nishikawa, Ah-Mee Park, Y Kira, I Imada, and K Utsumi. Mitochondrial generation of reactive oxygen species and its role in aerobic life. *Current Medicinal Chemistry*, 10:2495–2505, 2003.

[34] M. F. Beal. Less stress, longer life. *Nature Medicine*, 11:598–599, 2005.

[35] A. Sitaramayya. *Signal Transduction: Pathways, Mechanisms and Diseases*. Springer Verilag, Berlin, 2010.

[36] D. Hanahan and R. A. Weinberg. Hallmarks of cancer: The next generation. *Cell*, 144:646–674, 2011.

[37] D. Hanahan and R. A. Weinberg. The hallmarks of cancer. *Cell*, 100:57–70, 2000.

[38] W. C. Hahn and R. A. Weinberg. Rules for making human tumor cells. *New England Journal of Medicine*, pages 1593–1603, 2002.

[39] K. Sakamoto, K. Iwasaki, H. Sugiyama, and Y. Tsuji. Role of the tumor suppressor PTEN in antioxidant responsive element-mediated transcription and associated histone modifications. *Molecular Biology of the Cell*, 20:1606–1617, 2009.

[40] B. T. Hennessy, D. L. Smith, P. T. Ram, Y. Lu, and G. B. Mills. Exploiting the PI3K/AKT pathway for cancer drug discovery. *Nature Reviews Drug Discovery*, 4:989–1004, 2005.

[41] L. Wang, Y. Chen, P. Sternberg, and J. Cai. Essential roles of the PI3 kinase/Akt pathway in regulating Nrf2-dependent antioxidant functions in the RPE. *Investigative Ophthalmology and Visual Science*, 49:1671–1678, 2008.

[42] J. L. Martindale and N. J. Holbrook. Cellular response to oxidative stress: signaling for suicide and survival. *Journal of Cellular Physiology*, 192:1–15, 2002.

[43] A. Gross, J. M. McDonnell, and S. J. Korsmeyer. BCL-2 family members and the mitochondria in apoptosis. *Genes and Development*, 13:1899–1911, 1999.

[44] L. Coultas and A. Strasser. The role of the Bcl-2 protein family in cancer. *Seminars in Cancer Biology*, 13:115–123, 2003.

[45] M. Abramovici, M. A. Breuer, and A. D. Friedman. *Digital Systems Testing and Testable Design*. Wiley-IEEE Press, New York, 1990.

[46] M. A. Breuer and A. D. Friedman. *Diagnosis and Reliable Design of Digital Systems*. Springer Verilag, 1976.

[47] G L Semenza. HIF-1 and human disease: one highly involved factor. *Genes and Development*, 14(16):1983–1991, 2000.

[48] KangAe Lee, Robert A. Roth, and John J. LaPres. Hypoxia, drug therapy and toxicity. *Pharmacology and Therapeutics*, 113(2):229–246, 2007.

[49] Jeremy P.T. Ward. Oxygen sensors in context. *Biochimica et Biophysica Acta, Bioenergetics*, 1777(1):1–14, 2008.

[50] I. Beck, S. Ramirez, R. Weinmann, and J. Caro. Enhancer element at the 3'-flanking region controls transcriptional response to hypoxia in the human erythropoietin gene. *Journal of Biological Chemistry*, 266(24):15563–15566, 1991.

[51] G L Wang, B H Jiang, E A Rue, and G L Semenza. Hypoxia-inducible factor 1 is a basic-helix-loop-helix-PAS heterodimer regulated by cellular O_2 tension. *Proceedings of the National Academy of Sciences of the United States of America*, 92(12):5510–5514, 1995.

[52] Aimee Y. Yu, Maria G. Frid, Larissa A. Shimoda, Charles M. Wiener, Kurt Stenmark, and Gregg L. Semenza . Temporal, spatial, and oxygen-regulated expression of hypoxia-inducible factor-1 in the lung. *American Journal of Physiology, Lung Cellular and Molecular Physiology*, 275(4):L818–L826, 1998.

[53] Andrew C.R. Epstein, Jonathan M. Gleadle, Luke A. McNeill, Kirsty S. Hewitson, John O'Rourke, David R. Mole, Mridul Mukherji, Eric Metzen, Michael I. Wilson, Anu Dhanda, Ya-Min Tian, Norma Masson, Donald L. Hamilton, Panu Jaakkola, Robert Barstead, Jonathan Hodgkin, Patrick H. Maxwell, Christopher W. Pugh, Christopher J. Schofield, and Peter J. Ratcliffe. *C. elegans* EGL-9 and mammalian homologs define a family of dioxygenases that regulate HIF by prolyl hydroxylation. *Cell*, 107(1):43–54, 2001.

[54] P C Mahon, K Hirota, and G L Semenza. FIH-1: a novel protein that interacts with HIF-1α and VHL to mediate repression of HIF-1 transcriptional activity. *Genes and Development*, 15(20):2675–2686, 2001.

[55] David Lando, Daniel J. Peet, Dean A. Whelan, Jeffrey J. Gorman, and Murray L. Whitelaw. Asparagine hydroxylation of the HIF transactivation domain: A hypoxic switch. *Science*, 295(5556):858–861, 2002.

[56] Robert D. Guzy, Beatrice Hoyos, Emmanuel Robin, Hong Chen, Liping Liu, Kyle D. Mansfield, M. Celeste Simon, Ulrich Hammerling, and Paul T. Schumacker. Mitochondrial complex III is required for hypoxia-induced ROS production and cellular oxygen sensing. *Cell Metabolism*, 1(6):401–408, 2005.

[57] Qun Chen, Shadi Moghaddas, Charles L. Hoppel, and Edward J. Lesnefsky. Ischemic defects in the electron transport chain increase the production of reactive oxygen

species from isolated rat heart mitochondria. *American Journal of Physiology, Cell Physiology*, 294(2):C460–C466, 2008.

[58] Y Gong and F Agani. Oligomycin inhibits HIF-1α expression in hypoxic tumor cells. *American Journal of Cell Physiology*, 288(5):c1023–c1029, 2005.

[59] K Tani, M C Yoshida, H Satoh, K Mitamura, T Noguchi, T Tanaka, H Fujii, and S Miwa. Human M2-type pyruvate kinase: cDNA cloning, chromosomal assignment and expression in hepatoma. *Gene*, 73(2):509–516, 1988.

[60] Weibo Luo, Hongxia Hu, Ryan Chang, Jun Zhong, Matthew Knabel, Robert O'Meally, Robert N Cole, Akhilesh Pandey, and Gregg L Semenza. Pyruvate kinase M2 is a PHD3-stimulated coactivator for hypoxia-inducible factor 1. *Cell*, 145(5):732–744, 2011.

[61] Tiffany N. Seagroves, Heather E. Ryan, Han Lu, Bradly G. Wouters, Merrill Knapp, Pierre Thibault, Keith Laderoute, and Randall S. Johnson. Transcription factor HIF-1 is a necessary mediator of the Pasteur effect in mammalian cells. *Molecular and Cellular Biology*, 21(10):3436–3444, 2001.

[62] Heather R. Christofk, Matthew G. Vander Heiden, Marian H. Harris, Arvind Ramanathan, Robert E. Gerszten, Ru Wei, Mark D. Fleming, Stuart L. Schreiber, and Lewis C. Cantley. The M2 splice isoform of pyruvate kinase is important for cancer metabolism and tumour growth. *Nature*, 452(7184):230–233, 2008.

[63] Taro Hitosugi, Sumin Kang, Matthew G Vander Heiden, Tae-Wook Chung, Shannon Elf, Katherine Lythgoe, Shaozhong Dong, Sagar Lonial, Xu Wang, Georgia Z Chen, Jianxin Xie, Ting-Lei Gu, Roberto D Polakiewicz, Johannes L Roesel, Titus J Boggon, Fadlo R Khuri, D Gary Gilliland, Lewis C Cantley, Jonathan Kaufman, and Jing

Chen. Tyrosine phosphorylation inhibits PKM2 to promote the Warburg effect and tumor growth. *Science Signalling*, 2(97):ra73, 2009.

[64] Jung Whan Kim, Irina Tchernyshyov, Gregg L. Semenza, and Chi V. Dang. HIF-1-mediated expression of pyruvate dehydrogenase kinase: A metabolic switch required for cellular adaptation to hypoxia. *Cell Metabolism*, 3(3):177–185, 2006.

[65] Sriram Sridharan, Ritwik Layek, Aniruddha Datta, and Jijayanagaram Venkatraj. Boolean modeling and fault diagnosis in oxidative stress response. *BMC Genomics*, 13(Suppl 6):S4, 2012.

[66] Nicholas C. Denko. Hypoxia, HIF1 and glucose metabolism in the solid tumour. *Nature Reviews. Cancer*, 8(9):705–713, 2008.

[67] Kaisa R. Luoto, Ramya Kumareswaran, and Robert G. Bristow. Tumor hypoxia as a driving force in genetic instability. *Genome Integrity*, 4(1):5, 2013.

[68] Gregg L. Semenza. Targeting HIF-1 for cancer therapy. *Nature Reviews. Cancer*, 3(10):721–732, 2003.

[69] William R. Wilson and Michael P. Hay. Targeting hypoxia in cancer therapy. *Nature Reviews. Cancer*, 11(6):393–410, 2011.

[70] A. J. Levine and A. M. Puzio-Kuter. The control of the metabolic switch in cancers by oncogenes and tumor suppressor genes. *Science*, 330(6009):1340–1344, 2010.

[71] T van den Beucken, M Koritzinsky, and B Wouters. Translational control of gene expression during hypoxia. *Cancer Biology and Therapy*, 5(7):749–755, 2006.

[72] Garth Powis and Lynn Kirkpatrick. Hypoxia inducible factor-1α as a cancer drug target. *Molecular Cancer Therapeutics*, 3(5):647–654, 2004.

[73] Chiara Garulli, Cristina Kalogris, Lucia Pietrella, Caterina Bartolacci, Cristina Andreani, Maurizio Falconi, Cristina Marchini, and Augusto Amici. Dorsomorphin reverses the mesenchymal phenotype of breast cancer initiating cells by inhibition of bone morphogenetic protein signaling. *Cellular Signalling*, 26(2):352–362, 2014.

[74] Lionel Larue and Alfonso Bellacosa. Epithelial-mesenchymal transition in development and cancer: role of phosphatidylinositol 3' kinase/AKT pathways. *Oncogene*, 24(50):7443–7454, 2005.

[75] Catherine E. Forristal and Jean-Pierre Levesque. Targeting the hypoxia-sensing pathway in clinical hematology. *Stem Cells Translational Medicine*, 3(2):135–140, 2014.

[76] Gilles Mees, Rudi Dierckx, Christel Vangestel, Debby Laukens, Nancy Van Damme, and Christophe Van de Wiele. Pharmacologic activation of tumor hypoxia: a means to increase tumor 2-deoxy-2-[^{18}F] fluoro-D-glucose uptake? *Molecular Imaging*, 12(1):49–58, 2013.

[77] Daniele Fanale, Viviana Bazan, Stefano Caruso, Marta Castiglia, Giuseppe Bronte, Christian Rolfo, Giuseppe Cicero, and Antonio Russo. Hypoxia and human genome stability: Downregulation of BRCA2 expression in breast cancer cell lines. *BioMed Research International*, 2013:e746858, 2013.

[78] Lei Gong, Yuhua Wei, Xin Yu, Jirun Peng, and Xisheng Leng. 3-Bromopyruvic acid, a hexokinase II inhibitor, is an effective antitumor agent on the hepatoma cells : in vitro and in vivo findings. *Anti-Cancer Agents in Medicinal Chemistry*, 14(5):771–776, 2014.

[79] W. Keith Miskimins, Hyun Joo Ahn, Ji Yeon Kim, Sun Ryu, Yuh-Seog Jung, and Joon Young Choi. Synergistic anti-cancer effect of phenformin and oxamate. *PLoS ONE*, 9(1):e85576, 2014.

[80] Jie Cai, Evangelia Pardali, Gonzalo Sanchez-Duffhues, and Peter ten Dijke. BMP signaling in vascular diseases. *FEBS Journal*, 586(14):1993–2002, 2012.

[81] Mee Jung Kim and Senyon Choe. BMPs and their clinical potentials. *BMB Reports*, 44(10):619–634, 2011.

[82] Giovanni Melillo. Inhibiting hypoxia-inducible factor 1 for cancer therapy. *Molecular Cancer Research*, 4(9):601–605, 2006.

[83] Jie Xu, Jilin Wang, Bin Xu, Haiyan Ge, Xiaolin Zhou, and Jing-Yuan Fang. Colorectal cancer cells refractory to anti-VEGF treatment are vulnerable to glycolytic blockade due to persistent impairment of mitochondria. *Molecular Cancer Therapeutics*, 12(5):717–724, 2013.

[84] John Papaconstantinou and Sidney P. Colowick. The role of glycolysis in the growth of tumor cells II. the effect of oxamic acid on the growth of HeLa cells in tissue culture. *Journal of Biological Chemistry*, 236(2):285–288, 1961.

[85] Adam D. Moorhouse, Christian Spiteri, Pallavi Sharma, Mire Zloh, and John E. Moses. Targeting glycolysis: a fragment based approach towards bifunctional inhibitors of hLDH-5. *Chemical Communications*, 47(1):230–232, 2011.

[86] Deborah Huveldt, Laura J. Lewis-Tuffin, Brett L. Carlson, Mark A. Schroeder, Fausto Rodriguez, Caterina Giannini, Evanthia Galanis, Jann N. Sarkaria, and Panos Z. Anastasiadis. Targeting Src family kinases inhibits bevacizumab-induced glioma cell invasion. *PLoS ONE*, 8(2):e56505, 2013.

[87] E D Michelakis, L Webster, and J R Mackey. Dichloroacetate (DCA) as a potential metabolic-targeting therapy for cancer. *British Journal of Cancer*, 99(7):989–994, 2008.

[88] Ryan JO Dowling, Pamela J. Goodwin, and Vuk Stambolic. Understanding the benefit of metformin use in cancer treatment. *BMC Medicine*, 9(1):33, 2011.

[89] Xiaona Liu, Rishi Raj Chhipa, Shabnam Pooya, Matthew Wortman, Sara Yachyshin, Lionel M. L. Chow, Ashish Kumar, Xuan Zhou, Ying Sun, Brian Quinn, Christopher McPherson, Ronald E. Warnick, Ady Kendler, Shailendra Giri, Jeroen Poels, Koenraad Norga, Benoit Viollet, Gregory A. Grabowski, and Biplab Dasgupta. Discrete mechanisms of mTOR and cell cycle regulation by AMPK agonists independent of AMPK. *Proceedings of the National Academy of Sciences of the United States of America*, pages e435–e444, 2014.

[90] R Bellman. A problem in the sequential design of experiments. *Sankhya: The Indian Journal of Statistics*, 16(3/4):221–229, 1956.

[91] James John Martin. *Bayesian Decision Problems and Markov Chains*. Wiley, 1967.

[92] Sach Mukherjee and Terence P. Speed. Network inference using informative priors. *Proceedings of the National Academy of Sciences of the United States of America*, 105(38):14313–14318, 2008.

[93] Cyrus Derman. *Finite State Markovian Decision Processes*. Academic Press, 1970.

APPENDIX A

DESIGNING A TEST SEQUENCE

As an example on how to obtain the test sequence let us consider the sequential circuit shown in Fig. A.1.

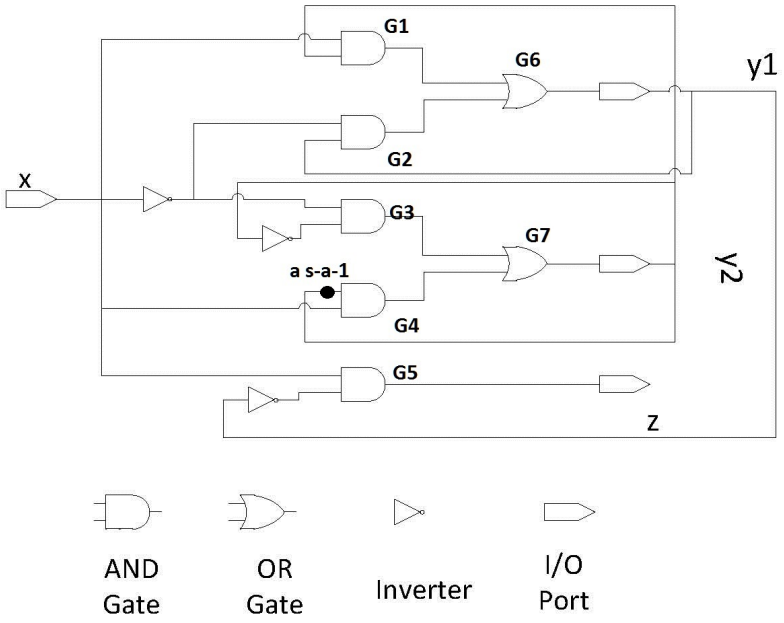

Figure A.1: Digital equivalent of a circuit

Let us also assume that the internal state is known and is y1=y2=0. Let us determine the test sequence that will determine the fault at location 'a' s-a-1. Time frame 0: Since y2=0 and we have the line s-a-1. As we need to propagate this fault we choose x=1 so that the output of G4 is going to be 0 for normal circuit and 1 for faulty circuit. The internal state is y1=0, y2=0/1. In the representation a/b, a corresponds to value in normal and b corresponds to value in fault network. The output is z=1. Time frame 1: Since the state y1 did not change we cannot produce a difference in the output between normal and faulty

network so we maintain x=1 and push the system to internal state y1=0/1, y2=0/1 and x=1. Time frame 2: Since there is difference in state y1 between normal and faulty circuit we can propagate this to z by choosing x=1 and z=1/0. Hence the test sequence x='111' will determine the fault at 'a' s-a-1.

APPENDIX B

RESULTS OF SIMULATION FROM SECTION 4

We show the results of convergence in this section. Let us assume the true CPT tables be given Fig. B.1. This true CPT tables will give a true TPM given in Table. B.1. The mean CPT tables after 100 and 10000 time-steps are shown in Fig. B.2 and B.3. The expected TPM after 100 and 10000 time-steps for Dirichlet and Beta models are shown in Table. B.2, B.3, B.4 and B.5. It was seen that with more and more data the model converged to true transition probabilities and the variance of the models was very small. This means that the expected TPM is the same as the true TPM.

$(B,C)_{t-1}$ \ A_t	0	1
00	0.85	0.15
01	0.25	0.75
11	0.35	0.65
10	0.05	0.95

$(C,D)_{t-1}$ \ B_t	0	1
00	0.8	0.2
01	0.35	0.65
11	0.25	0.75
10	0.1	0.9

$(D,A)_{t-1}$ \ C_t	0	1
00	0.95	0.05
01	0.2	0.8
11	0.2	0.8
10	0.05	0.95

$(A,B)_{t-1}$ \ D_t	0	1
00	0.9	0.1
01	0.25	0.75
11	0.25	0.75
10	0.1	0.9

Figure B.1: True CPT values

$(B,C)_{t-1}$ \ A_t	0	1
00	0.5714	0.4286
01	0.2	0.8
11	0.3125	0.6875
10	0.0625	0.9375

$(C,D)_{t-1}$ \ B_t	0	1
00	0.75	0.25
01	0.4	0.6
11	0.381	0.619
10	0.0405	0.9595

$(D,A)_{t-1}$ \ C_t	0	1
00	0.8	0.2
01	0.2308	0.7692
11	0.4167	0.5833
10	0.0789	0.9211

$(A,B)_{t-1}$ \ D_t	0	1
00	0.8	0.2
01	0.4615	0.5385
11	0.4118	0.5882
10	0.1325	0.8675

Figure B.2: Mean CPT values after 100 time-steps

Table B.1: True TPM from true CPT values

0.5814	0.0646	0.0306	0.0034	0.1454	0.0162	0.0077	0.0009	0.1026	0.0114	0.0054	0.0006	0.0257	0.0029	0.0014	0.0002
0.0536	0.0060	0.2142	0.0238	0.0995	0.0111	0.3978	0.0442	0.0095	0.0011	0.0378	0.0042	0.0176	0.0020	0.0702	0.0078
0.0534	0.0059	0.0028	0.0003	0.1603	0.0178	0.0084	0.0009	0.1603	0.0178	0.0084	0.0009	0.4809	0.0534	0.0253	0.0028
0.0045	0.0005	0.0180	0.0020	0.0405	0.0045	0.1620	0.0180	0.0135	0.0015	0.0540	0.0060	0.1215	0.0135	0.4860	0.0540
0.0665	0.1995	0.0035	0.0105	0.0166	0.0499	0.0009	0.0026	0.1235	0.3705	0.0065	0.0195	0.0309	0.0926	0.0016	0.0049
0.0061	0.0184	0.0245	0.0735	0.0114	0.0341	0.0455	0.1365	0.0114	0.0341	0.0455	0.1365	0.0211	0.0634	0.0845	0.2535
0.0030	0.0089	0.0002	0.0005	0.0089	0.0267	0.0005	0.0014	0.0564	0.1692	0.0030	0.0089	0.1692	0.5077	0.0089	0.0267
0.0003	0.0008	0.0010	0.0030	0.0023	0.0068	0.0090	0.0270	0.0048	0.0143	0.0190	0.0570	0.0428	0.1283	0.1710	0.5130
0.0340	0.1020	0.1360	0.4080	0.0085	0.0255	0.0340	0.1020	0.0060	0.0180	0.0240	0.0720	0.0015	0.0045	0.0060	0.0180
0.0037	0.0112	0.0707	0.2120	0.0069	0.0207	0.1312	0.3937	0.0007	0.0020	0.0125	0.0374	0.0012	0.0037	0.0232	0.0695
0.0031	0.0094	0.0125	0.0375	0.0094	0.0281	0.0375	0.1125	0.0094	0.0281	0.0375	0.1125	0.0281	0.0844	0.1125	0.3375
0.0003	0.0009	0.0059	0.0178	0.0028	0.0084	0.0534	0.1603	0.0009	0.0028	0.0178	0.0534	0.0084	0.0253	0.1603	0.4809
0.0056	0.0504	0.0224	0.2016	0.0014	0.0126	0.0056	0.0504	0.0104	0.0936	0.0416	0.3744	0.0026	0.0234	0.0104	0.0936
0.0006	0.0055	0.0116	0.1047	0.0011	0.0102	0.0216	0.1945	0.0011	0.0102	0.0216	0.1945	0.0021	0.0190	0.0401	0.3612
0.0003	0.0023	0.0010	0.0090	0.0008	0.0068	0.0030	0.0270	0.0048	0.0428	0.0190	0.1710	0.0143	0.1283	0.0570	0.5130
0.0000	0.0002	0.0005	0.0043	0.0002	0.0020	0.0043	0.0385	0.0005	0.0043	0.0090	0.0812	0.0043	0.0385	0.0812	0.7310

Table B.2: Model expected TPM after 100 time-steps for Dirichlet model

$$
\begin{pmatrix}
0.0625 & 0.0625 & 0.0625 & 0.0625 & 0.0625 & 0.0625 & 0.0625 & 0.0625 & 0.0625 & 0.0625 & 0.0625 & 0.0625 & 0.0625 & 0.0625 & 0.0625 & 0.0625 \\
0.0588 & 0.0588 & 0.0588 & 0.0588 & 0.0588 & 0.0588 & 0.1176 & 0.0588 & 0.0588 & 0.0588 & 0.0588 & 0.0588 & 0.0588 & 0.0588 & 0.0588 & 0.0588 \\
0.0625 & 0.0625 & 0.0625 & 0.0625 & 0.0625 & 0.0625 & 0.0625 & 0.0625 & 0.0625 & 0.0625 & 0.0625 & 0.0625 & 0.0625 & 0.0625 & 0.0625 & 0.0625 \\
0.0625 & 0.0625 & 0.0625 & 0.0625 & 0.0625 & 0.0625 & 0.0625 & 0.0625 & 0.0625 & 0.0625 & 0.0625 & 0.0625 & 0.0625 & 0.0625 & 0.0625 & 0.0625 \\
0.0625 & 0.0625 & 0.0625 & 0.0625 & 0.0625 & 0.0625 & 0.0625 & 0.0625 & 0.0625 & 0.0625 & 0.0625 & 0.0625 & 0.0625 & 0.0625 & 0.0625 & 0.0625 \\
0.0588 & 0.1176 & 0.0588 & 0.0588 & 0.0588 & 0.0588 & 0.0588 & 0.0588 & 0.0588 & 0.0588 & 0.0588 & 0.0588 & 0.0588 & 0.0588 & 0.0588 & 0.0588 \\
0.0556 & 0.0556 & 0.0556 & 0.0556 & 0.0556 & 0.0556 & 0.0556 & 0.0556 & 0.0556 & 0.0556 & 0.0556 & 0.0556 & 0.0556 & 0.1667 & 0.0556 & 0.0556 \\
0.0435 & 0.0435 & 0.0435 & 0.0435 & 0.0435 & 0.087 & 0.0435 & 0.0435 & 0.0435 & 0.0435 & 0.0435 & 0.0435 & 0.0435 & 0.087 & 0.1739 & 0.1304 \\
0.0625 & 0.0625 & 0.0625 & 0.0625 & 0.0625 & 0.0625 & 0.0625 & 0.0625 & 0.0625 & 0.0625 & 0.0625 & 0.0625 & 0.0625 & 0.0625 & 0.0625 & 0.0625 \\
0.0625 & 0.0625 & 0.0625 & 0.0625 & 0.0625 & 0.0625 & 0.0625 & 0.0625 & 0.0625 & 0.0625 & 0.0625 & 0.0625 & 0.0625 & 0.0625 & 0.0625 & 0.0625 \\
0.0588 & 0.0588 & 0.0588 & 0.0588 & 0.0588 & 0.0588 & 0.0588 & 0.0588 & 0.0588 & 0.0588 & 0.0588 & 0.0588 & 0.0588 & 0.1176 & 0.0588 & 0.0588 \\
0.0417 & 0.0417 & 0.0417 & 0.0417 & 0.0417 & 0.0417 & 0.0417 & 0.0833 & 0.0417 & 0.0417 & 0.0833 & 0.0417 & 0.0417 & 0.0417 & 0.0417 & 0.2917 \\
0.0625 & 0.0625 & 0.0625 & 0.0625 & 0.0625 & 0.0625 & 0.0625 & 0.0625 & 0.0625 & 0.0625 & 0.0625 & 0.0625 & 0.0625 & 0.0625 & 0.0625 & 0.0625 \\
0.0455 & 0.0455 & 0.0455 & 0.0455 & 0.0455 & 0.0455 & 0.0455 & 0.1364 & 0.0455 & 0.0455 & 0.0455 & 0.0909 & 0.0455 & 0.0455 & 0.0455 & 0.1818 \\
0.0435 & 0.0435 & 0.0435 & 0.0435 & 0.0435 & 0.0435 & 0.0435 & 0.0435 & 0.0435 & 0.0435 & 0.0435 & 0.087 & 0.0435 & 0.087 & 0.0435 & 0.2609 \\
0.0108 & 0.0108 & 0.0108 & 0.0108 & 0.0108 & 0.0108 & 0.0108 & 0.0538 & 0.0108 & 0.0108 & 0.0108 & 0.0753 & 0.0108 & 0.0215 & 0.0645 & 0.6667
\end{pmatrix}
$$

Table B.3: Model expected TPM after 10000 time-steps for Dirichlet model

$$
\begin{pmatrix}
0.2813 & 0.0625 & 0.0313 & 0.0313 & 0.1563 & 0.0313 & 0.0313 & 0.0313 & 0.0938 & 0.0313 & 0.0313 & 0.0313 & 0.0625 & 0.0313 & 0.0313 & 0.0313 \\
0.0345 & 0.0172 & 0.1552 & 0.0345 & 0.1034 & 0.0172 & 0.2931 & 0.0517 & 0.0345 & 0.0172 & 0.0517 & 0.0517 & 0.0172 & 0.0172 & 0.0862 & 0.0172 \\
0.0411 & 0.0274 & 0.0137 & 0.0137 & 0.1370 & 0.0137 & 0.0274 & 0.0137 & 0.1370 & 0.0137 & 0.0137 & 0.0137 & 0.4521 & 0.0274 & 0.0411 & 0.0137 \\
0.0038 & 0.0038 & 0.0077 & 0.0038 & 0.0423 & 0.0115 & 0.1423 & 0.0115 & 0.0192 & 0.0038 & 0.0615 & 0.0115 & 0.1269 & 0.0077 & 0.4885 & 0.0538 \\
0.0169 & 0.3051 & 0.0169 & 0.0169 & 0.0169 & 0.0339 & 0.0169 & 0.0169 & 0.1017 & 0.2034 & 0.0169 & 0.0169 & 0.1017 & 0.0847 & 0.0169 & 0.0169 \\
0.0125 & 0.0250 & 0.0250 & 0.0875 & 0.0375 & 0.0375 & 0.0250 & 0.1000 & 0.0125 & 0.0750 & 0.0250 & 0.1250 & 0.0125 & 0.0750 & 0.0750 & 0.2500 \\
0.0109 & 0.0055 & 0.0055 & 0.0055 & 0.0164 & 0.0219 & 0.0055 & 0.0109 & 0.0492 & 0.1530 & 0.0055 & 0.0164 & 0.1585 & 0.4918 & 0.0164 & 0.0273 \\
0.0014 & 0.0014 & 0.0042 & 0.0070 & 0.0042 & 0.0056 & 0.0042 & 0.0308 & 0.0056 & 0.0182 & 0.0182 & 0.0532 & 0.0574 & 0.1176 & 0.1723 & 0.4986 \\
0.0476 & 0.1111 & 0.0794 & 0.2857 & 0.0317 & 0.0317 & 0.0635 & 0.0952 & 0.0159 & 0.0159 & 0.0317 & 0.0952 & 0.0159 & 0.0317 & 0.0159 & 0.0317 \\
0.0111 & 0.0056 & 0.0889 & 0.2056 & 0.0056 & 0.0222 & 0.0722 & 0.4056 & 0.0111 & 0.0056 & 0.0111 & 0.0500 & 0.0056 & 0.0056 & 0.0167 & 0.0778 \\
0.0066 & 0.0066 & 0.0066 & 0.0596 & 0.0199 & 0.0331 & 0.0199 & 0.0861 & 0.0132 & 0.0397 & 0.0199 & 0.1391 & 0.0199 & 0.0728 & 0.1192 & 0.3377 \\
0.0009 & 0.0009 & 0.0091 & 0.0210 & 0.0037 & 0.0100 & 0.0566 & 0.1525 & 0.0027 & 0.0027 & 0.0174 & 0.0548 & 0.0110 & 0.0256 & 0.1543 & 0.4767 \\
0.0047 & 0.0558 & 0.0233 & 0.1953 & 0.0093 & 0.0186 & 0.0047 & 0.0512 & 0.0140 & 0.1209 & 0.0233 & 0.3209 & 0.0047 & 0.0419 & 0.0186 & 0.0930 \\
0.0032 & 0.0064 & 0.0113 & 0.1159 & 0.0016 & 0.0145 & 0.0242 & 0.1932 & 0.0016 & 0.0032 & 0.0258 & 0.2013 & 0.0048 & 0.0193 & 0.0386 & 0.3349 \\
0.0009 & 0.0027 & 0.0027 & 0.0101 & 0.0009 & 0.0073 & 0.0027 & 0.0302 & 0.0046 & 0.0449 & 0.0174 & 0.1687 & 0.0174 & 0.1210 & 0.0486 & 0.5197 \\
0.0002 & 0.0002 & 0.0009 & 0.0045 & 0.0005 & 0.0028 & 0.0026 & 0.0385 & 0.0009 & 0.0045 & 0.0072 & 0.0864 & 0.0045 & 0.0362 & 0.0847 & 0.7255
\end{pmatrix}
$$

Table B.4: Model expected TPM after 100 time-steps for beta model

0.1667	0.0833	0.0556	0.0278	0.1667	0.0833	0.0556	0.0278	0.0833	0.0417	0.0278	0.0139	0.0833	0.0417	0.0278	0.0139
0.0485	0.0242	0.0848	0.0424	0.1131	0.0566	0.1980	0.0990	0.0242	0.0121	0.0424	0.0212	0.0566	0.0283	0.0990	0.0495
0.0152	0.0076	0.0051	0.0025	0.0758	0.0379	0.0253	0.0126	0.0682	0.0341	0.0227	0.0114	0.3409	0.1705	0.1136	0.0568
0.0038	0.0019	0.0066	0.0033	0.0403	0.0202	0.0706	0.0353	0.0169	0.0084	0.0295	0.0148	0.1815	0.0907	0.3176	0.1588
0.0556	0.1111	0.0185	0.0370	0.0556	0.1111	0.0185	0.0370	0.0694	0.1389	0.0231	0.0463	0.0694	0.1389	0.0231	0.0463
0.0162	0.0323	0.0283	0.0566	0.0377	0.0754	0.0660	0.1320	0.0202	0.0404	0.0354	0.0707	0.0471	0.0943	0.0825	0.1650
0.0026	0.0053	0.0009	0.0018	0.0132	0.0263	0.0044	0.0088	0.0390	0.0781	0.0130	0.0260	0.1952	0.3904	0.0651	0.1301
0.0007	0.0013	0.0011	0.0023	0.0070	0.0140	0.0123	0.0245	0.0097	0.0193	0.0169	0.0338	0.1039	0.2078	0.1818	0.3636
0.0182	0.0818	0.0424	0.1909	0.0182	0.0818	0.0424	0.1909	0.0091	0.0409	0.0212	0.0955	0.0091	0.0409	0.0212	0.0955
0.0008	0.0035	0.0356	0.1601	0.0018	0.0082	0.0830	0.3736	0.0004	0.0018	0.0178	0.0801	0.0009	0.0041	0.0415	0.1868
0.0017	0.0074	0.0039	0.0174	0.0083	0.0372	0.0193	0.0868	0.0074	0.0335	0.0174	0.0781	0.0372	0.1674	0.0868	0.3905
0.0001	0.0003	0.0028	0.0124	0.0007	0.0029	0.0296	0.1332	0.0003	0.0012	0.0124	0.0557	0.0029	0.0132	0.1332	0.5993
0.0043	0.0623	0.0101	0.1454	0.0043	0.0623	0.0101	0.1454	0.0054	0.0779	0.0127	0.1818	0.0054	0.0779	0.0127	0.1818
0.0002	0.0027	0.0085	0.1220	0.0004	0.0063	0.0199	0.2846	0.0002	0.0034	0.0106	0.1524	0.0005	0.0078	0.0248	0.3557
0.0002	0.0030	0.0005	0.0069	0.0010	0.0148	0.0024	0.0344	0.0031	0.0438	0.0071	0.1022	0.0153	0.2189	0.0356	0.5109
0.0000	0.0001	0.0003	0.0049	0.0001	0.0012	0.0037	0.0529	0.0001	0.0016	0.0051	0.0729	0.0012	0.0172	0.0547	0.7840

Table B.5: Model expected TPM after 10000 time-steps for beta model

0.5578	0.0487	0.0267	0.0023	0.1709	0.0149	0.0082	0.0007	0.1140	0.0100	0.0055	0.0005	0.0349	0.0031	0.0017	0.0001
0.0574	0.0050	0.2229	0.0195	0.0989	0.0086	0.3843	0.0336	0.0117	0.0010	0.0456	0.0040	0.0202	0.0018	0.0786	0.0069
0.0519	0.0045	0.0025	0.0002	0.1587	0.0139	0.0076	0.0007	0.1645	0.0144	0.0079	0.0007	0.5027	0.0439	0.0240	0.0021
0.0047	0.0004	0.0181	0.0016	0.0405	0.0035	0.1574	0.0137	0.0148	0.0013	0.0574	0.0050	0.1284	0.0112	0.4985	0.0435
0.0666	0.1982	0.0032	0.0095	0.0204	0.0607	0.0010	0.0029	0.1171	0.3486	0.0056	0.0167	0.0359	0.1068	0.0017	0.0051
0.0069	0.0204	0.0266	0.0792	0.0118	0.0352	0.0459	0.1366	0.0121	0.0359	0.0468	0.1393	0.0208	0.0618	0.0807	0.2401
0.0029	0.0087	0.0001	0.0004	0.0089	0.0265	0.0004	0.0013	0.0563	0.1674	0.0027	0.0080	0.1720	0.5118	0.0082	0.0245
0.0003	0.0008	0.0010	0.0030	0.0023	0.0068	0.0088	0.0263	0.0051	0.0150	0.0196	0.0584	0.0439	0.1307	0.1706	0.5075
0.0309	0.0981	0.1214	0.3851	0.0095	0.0301	0.0372	0.1180	0.0063	0.0201	0.0248	0.0787	0.0019	0.0061	0.0076	0.0241
0.0035	0.0112	0.0695	0.2206	0.0061	0.0192	0.1199	0.3803	0.0007	0.0023	0.0142	0.0451	0.0012	0.0039	0.0245	0.0777
0.0029	0.0091	0.0113	0.0358	0.0088	0.0279	0.0345	0.1096	0.0091	0.0289	0.0358	0.1135	0.0279	0.0884	0.1094	0.3470
0.0003	0.0009	0.0056	0.0179	0.0025	0.0079	0.0491	0.1557	0.0009	0.0029	0.0179	0.0568	0.0079	0.0250	0.1555	0.4933
0.0055	0.0508	0.0218	0.1994	0.0017	0.0156	0.0067	0.0611	0.0098	0.0893	0.0383	0.3506	0.0030	0.0274	0.0117	0.1074
0.0006	0.0058	0.0125	0.1142	0.0011	0.0100	0.0215	0.1969	0.0011	0.0102	0.0219	0.2008	0.0019	0.0175	0.0378	0.3462
0.0002	0.0022	0.0010	0.0087	0.0007	0.0068	0.0029	0.0266	0.0047	0.0429	0.0184	0.1684	0.0143	0.1311	0.0562	0.5147
0.0000	0.0002	0.0005	0.0044	0.0002	0.0019	0.0041	0.0379	0.0005	0.0043	0.0092	0.0842	0.0040	0.0370	0.0799	0.7317

A_t / $(B,C)_{t-1}$	0	1
00	0.8303	0.1697
01	0.2399	0.7601
11	0.3625	0.6375
10	0.0492	0.9508

B_t / $(C,D)_{t-1}$	0	1
00	0.7655	0.2345
01	0.3672	0.6328
11	0.2465	0.7535
10	0.1032	0.8968

C_t / $(D,A)_{t-1}$	0	1
00	0.9544	0.0456
01	0.2048	0.7952
11	0.203	0.797
10	0.0482	0.9518

D_t / $(A,B)_{t-1}$	0	1
00	0.9197	0.0803
01	0.2515	0.7485
11	0.2397	0.7603
10	0.0985	0.9015

Figure B.3: Mean CPT values after 10000 time-steps